

**NAFEMS**

# Proceedings Document

Extended Abstracts

# **Using Optimisation in the Design of the RWUAS** **Air Vehicle Structure**

**Gordon MacKenzie** BEng CEng FRAeS  
**Head of Airframe Analysis & Simulation Leonardo Helicopters**

## **SUMMARY**

Leonardo is a global company in the Aerospace, Defence and Security sector with an integrated offer of high-tech and dual-use solutions. Leonardo Helicopters develops the latest generation rotorcraft which meet the most demanding current and future operational requirements in all conditions and environments. Leonardo Helicopters' products, systems and services are used across approximately 150 companies worldwide.

The Rotary-Wing Unmanned Air System or RWUAS, is one of the latest unmanned capabilities being developed by Leonardo. It is a highly configurable multi-role Vertical Take Off and Landing (VTOL) vehicle with modular bays for a wide variety of mission payloads. This wide variation in usage creates significant challenges in producing an optimum light weight, cost effective structure.

Optimisation is a key element in maximising the potential of any product. The intention within this project is to develop new methods using optimisation to help determine the preliminary sizing, best architecture and cost effective materials technology for the structure. This will be applied from the very early conceptual design phase right through to the development of the mature design. To achieve this, instead of focusing solely on minimising mass, a more holistic multi-disciplinary approach is adopted involving a broad spectrum of functions using the HyperStudy™ tool from Altair.

This presentation outlines the new methods under development by Leonardo Helicopters Division Structural Design Office.

## **1: Using Optimisation to Determine Preliminary Sizing**

The aircraft is designed to perform a series of different missions. Each mission has a specific set of requirements regarding operational range, payload to be carried, loiter time and severity of manoeuvres etc. Normally these missions would be rolled into one analysis and the aircraft sized to meet the envelope created. Until now no assessment has ever been performed on the impact of these mission requirements on the structural mass of the air vehicle or whether performance improvements can be gained from small architectural changes.

To begin with, each mission can be broken down into a set of applied loads plus a corresponding aircraft mass distribution resulting in a set of finite element models each with the same stiffness matrix but different mass matrices. An optimisation process has been developed to size the primary structural components for each mission with a view to understanding the impact of each mission on the structural weight. This is done by creating design variables for the key features of the primary structural elements and then running the optimiser for each specific model. The results for the optimisation performed in HyperStudy™ can then be compared as shown in the example in figure 1 for the dummy test model.

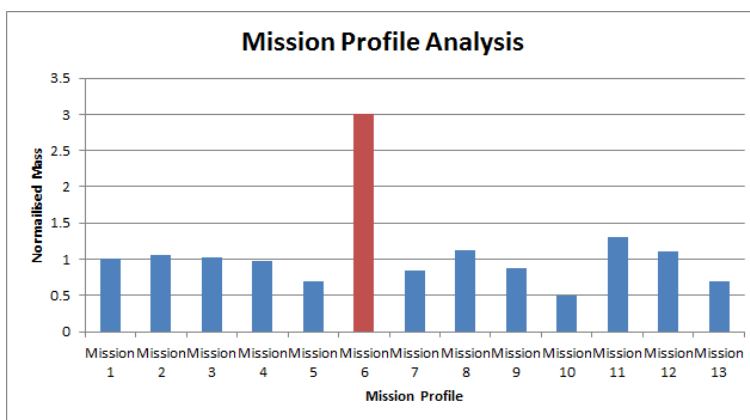


**Figure 1: Development Model Mission Profile Analysis.**

In this case, clearly we would examine mission 6 to see if it was really a key requirement for the aircraft and eliminate it from the design if possible.

Once the mission configuration is agreed, the output from this stage is the envelope of the minimum design variable values necessary for structural integrity.

Multiple analysis models add complexity and time to any further analysis processes. However, it is likely that only a subset of the missions will design the structure therefore the output from these optimisation runs can also be used to select only that key subset of models in order to improve computing times. As there are of the order of tens of design variables, an automated process for load case selection was developed using MS Excel™.

## 2: Assessing the Optimum Architecture

The basic architecture of the structure is defined as the placement of frames, intercostals and ribs. The goal of this optimisation is to achieve the maximum stiffness possible while maintaining any given functional constraints.

The method developed is based on shape optimisation. Here the shapes define the positions that the components such as frames and intercostals can adopt. An example is shown in figure 2 where the shape functions are defined using HyperMesh™, again from Altair. Each selected feature shown in the figure was allowed to move by  $\pm 100\text{mm}$ .

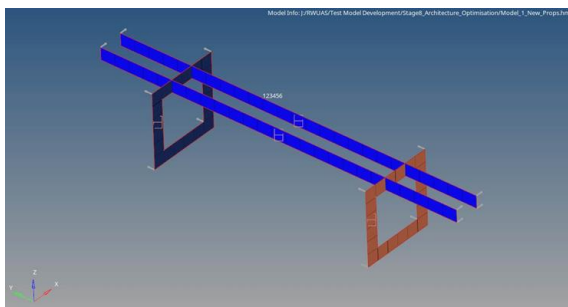


Figure 2: Shape Variable Example.

The objective function is the element strain energy which is minimised using optimisation routines in HyperStudy™ thus maximising the airframe stiffness for zero weight penalty.

## 3: Reviewing Material Technologies

Parts of the structure benefit from a deeper understanding of the possible effects material selection and manufacturing techniques may have on the cost of those components, such that a trade-off between cost and weight may be performed. A typical example of this would be the skin panel elements where a range of manufacturing methods are available such as aluminium skinned honeycomb, machined integrally stiffened aluminium panels, carbon monocoque panels (unstiffened) or carbon skinned honeycomb. All of these come with associated weight and cost penalties and in particular the cost penalty may shift with manufacturing batch size.

To develop the method, a set of materials and associated construction methods were investigated for the airframe skin panels. The method uses various MS Excel™ models to pass stiffness and mass data to the FE models, which provide the responses corresponding to the optimisation constraints plus a bespoke costing model developed in MS Excel™ which is used to provide a cost estimate for the corresponding configuration for different manufacturing



batch sizes. The control of data between models and the optimisation itself is performed using HyperStudy™.

For each panel a material model was created in MS Excel™ which allowed a discrete set of material properties to be passed to the FE model by HyperStudy™ to represent either carbon or aluminium.

As the FE model used shell elements for the skin panels, a method was developed using MS Excel™ to calculate an equivalent stiffness which could be applied to the corresponding property cards and an equivalent density which could be applied to the corresponding material cards. This allowed stiffened and unstiffened panels to be represented using the same FE mesh.

Finally a costing model was created in MS Excel™ which used the panel properties, process cost information and anticipated batch numbers to calculate the individual panel costs.

A typical output for the dummy test model is shown in figure 3.

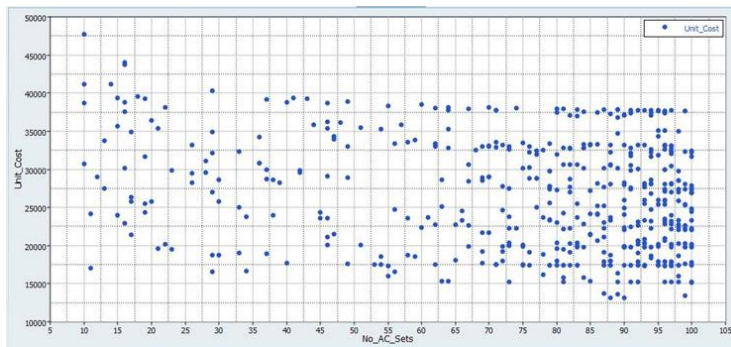


**Figure 3: Development Model Output From Cost Optimisation**

The aim of figure 3 is to assess the optimum technologies for consideration at particular production batch levels.

#### **4: Robust Design**

All forms of optimised designs by definition will have reduced strength margins. This is an issue as in the early phase of product design many of the input conditions will also be in a volatile state. Therefore having sized the airframe structure and selected the manufacturing technologies it is important to ensure that the design can tolerate some level of future change. A method was developed to do this using a stochastic approach in HyperStudy™ to see how sensitive the stress responses were to a bounded set of random variations in the input loadings.

# **AUTOMATED SHAPE OPTIMIZATION TECHNOLOGY COUPLED WITH UPFRONT CFD**

**Sean Horgan**

**Managing Director – 80/20 Engineering Ltd**

## **SUMMARY**

### **Robust Geometry Variation for the CFD-Driven Optimization of Complex Geometries.**

With the rapid development in computer technology over the last decades, both in terms of computing power and affordability, the use of simulation – specifically CFD – has increased significantly.

Not only is CFD being utilized to a much larger extent, reducing the need for physical testing, but also earlier in the product development process. Using CFD late in the design process, does serve to validate a completed design or give some guidance for late changes, however, employing it early in the process turns CFD into a real design tool.

Implementing UpFront CFD is the obvious first step in achieving this but then how does an organization get to evaluate all the many design variants that are possible before making a decision to build or manufacture?

One of the main challenges in CFD-driven shape optimization is the flexible and robust parametric variation of complex – often free-formed geometries, keeping the number of degrees-of-freedom within reasonable bounds and taking into account all necessary constraints.

This paper presents a possible solution by introducing a new state-of-the-art automated workflow based on combining a specialized software environment (CAESES®) with any of the flow (CFD) solvers found in use within industry today.

The industrial application from Diplomatic Motion Solutions used will illustrate how a control valve's internal channel shape was optimized utilizing an UpFront CFD-driven methodology bringing the whole process into one automated environment.

***80/20 Engineering** is a specialist Fluid Flow Simulation and Thermal Analysis Consultancy Company. We have a long track record of helping companies implement CFD software within 'Fluid Machinery' design environments and we believe CFD simulation will play an ever-increasing role within this challenging product development application area.*

## Hydraulic Spool Valve from Duplomatic Motion Solutions based in Italy.

Duplomatic MS are a medium sized company whose business serves the Motion Control Marketplace. They have been users of UpFront CFD to assist in the design of their valve systems for some time now.

The goal of this study was to optimize a Directional Spool valve to achieve the highest mass flow rate possible through the modification of the various internal flow channels.

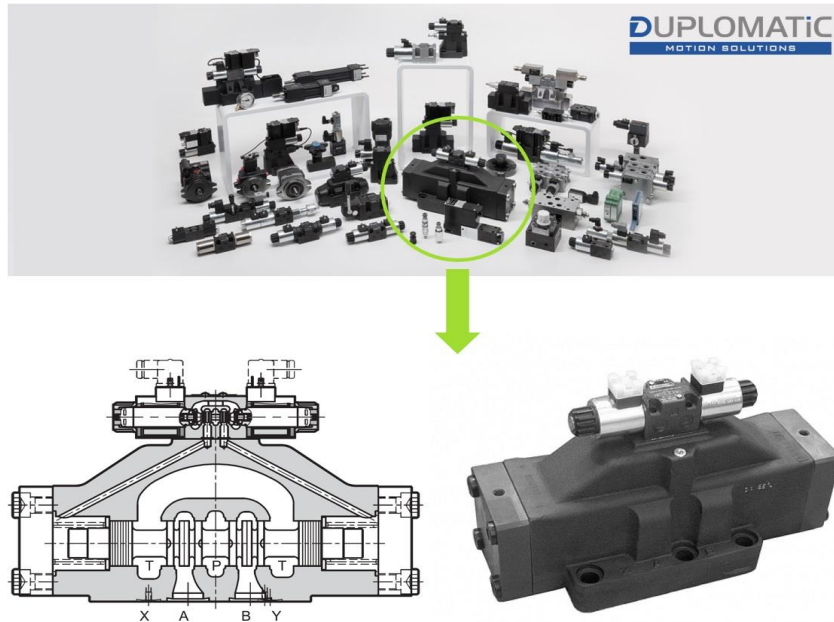


Figure 1 – Showing the Duplomatic product range and the specific Directional Spool Valve being study.

In more detail, the mechanical design was a four-way spool valve which is a pilot operated, solenoid or hydraulic control. In particular, the shape of the two ports of the valve shown in Figure 2 require optimization for an imposed pressure drop of 5 bar.

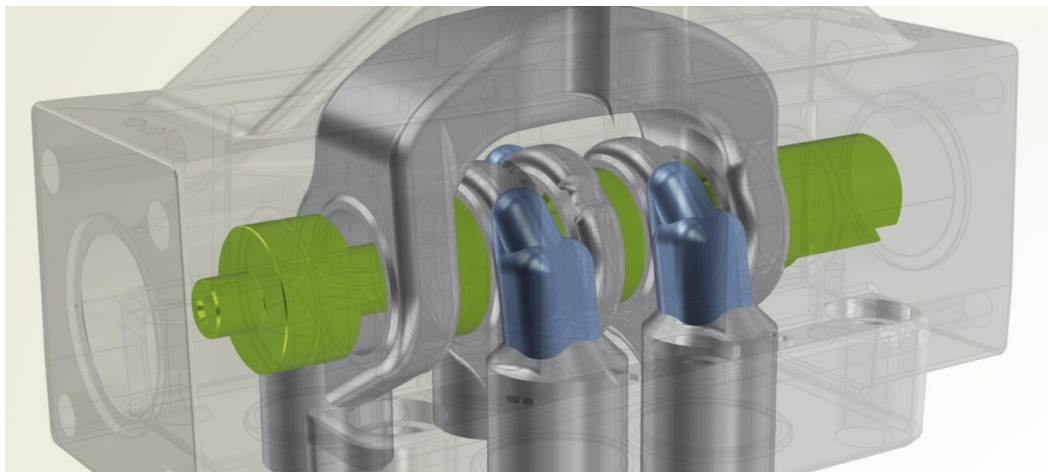


Figure 2 – Showing the specific configuration of flow path that is to be presented here.

Ten geometrical parameters were set-up to be varied, a total of 240 CFD simulations were automatically run involving Design of Experiments (DOE), to capture the most influential parameters, followed by the optimization of the best designs identified.

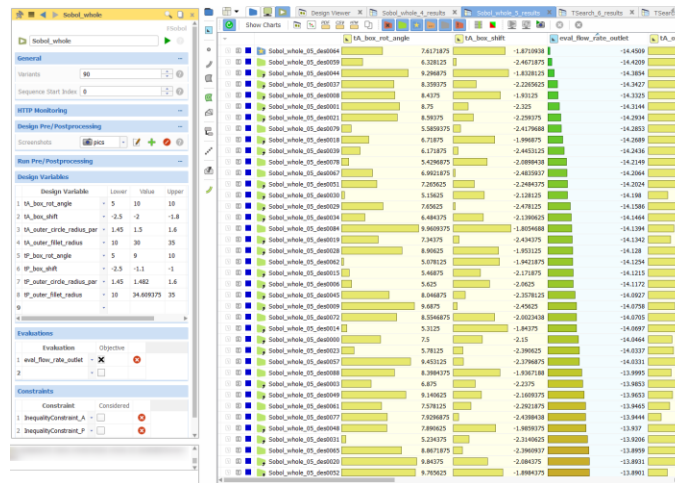


Figure 3 – Showing the number of variants, the design variables used in the upper and lower bound DoE, results, constraints and the ranked objective function.

### Automating the Shape Optimization Process

The overall optimization process was structured into three phases. In the first step, a preliminary DoE that included all 10 parameters for one of the two ports was carried out with 100 design variants. Based on those results, the 4 most influential design variables, i.e., the parameters with the strongest correlation to the objective function (box rotation, shift, outer radius and bottom fillet radius), were identified and selected for a second DoE of 90 design runs. The final phase was based on the best design from the previous step and a single objective optimization run using a further 50 designs.

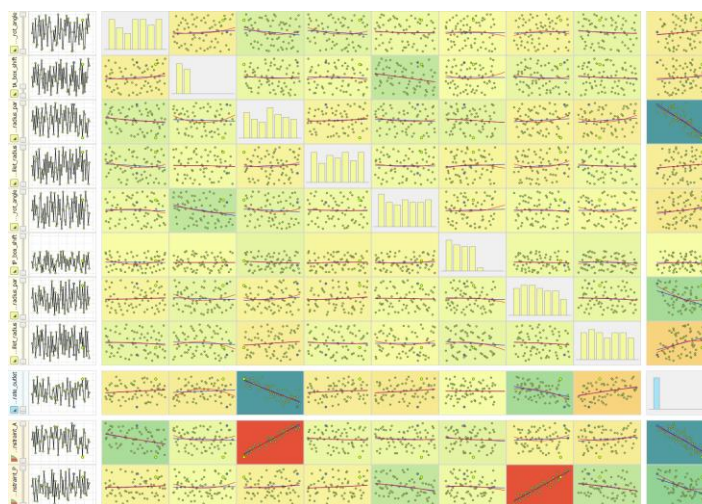


Figure 4 – Showing the total spectrum of Optimization results obtained using colour coded charts for easy comparison.

## UpFront CFD

In this example, Simerics-MP® was the CFD tool integrated into the optimization process using the CAESES® Software Connector for the analysis of the generated geometry variants. The geometry is saved in STL Extract Colours format, where each is defined for a part of the geometry and exported into a separate STL file. This allows for the CFD software to easily identify boundary patches, keeps the associativity to the related settings (e.g. mesh settings or boundary conditions) thereby allowing automated mesh regeneration. The simulation setup is carried out once, which will subsequently be exported for each variant.

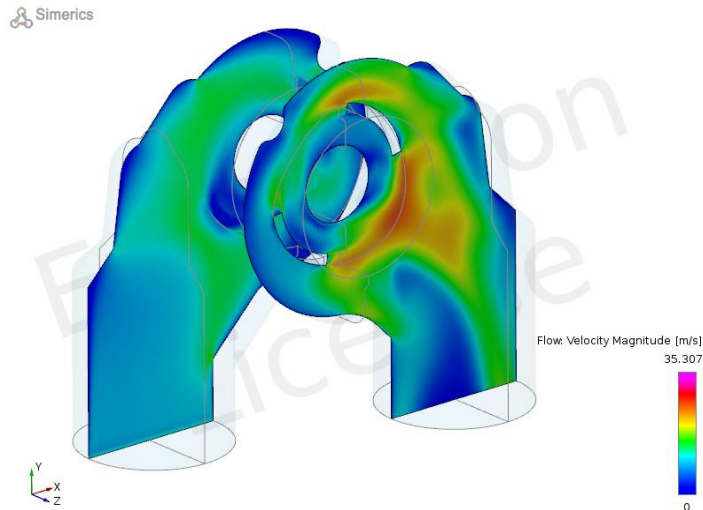


Figure 5 – Showing the velocity flow pattern on separate cutting planes through the one of the 240 automatically generated CFD runs.

## Conclusions

The study shows how Duplomatic MS used automated shape optimization technology coupled with UpFront CFD. This resulted in a product performance improvement of **8.65% on the mass flow rate** and was undertaken 10 times faster than using the more traditional iterative design and CFD simulation process.

## Acknowledgements

1. Friendship Systems AG, Benzstrasse 2 | D-14482 Potsdam | Germany
2. Duplomatic MS S.p.A, Via Mario Re Depaolini 24, 20015 Parabiago (MI) Italy

## References:

1. Mattia Brenner, Friendship Systems, Presentation at Simerics European User Meeting, February 4<sup>th</sup>- 5<sup>th</sup> 2020.
2. CAESES® is a highly specialized Design environment that addresses the aforementioned parametric variation challenge and is being used in industries like energy, maritime, and automotive: [8020engineering.com/caeses](http://8020engineering.com/caeses)

**Sean Horgan**, 80/20 Engineering Ltd, Aston Court, Kingsmead Business Park, High Wycombe, HP11 1JU. Tel: 07879 432669 [sean.horgan@8020engineering.com](mailto:sean.horgan@8020engineering.com)

# Uncertainty in simulation and test

*Jack Reijmers  
Nevesbu – The Netherlands*

## SUMMARY

Comparing the result of a physical test with numerical simulation usually shows a difference. When this difference is significant a closer look at the numerical results seems obvious. However, it is disputable to rank test results beyond doubt. Assessment of measuring also deserves attention.

With a specific experiment the difference between simulation and test was investigated. The test comprised a U-shaped plate under tension with strain gauges at several locations. For one location, with a clearly defined unidirectional stress state, the FE model was verified by mesh refinement and variation in element type. At a location with a biaxial stress state the strain result of a rosette was compared with FE analysis.

Comparison of the FE result with the measurement at a location with a unidirectional stress state showed a good match. This provided confidence in the numerical simulation. However, for a biaxial stress with a rosette a large bias was found. With a moderate shift in the location of strain assessment the difference with the FE result could be eliminated.

The study indicates that attention must be paid to the measurement. Verification of the FE model establishes a reliable result of the numerical simulation. On the other hand, strains delivered by a rosette are not given for one exact location. Especially in case of large strain gradient, a small shift in position of the rosette makes the difference between a satisfactory match and a disappointing comparison between simulation and test.

### **1: Measurement by strain gauges**

It must be realized that strain gauges are accurate up to a certain level. In fact, a change in resistance is measured, and this is converted to strain by the k-factor with a specified accuracy. Stresses follow with the Young's modulus,  $E$ , and the Poisson ratio,  $\nu$ , by Hooke's law. Figure 1 show a plate with 8 single strain gauges, 3 rosettes ( $0^\circ$ - $90^\circ$ ) and 3 rosettes ( $0^\circ$ - $45^\circ$ - $90^\circ$ ). Two forces,  $P$ , pull the legs of the U-shaped plate apart. This test was part of a course in experimental stress and vibration investigations (vakgroep technische mechanica, 1978). Strains are measured at zero load ( $P_0 = 0$ ) and  $P_{II} = 7159$  N, and the absolute

error in the (micro) strain is  $\pm 1$ . For strain gauge 5:  $\mu\epsilon_o = -11$  and  $\mu\epsilon_{II} = -593$ . The strain gauge measures a change in electrical resistance and the k-factor, which converts this value to strain, is about 2. This factor is applied in the test set-up but must be corrected for the specified k-factor. For strain gauge 5:  $2.105 \pm 5\%$ , and this leads to:

$$\epsilon_5 = \frac{2}{2.105 \pm 0.5\%} \cdot \{(539 \pm 1) - (-11 \pm 1)\} \rightarrow 518 < \epsilon_5 < 528$$

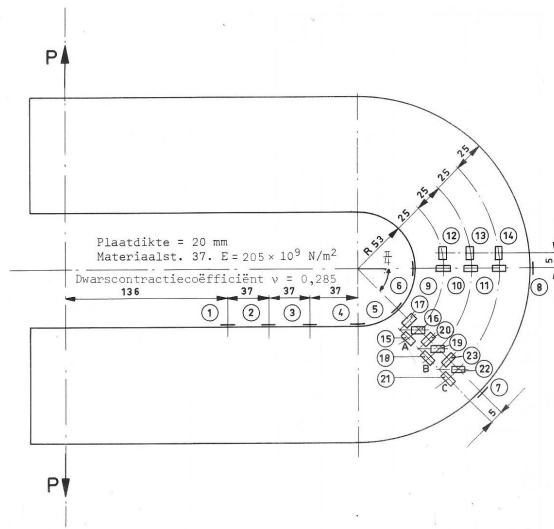


**Figure 1: Tested plate**

The application of rosettes implies that 3 strains must be converted to principal strains according to the formula:

$$\epsilon_{1,2} = \frac{(\epsilon_a + \epsilon_c) \pm \sqrt{2 \cdot \{(\epsilon_a - \epsilon_b)^2 + (\epsilon_b - \epsilon_c)^2\}}}{2}$$

The calculation of the accumulated error is rather complicated and carried out by considering the minimum and maximum value for each strain component. For location A in Figure 1 (number 15, 16 and 17) this results in  $\epsilon_1 = 153 \pm 8$ .

This error ( $\pm 5\%$ ) must be kept in mind when results of numerical simulation are compared with experimental outcome.

## 2: Numerical simulation

Figure 2 shows the FE model of the plate, presented in Figure 1. Around the transition of the rectangular to the curved plate the elements are square (aspect ratio 1).

Mesh refinement and application of element types are applied to assess convergence of the measured strain at location 5 and 7 (unidirectional stress state).

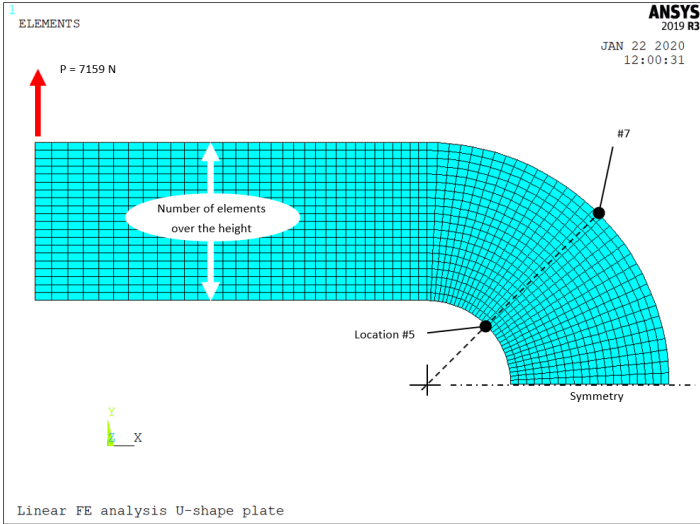


**Figure 2: FE model**

The FE code applied was ANSYS (Release 2019 R3), and the number of elements over the height varied from 10 to 20. The study covered 5 types of elements: 4-node shell181 with reduced and full integration, 8-node shell281, 4 node plane182 and 8 node plane183. Figure 3 shows convergence of the result, and the 4-noded shell181 with reduced integration behaves poorly.

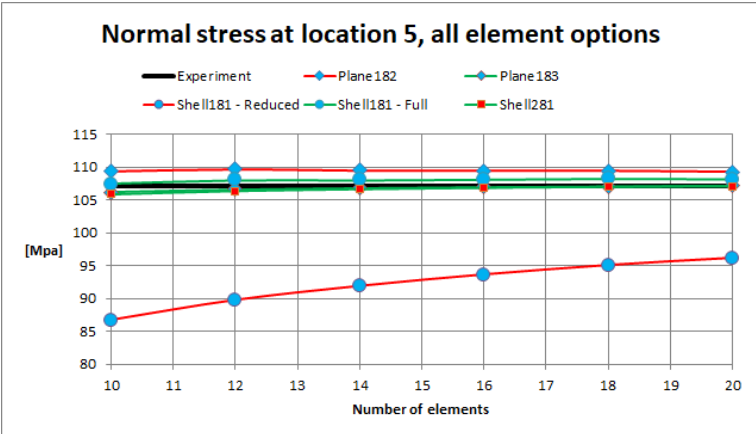


**Figure 3: Convergence investigation**

Further analysis is carried out with the 8-noded plane183. From Figure 3 follows that the influence of mesh refinement is small, however, a mesh with 20 elements over the height is maintained. The resulting element size provides a convenient base for the interpolation of strains.



Location A in Figure 1 contains a rosette and may be considered as a representation of strain at 25 mm from the edge under an angle of  $45^\circ$ . The strain gauge in tangential direction (number 17) gives a strain of  $139 \mu\epsilon$ . The FE analysis at this location shows:  $117 \mu\epsilon$ , and this is 16% lower. However, it must be realized that the three strain gauges of the rosette are not located at the same point. According to Figure 1 the distance between the strain gauges amounts to 5 mm. This implies that number 17 lies 20 mm from the edge and the FE analysis shows  $170 \mu\epsilon$  at this point in tangential direction (22% higher than measured). This shift in location shows clearly the necessity of comparing measurement and simulation at the correct point.

The effect is illustrated in Figure 4. The large gradient in tangential strain follows from (a) and a detail around location A is presented in (b). This figure also shows the accuracy of the measurement. The numerical result matches the measured strain when location between 22.5 and 23.5 mm is assessed.

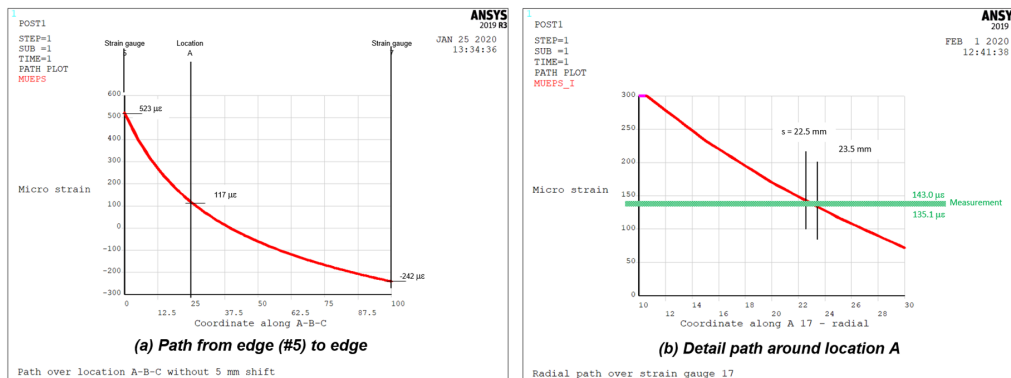


**Figure 4: Influence of location shift**

That the uncertainty in FE analysis causes a difference between simulation and measured value seems a logical conclusion. However, in this case a closer look at the location of measuring is imperative. Considering the uncertainty of the exact location of the rosette components gives a higher impact on the bias than shortcomings of FE analysis.

## REFERENCES

- [1] Vakgroep technische mechanica, 1978, A guide to the practicum experimental stress and vibration research (in Dutch), Delft University of Technology.

# **3D Electromagnetic Eddy-Current problems within the Finite Element Framework of computing platform FEniCS**

*Nunzio Palumbo, Sandeep Shrivastava, Neeraj Cherukunnath, James McDonagh, Suvro Mukherjee, Ed Green*

## **SUMMARY**

Aerospace industry is driving more electric solutions to support aviation sustainability.

As part of the journey towards electrification, industry needs large scale, fast and efficient coupled multi-physics simulations. High Performance Computing (HPC) along with iterative solution schemes offer means of achieving this.

Under the EPSRC funded ASiMoV project, Rolls Royce plc is working with a number of partners to develop a coupled electro-thermo-mechanical simulation capability for large scale engineering systems.

Electromagnetic phenomena are most commonly formulated and solved using the finite element method (FEM). Based on the operating frequency, electric machine problems can be categorized into high & low frequency applications where low frequency includes eddy current and magnetostatic problems.

Here, 3D electromagnetic eddy-current problems are investigated within the finite element framework of computing platform FEniCS. Simulation speed is addressed by the use of parallel iterative sparse solvers in a High Performance Computing environment.

The numerical procedure involves solving the time harmonic Maxwell's equations by means of the Coulomb gauged magnetic vector potential  $A$  and the electric scalar potential  $V$  (known as the A-V formulation). The numerical method as well as the implementation within FEniCS is described. The weak formulation derived in FEniCS for the integration of the Maxwell's equations is also presented.

After briefly presenting the numerical procedure, this paper will focus on the models that have been implemented using FEniCS open-source computing platform. A brief description of the models will be given as well as the main results obtained. For each test case, some results, especially current density and magnetic flux density predictions at different frequencies have been extracted and qualitatively compared to the associated reference model that is implemented using commercial off the shelf software (e.g. OPERA 3D - Simulia by Dassault Systemes®).

## 1: Computational Simulation Procedure

The finite element method (FEM) for solving partial differential equations is one of the most efficient simulation tools for electromagnetism analysis.

In this section the FEM formulation of electric machine problems is described using both magnetic vector and electric scalar potentials (A-V formulation).

Based on the operating frequency, electric machine problems can be categorized into eddy current problems and magneto static problems.

In this section, we derive the A-V formulation which is suitable for eddy current problems assuming that only linear material is involved. For the sake of brevity and simplicity the A-V formulation is derived in the frequency domain only herein.

Typical computational domain for electromagnetic problems consists of conducting regions including the excited coils ( $\Omega_c$ ) and the non-conducting region such as air ( $\Omega_0$ ). The material property inside the computational domain can be described by permeability  $\mu$  and conductivity  $\sigma$  (equal to zero in the non-conducting region  $\Omega_0$ ).

The starting point is the differential form of the Maxwell's equations and constitutive relations. A magnetic vector potential  $\mathbf{A}$  is introduced which satisfies

$$\mathbf{B} = \nabla \times \mathbf{A}$$

where  $\mathbf{B}$  is the magnetic flux density.

The Faraday law in the frequency domain becomes

$$\nabla \times \mathbf{E} = -\frac{\partial \mathbf{B}}{\partial t} - \Delta V = -j\omega \mathbf{A} - \Delta V$$

where  $\mathbf{E}$  is the electric field intensity,  $V$  is the electric scalar potential and  $\omega$  the angular frequency,  $2\pi f$ , with  $f$  the frequency in Hz.

Using the constitutive equation  $\mathbf{J} = \sigma \mathbf{E}$ , with  $\mathbf{J}$  electric current density, and substituting in the Ampere's law (the displacement current term is negligible for low frequency problems) we obtain the first governing equation for eddy current problems (second order equation)

$$\nabla \times \left( \frac{1}{\mu} \nabla \times \mathbf{A} \right) = \mathbf{J}_s - j\omega \sigma \mathbf{A} - \sigma \nabla V \quad (1)$$

with  $\mathbf{J}_s$  electric current density source (applied excitation).

Conservation of charge also needs to be satisfied in eddy current problems. We obtain the second governing equation for eddy current problems in the frequency domain (first order equation)

$$\nabla \cdot (\sigma \mathbf{E}) = 0 \rightarrow \nabla \cdot (-j\omega\sigma \mathbf{A} - \sigma \nabla V) = 0 \quad (2)$$

Equations (1-2) are the governing equations for eddy current problems.

Although the magnetic vector potential  $\mathbf{A}$  is not unique,  $\mathbf{A}$  can be uniquely defined when a gauge condition is enforced (Coulomb gauge)

$$\nabla \cdot \mathbf{A} = 0$$

On the outer boundary  $\Gamma_\infty$  Dirichlet type boundary condition is imposed. Tangential magnetic flux density (zero normal component,  $\mathbf{n}_\infty \cdot \mathbf{B} = 0$ ) is imposed by using the magnetic vector potential  $\mathbf{A}$

$$\mathbf{n}_\infty \times \mathbf{A} = 0 \quad \text{on } \Gamma_\infty$$

On the interface boundary  $\Gamma_c$ , the boundary conditions for the electric scalar potential (zero normal component of the induced currents) are satisfied:

$$\mathbf{n}_c \cdot (\sigma \mathbf{E}) = 0 \quad \text{on } \Gamma_c$$

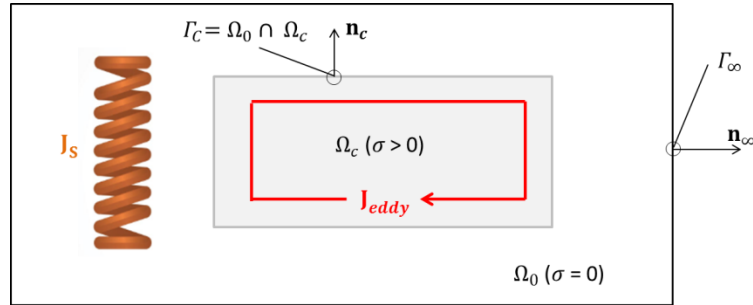


**Figure 1: Typical computational electromagnetic domains. An alternating source current in the coil induces eddy-currents in the conductor.**

The A-V formulation coupled with a motion voltage term has been used for rotating electrical machine problems.

The formulations presented herein were applied to compute magnetic flux density and eddy currents. For electrical machines power dissipation of rotor, torque and induced voltage were also computed.

## 2: Eddy-Current problems within FEniCS

A series of eddy current problems have been implemented using FEniCS, a multi-purpose open-source computing platform, developed by the University of Cambridge, for solving partial differential equations.

Problems are 3-dimensional large scale finite elements consisting of 1+ millions linear tetrahedral elements. The purpose of the problems is to test the formulation (mathematical model) used to build the model, boundary conditions, software correctness, accuracy, scalability, and solver performance.

The linear problems have been solved in both the frequency and time domain.

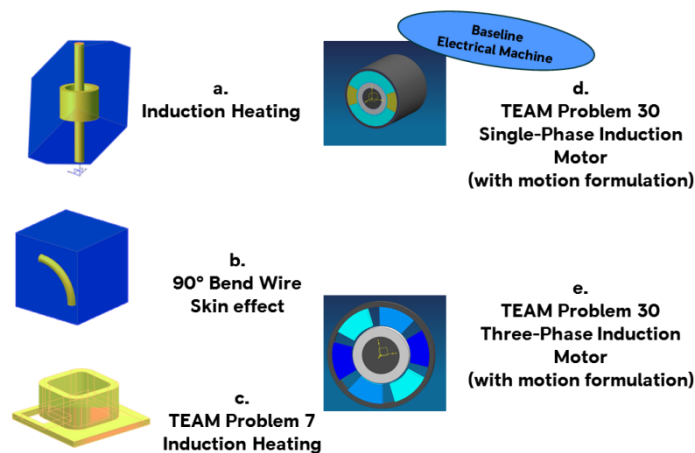


**Figure 2:** Eddy current problems implemented in FEniCs.

The induction heating problems (a. & c.), including Problem No. 7 of TEAM Workshop, consist of a magnetic field produced by an induction coil excited with a time varying current density. That generates electromotive forces and eddy currents in the conducting regions (e.g. steel rod, aluminium plate). The skin effect problem (b.) describes the skin effect caused by opposing induced eddy currents in a wire. Higher is the frequency, smaller the skin depth becomes. Problem No. 30 of TEAM Workshop (d. & e.) consists of a single phase and three phase induction motors in which eddy currents are induced by the time harmonic current in the stator windings and the rotation of the rotor.

FEniCS implementation consisted of: a. Initialise Sub-Systems; b. Read mesh; c. Define equations; d. Apply boundary conditions; e. Solve; f. Write solution. Results were subsequently post-processed using Paraview, an open-source, multi-platform data analysis and visualization application.

### 3: Results

The numerical computations were performed using a development version of FEniCS (version X). The programmes have been run on a HPC at the Centre for Modelling & Simulation (CFMS) in Bristol and ARCHER in Edinburgh.

FEniCS uses PETSc for the numerical solution of the partial differential equations on high-performance computers. All models were solved via direct solver as a preconditioner based on LU factorisation. The use of an iterative method for scalability purposes has not been thoroughly explored yet.

Results have been verified using Opera3D v2018 by Dassault Systemes<sup>®</sup> and, in some cases, compared with benchmark problems (e.g. TEAM Workshop). Figure 3 presents a comparison between results obtained using FEniCS and Opera software for the induction heating problem (Problem a.) in the frequency domain. Solutions seem to be comparable from a qualitative and quantitative perspective for all the models implemented and for all the frequency range investigated.

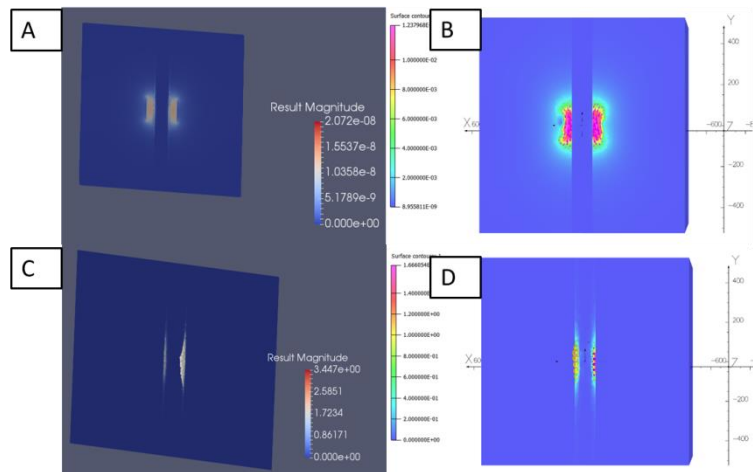


**Figure 3: Induction Heating (Problem a.) in frequency domain: Comparison FEniCS vs Opera. Images A & B: magnetic flux density at 1kHz; Images C & D: eddy currents at 1kHz.**

Since FEniCS is being used as a platform for massively scalable models within the ASiMoV project, a preliminary performance study has been conducted to better understand the differences between the C++ and Python programming languages interfaces in terms of wall time performance. Using two of the electromagnetic problems (Problem a. & b.) the timing of key sections of the models has been investigated. Not only this helps determine the better performing interface, it also identifies key areas where time is being spent within the code. Figure 4 shows the assessment, the assembling matrix section and the solution writing are the most time consuming sections of the code

(besides solving time), especially in the Python interface. This behaviour is more evident for low number of cores.

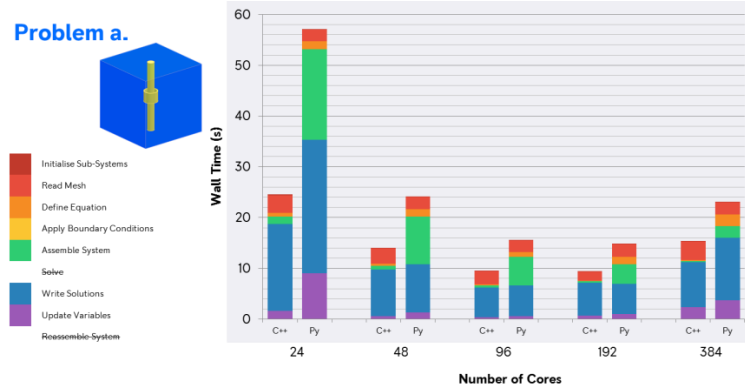


**Figure 4: Induction Heating (Problem a.) in time domain: Comparison FEniCS C++ vs Python interfaces: Wall time.**

A comparison between the computed rotor losses of the TEAM Problem No. 30a by Marcsa et al. and the implementation in FEniCS has been performed. Figure 5 shows computed losses as a function of rotational speed (at fixed frequency). The rotor losses curves seem comparable in trend and absolute values. Meshes between the two models were not identical.

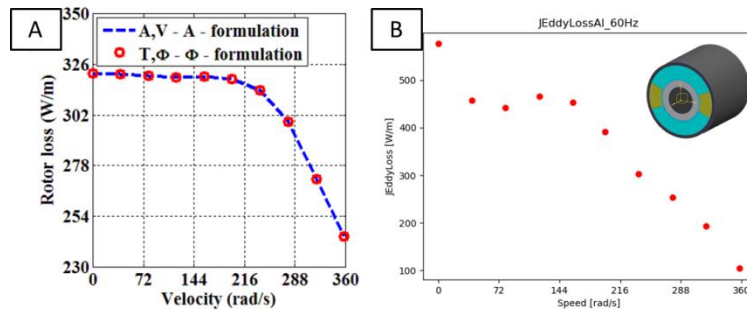


**Figure 5: Team Problem 30 Single phase induction motor (Problem d.) in frequency domain: Comparison rotor losses: A. Marcsa et al; B. FEniCS.**

#### 4: Conclusion

Implementation of linear eddy currents problems within finite element framework of computing platform FEniCS has been successfully demonstrated. Simulation speed is addressed by the use PETCs solver in a high performance computing environment. The aim of further research is to explore the use of iterative solver to massively improve scalability and implement a computational solution capable to simulate the multiphysics nature of eddy current problems.

The permission of Rolls-Royce to publish this paper is gratefully acknowledged. This research forms part of the Rolls-Royce led EPSRC Prosperity Partnership (Grant Ref: EP/S005072/1) entitled “Strategic Partnership in Computational Science for Advanced Simulation and Modelling of Virtual Systems – ASiMoV”. Access to the UK national supercomputer service (ARCHER) is gratefully acknowledged.

We acknowledge Prof. Garth N. Wells at University of Cambridge and his Team for their contribution and support.



## REFERENCES

- [1] Yao, W., 2010. Finite element analysis of 3D electric machine problems.
- [2] Beckstein, P., Galindo, V. and Vukčević, V., 2017. Efficient solution of 3D electromagnetic eddy-current problems within the finite volume framework of OpenFOAM. *Journal of computational physics*, 344, pp.623-646.
- [3] Marcsa, D. and Kuczmann, M., 2008. Induction motors simulation by finite element method and different potential formulations with motion voltage term. Szechenyi Istvan University.
- [4] Marcsa, D. and Kuczmann, M., 2008, November. Finite element analysis of single-phase induction motors. In *COMSOL Conference Budapest*.

# **Supporting the design of composite components using multiphysics simulations**

*Dr Olivia Stodieck  
DaptaBlade Ltd, Unit Dx St Philips Central, Albert Road, Bristol, United  
Kingdom, BS2 0XJ, Email: olivia.stodieck@daptablade.com*

## **SUMMARY**

This paper focuses on the design of composite components using multi-physics and coupled disciplinary simulations within the context of the 20 months ATI funded MASCoTS project. The concepts of fibre steering and aeroelastic tailoring for wing and blade structures will be introduced. The aeroelastic design workflow, which requires the coupling of the structures and aero loads models, will be described. Typical design objectives and constraints, including manufacturing constraints will be discussed. It will be shown that the multidisciplinary analysis workflow can be automated using a formal design optimisation approach, which allows for faster design iterations and improved product performance.

## **1: Introduction**

Aircraft wings are light-weight structures that tend to deflect and bend in flight. By designing wings with flexibility in mind right from the start, the wing shape can be tailored for different flight conditions. The weight and drag can be reduced and the external loads can be controlled, leading to an overall improved aircraft performance. The benefits of composite wing aeroelastic tailoring have been widely researched since the 1980s [1] and it has been demonstrated that tailoring can increase an aircraft's range, payload or endurance, increase flutter or divergence airspeeds, increase stability in gusty winds and/or improve manoeuvrability [2,3]. Aeroelastic tailoring is currently experiencing something of a resurgence, both due to an increasing interest in high-aspect-ratio aircraft configurations (Fig.1) and the availability of novel materials and construction methods.

One novel material technology which promises such improvements is Continuous Tow Shearing (CTS) which has been developed by iCOMAT in Bristol. A consortium of Daptablade, iCOMAT, MSC Software and TWI has been formed to increase the technology readiness level of CTS and to make it industrially usable. This will be achieved within the 20 months ATI funded

MASCoTS project. The project will focus on the development of the design, analysis and manufacturing technologies for CTS components. Physical testing will be conducted to demonstrate the hardware and software capabilities.



**Figure 1 - High-aspect-ratio wing designs: Boeing SUGAR volt concept plane (Left), NASA Helios (right)**

## 2: Composite fibre steering technologies

Composite structures are designed by stacking straight-fibre layers in different orientations. As structures have complex load paths, this approach often leads to oversized components. It is more efficient to design with layers of curved fibres, changing their orientation to follow the load path.

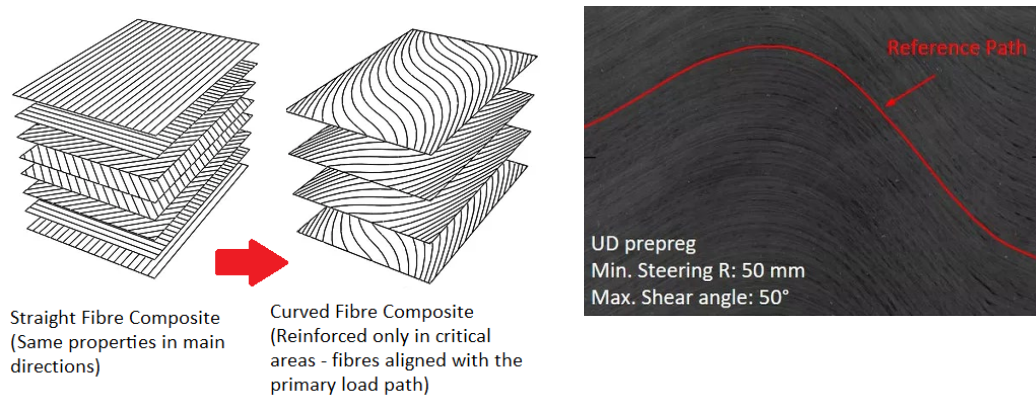


**Figure 2 – Straight vs. curved fibre composites (left), Continuous tow shearing (right)**

Current solutions for fibre steering are automatic tape laying (ATL) and tailored fibre placement (TFP). These both have limitations. ATL cannot steer with a tight radius and steering causes fibre wrinkling and gaps, compromising the structural performance. TFP is a slow process so cannot deposit material fast enough for anything of a significant size. Also, the stitching used for TFP compromises the structural performance. iCOMAT have created a new tape

laying process, continuous tow shearing (CTS), which promises to rival the speed of ATL but without the wrinkling and gaps. It also can lay material around tight radii (Figure 2).

### 3: Aeroelastic design of composites wings

Curved fibre composites can also be designed to improve the passive aeroelastic behaviour of wing structures. For example, peak gust loads and structural weight can be reduced by continuously changing the main fibre direction on the wing skins (Figure 3). By rotating the main fibre direction, a beneficial wash-out bend-twist coupling behaviour is introduced on the outer wing, without reducing the laminate strength at the wing root. The wing twists as it bends (Figure 4), which effectively reduces the peak lift forces generated.

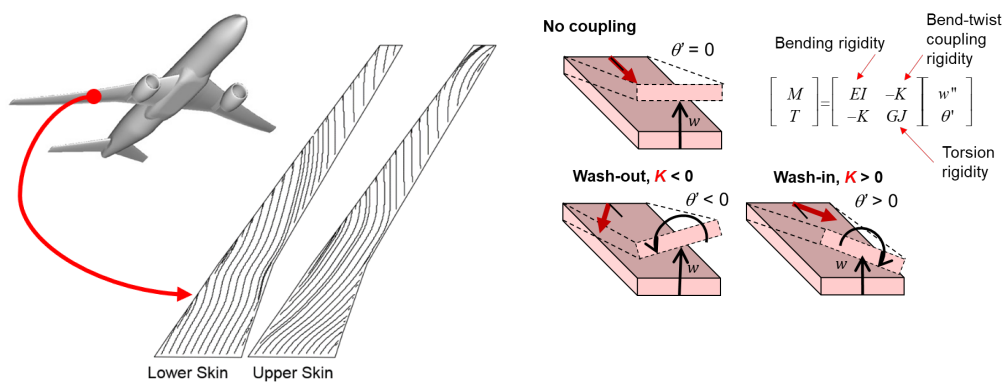


Figure 3 - Optimised curved fibre directions on the NASA CRM wing skins [3]

Figure 4 - Passive stiffness design (red arrow = main fibre direction)

### 4: Automation of the multidisciplinary workflow

The use of multidisciplinary design analysis and optimization (MDAO) tools for the preliminary design of aircraft structures can lead to significant aircraft performance improvements. These tools allow unconventional configurations and materials to be explored in a systematic way, while satisfying a wide range of constraints. The use of MDAO for the design of wing structures subject to aerodynamic, stress, and aeroelastic constraints can be further improved by chaining simulations of various fidelities (Figure 5). The structural optimization variables are defined with respect to a detailed 3D finite element model (FEM), which is also used for stress analysis purposes, but the wing is modelled as a beam for aeroelastic analysis purposes. A key requirement for such an approach is an efficient, yet sufficiently accurate, means of reducing a FEM to a beam model in an automated fashion. Such a method was developed in previous work [4], where it was shown that this approach would be suitable for integration with a gradient-based optimisation algorithm, which is essential

for any design problem with hundreds of variables or more. This multi-fidelity MDAO approach will be further explored within the MASCoTS project.

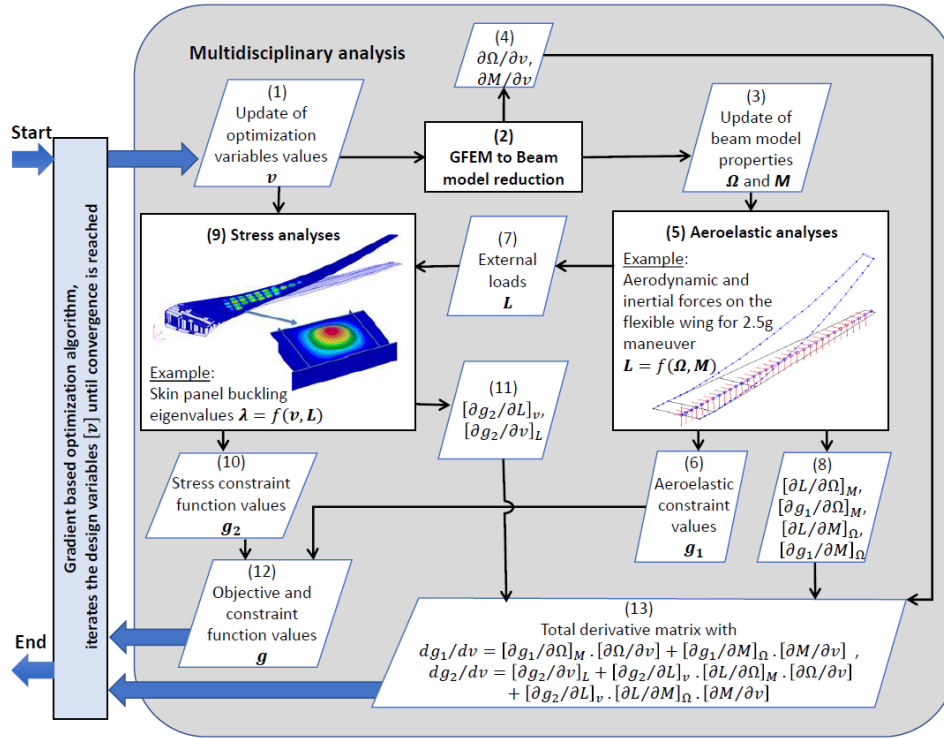


Figure 5 - Aeroelastic design optimization with detailed stress constraints [4]

## REFERENCES

- [1] M. H. Shirk, T. J. Hertz and T. A. Weisshaar, "Aeroelastic tailoring - Theory, practice, and promise", J. Aircraft, 1986 [23/1], pp. 6-18, doi:10.2514/3.45260
- [2] F. E. Eastep, V. A. Tischler and V. B. Venkayya and N. S. Khot, "Aeroelastic Tailoring of Composite Structures", J. Aircraft, 1999 [36/6], pp. 1041-1047, doi:10.2514/2.2546
- [3] O. Stodieck, J.E. Cooper, P. Weaver, P. Kealy, "Aeroelastic Tailoring of a Representative Wing-Box Using Tow-Steered Composites", AIAA Journal, 2017 [55], pp. 1425-1439, doi:10.2514/1.J055364
- [4] O. Stodieck, J.E. Cooper, S.A. Neild, M. H. Lowenberg, and L. Iorga, "Slender-Wing Beam Reduction Method for Gradient-Based Aeroelastic Design Optimization", AIAA Journal, 2018 [56], pp. 4529-4545, doi:10.2514/1.J056952

# **Rapid 3D Inspection of AM Components using CT: From Defect Detection to Thermal Performance Simulation**

*Celia A. M. Butler<sup>1,2</sup>, David Harman<sup>1</sup>, Bethan Nye<sup>3</sup>, Borja Lazaro Toralles<sup>3</sup>, Nathanael Turner<sup>3</sup>, and Nick Brierley<sup>3</sup>*

*<sup>1</sup>Synopsys NE Ltd., Exeter, United Kingdom*

*<sup>2</sup>University of Exeter, Exeter, United Kingdom*

*<sup>3</sup>Manufacturing Technology Centre, Coventry, United Kingdom*

## **SUMMARY**

Metal Additive Manufacturing (AM) can be used to produce topologically complex designs, which are difficult or impossible to engineer using traditional manufacturing techniques. Non-destructive inspection and testing of such structures can be challenging due to internal or inaccessible features. Inability to find and correct for defects in built parts can lead to increased performance testing, potentially more failures and therefore more scrappage of parts, wasting precious time and resources.

Here a “hot box” heat exchanger is presented as an industrial example of how X-ray Computed Tomography (CT) can be used as part of a non-destructive testing process to inspect complex structures.

From the CT scan, an image-based model was built to identify and analyse defects and deviations from the original design. At this stage, the part could be deemed fit for use if any deviations fall within allowed tolerances or inspected further using image-based simulation. Inspection at this stage also means changes can be made to the manufacturing process for future manufacturing runs (such as a design change for trapped powder extraction).

Image-based simulation allows virtual performance testing of the “real” part (as opposed to a CAD idealisation). This includes any defects, pores, warping, etc. which could have occurred during the manufacturing process.

In the “hot box” heat exchanger example, defects in the structure were identified. This was mainly in the form of trapped powder in narrow channels, and some deviation to the lattice structure. An image-based simulation of the “as-built” structure was undertaken to show the impact of these deviations

from the “as-designed” structure. This simulation focuses on the thermal performance of key areas of the “hot box”.

The ability to perform dimensional, integrity and surface inspection in a single workflow proved to be highly beneficial for the current production process of the “hot box”. It has the potential to reduce inspection time and remove the need for additional inspection equipment, therefore reducing costs, cycle times, and potentially increasing workable floorspace.

## 1: The “hot box”

Manufacturers repeatedly ask the following questions: “What are the differences between my design and the part that is actually manufactured via AM, and more importantly, how will these differences affect performance in the real world?” This industrial use case shows how to use CT and image-based simulation to answer these questions.

The “hot box” (shown in Figure 1) is a test jig designed to ascertain performance of a particular structure before a bespoke heat exchanger is designed. It has a lattice structure through which air passes, and cross-corrugated channels for liquid coolant, making this a complex design, impossible to traditionally manufacture and subsequently inspect without cutting the part open.

It was manufactured using AM from AlSi10Mg by HiETA Technologies Ltd., and was CT scanned at the Manufacturing Technology Centre (for details see: Turner et. al. 2019) to visualise and quantify defects, and the output reconstructed to be used to build an image-based model for simulated tests.

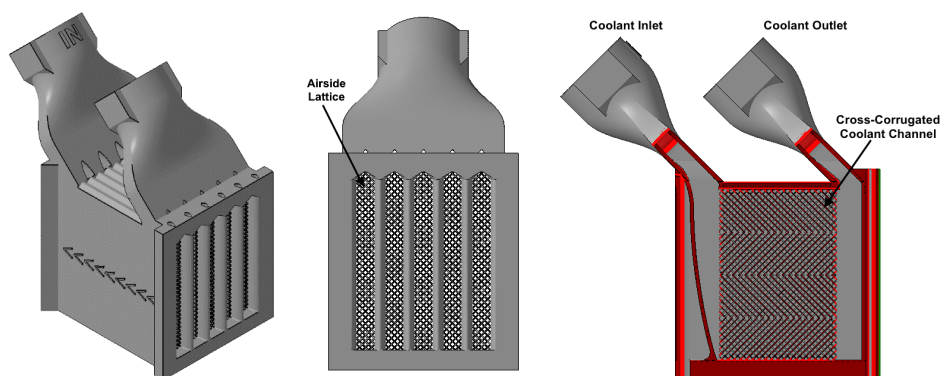


Figure 1: “Hot box” heat exchanger, image courtesy of HiETA Technologies

## 2: Visualising defects

Images obtained from the CT scan were reconstructed into a 3D image volume and used to inspect the topology of the structure. The reconstructed image data



was imported into Simpleware™ ScanIP (Synopsys, Inc. Mountain View, CA) for image processing and mesh generation. Accurate surfaces were determined using automated segmentation tools, including the local surface correction filter to counter beam hardening effects.

The Simpleware Surface Deviation tool compared the “as-designed” CAD surface to the “as-built” AM surface, and identified 3 areas where they differed. These regions are shown in Figure 2 below - trapped powder (dark blue, both images) and deviation from the designed lattice structure (right image, dark blue and red)

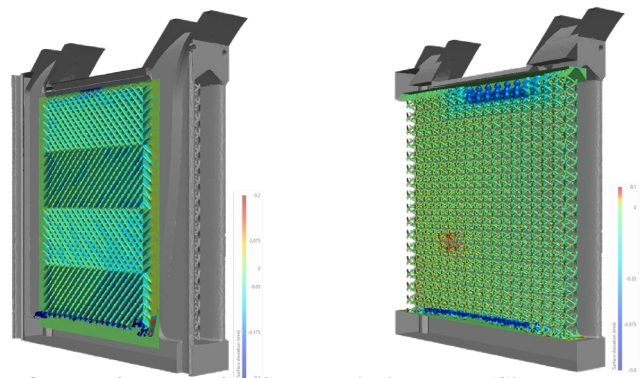


**Figure 2: Output from the Surface Deviation Tool (Simpleware ScanIP) between the “as-designed” and “as-built” image-based model.**

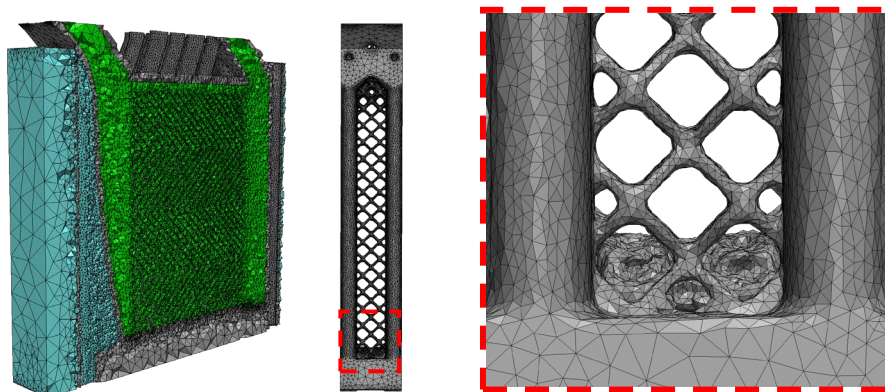


**Figure 3: Multipart CFD mesh (generated using Simpleware ScanIP)**

### **3: Meshing for simulation**

In order to understand the performance of the AM part including its defects, a full volumetric mesh suitable for CFD simulation was generated (“image-based model”) using the Simpleware FE Module. This image-based mesh comprised three parts: Metal, Fluid and Air, complete with assigned boundaries for inlets and outlets for fluid flow regions.



#### 4: Thermal simulation comparison

Simulation and comparison of thermal behaviour was conducted in COMSOL Multiphysics®, with coupled heat transfer and laminar flow. The temperature distribution in coolant flow through the channels is shown in Figure 4.

Deviation from “as-built” geometry is most apparent towards the base of the heat exchanger, and not only is the overall cooling from inlet to outlet greater in the “as-built” geometry, but is visibly less uniform in the vertical axis. This particular scenario shows that the “as-built” part performs worse than the “as-designed” part due to geometrical deviations.

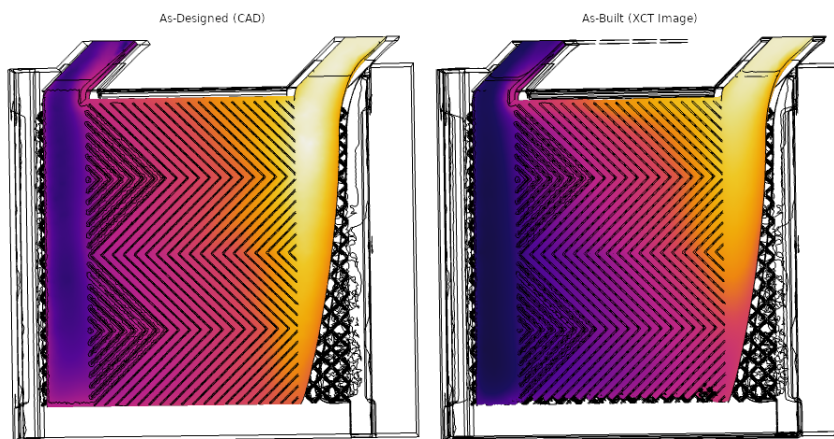


**Figure 4: Thermal Simulation showing difference between “as-designed” CAD based simulation and “as-built” image based simulation.**

#### 5: Conclusion

This industrial use case shows the importance of X-ray CT and image-based modelling for non-destructive inspection and testing. This workflow allows users to close the design loop and truly understand how any unexpected defects and inconsistencies in the manufactured part can affect real world performance, allowing better allocation of time and physical test resources.

#### REFERENCES

- [1] Turner, N., Brierley, N. and Townsend, A., 2019. 3-in-1 X-ray Computed Tomography. In: 9th Conference on Industrial Computed Tomography (iCT), 13-15 February 2019, Padova, Italy. [Online] NDT net [Accessed 14 April 2019]. Available from: <https://www.ndt.net/search/docs.php3?showForm=off&id=23702>

# **Structural simulation of components with defects** **– a workflow from Computed Tomography to** **Finite Element Simulation**

*Beate Lauterbach, Johannes Fieres, Karl-Michael Nigge  
Volume Graphics GmbH, Heidelberg, Germany*

## **SUMMARY**

Deviations between the designed and the manufactured part can be identified by means of non-destructive inspection methods, e.g. computed tomography (CT). Beside major geometrical differences like shrinkage and distortion, surface and internal defects become visible. As in general defects are sources of stress concentration, it is important to evaluate their impact on the structural performance of a component. Thus, including microdefects into a structural mechanics simulation would be desirable.

Building a Finite Element Model that includes a huge number of microstructural defects will create an enormous effort in FE mesh generation. To resolve stress concentrations in the vicinity of each defect, fine discretization is necessary. This will result in very large simulation models that can hardly be handled. The simulation effort can be reduced significantly including only the critical defects that will affect the structural performance in the FEM simulation.

By using a specific finite element variant, a so called immersed-boundary solver, an accurate pre-simulation including all detected pores can be done easily. These immersed-boundary methods do not require a geometry conforming mesh but operate directly on the image data, which is a big advantage for simulation of components with very complex geometrical features. This approach is implemented in the Structural Mechanics Simulation module of VGSTUDIO MAX by Volume Graphics. It simulates local stress distributions for linear elastic material properties directly on computed tomography (CT) scans which accurately represent complex material structures and internal discontinuities. From the stress fields calculated by the immersed boundary finite element simulation, the microstructural defects can be sorted with respect to their severity and thus critical pores can be identified. This reduction of geometrical complexity makes a classical FEM simulation feasible which allows the use of the wide range of functionalities that are offered by a fully capable finite element software (e.g. non-linear material models). The volume meshing module in VGSTUDIO MAX enables efficient

creation of a tetrahedral mesh on the CT scan and therefore bridges the gap between image data and classical FEM simulation.

A workflow from CT scanning, analyzing most critical defects and efficient meshing to nonlinear structural simulation with ANSYS maintaining the relevant features of the scanned object will be presented. It enables to assess the mechanical performance of the manufactured part.

### 1: Motivation

The actual stress field around a pore is affected by many parameters, e.g. size, shape, and location of the defect as well as the loading state of the component. A small pore situated in a highly loaded area can lead to higher stress concentration than a large pore in a barely loaded area. To assess the severity of a certain defect, knowledge of the stress concentration within the real manufactured part, including all defects, allows for the distinction between possibly dangerous and rather harmless defects. While the former should be considered for the assessment of the component performance, the latter can possibly be neglected or only covered in an averaged manner.

### 2: Defect Detection

By computed tomography (CT) external as well as internal surfaces can be identified. This includes surface imperfections and undesired defects. By taking a sequence of X-ray exposures of a rotating component, a 3D image of the component can be reconstructed. Based on the gray values of the voxels, the CT image can be segmented, and surfaces can be identified. From this, the component's porosity can be calculated (Figure 1). This way, the 3D representation of the physical component can serve as a basis for structural mechanics simulations.

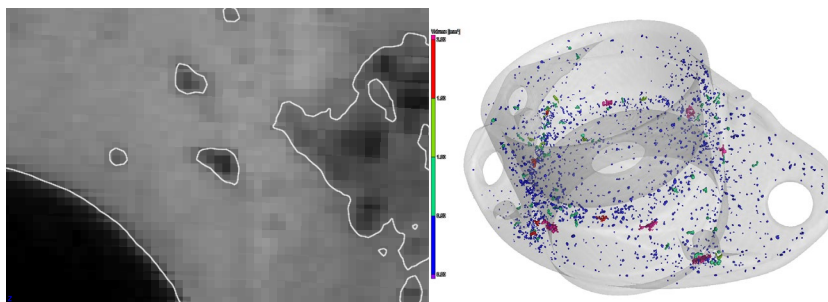
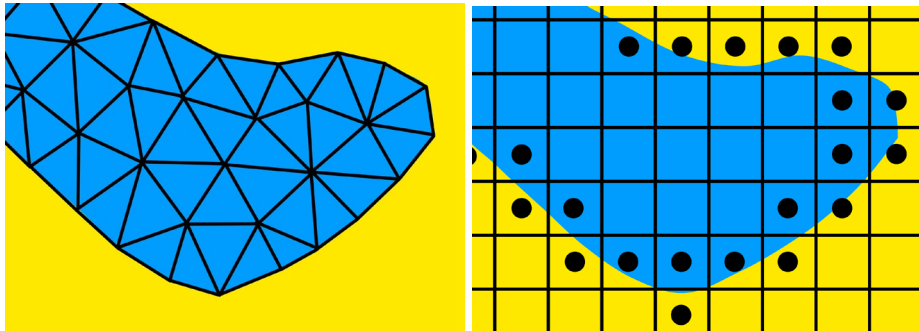


Figure 1: Surface determination (left) and porosity detected from CT data (right)

### 3: Micromechanical Simulation

Classical finite element methods may not always be well suited for micromechanical simulations of components with defects, because they require

the generation of geometry-conforming meshes that must be fine enough to capture all relevant geometric details, but coarse enough to keep the computational effort at a practical level. To avoid this problem, immersed-boundary finite element methods have recently been used to enable mechanical simulation (see, e.g. [1]). Such methods do not require the generation of a boundary-conforming mesh and are suited for the simulation of arbitrarily complex domains. Figure 2 shows the differences between the classical finite element method and the immersed boundary finite element method.



**Figure 2:** Classical FEM mesh (left) and Immersed Boundary FEM mesh (right)

Figure 3 shows the results of a linear-elastic simulation with the Structural Mechanics Simulation module (SMS) of VGSTUDIO MAX which is based on immersed-boundary FEM on an aluminum cast component including several thousand defects. The left image shows the simulated load case. The red areas indicate the applied fixation of the simulated sample, whereas the green area shows the area of applied load. First, a simulation on the CAD data set has been performed and the von Mises stress values have been evaluated (middle image). In the right image, the results based on the CT scan, including all detected defects, are shown. The presence of defects leads to a local increase in the stress that can be quantified by the simulation.

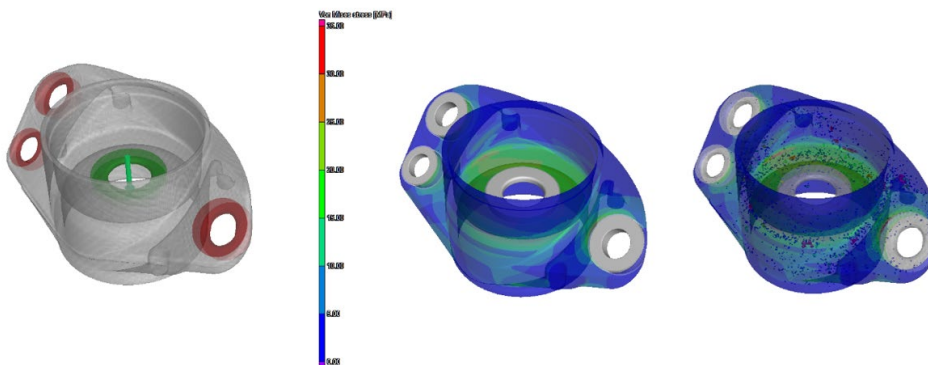


**Figure 3:** Linear-elastic simulation: simulated load case (left), results based on CAD data (middle), and results based on CT data, including internal defects (right)

#### 4: Nonlinear Finite Element Simulation

A classical finite element simulation approach, which is necessary for example to work with nonlinear models, can be enhanced by making use of the detailed porosity analyses. In general, it would be possible to build a classical finite element model that includes all detected defects by generating a mesh that follows all pore boundaries. Clearly, this would lead to many finite elements, and the computational effort will increase significantly. Due to this, the created model might not be usable.

By filtering out only those defects that cause a relevant stress concentration for the finite element model build, the model size can be greatly reduced. This can be done with little effort by a pre-simulation with the linear immersed-boundary solver SMS. The computed stress field allows for rating the severity of the defects within the component.

Meshing of the scanned component according to the external surfaces and the reduced number of internal surfaces can be done efficiently in VGSTUDIO MAX by using the Volume Meshing module. This module enables the creation of a tetrahedral mesh for a user-specified element size including mesh refinement around the pores based on CT data (Figure 4).

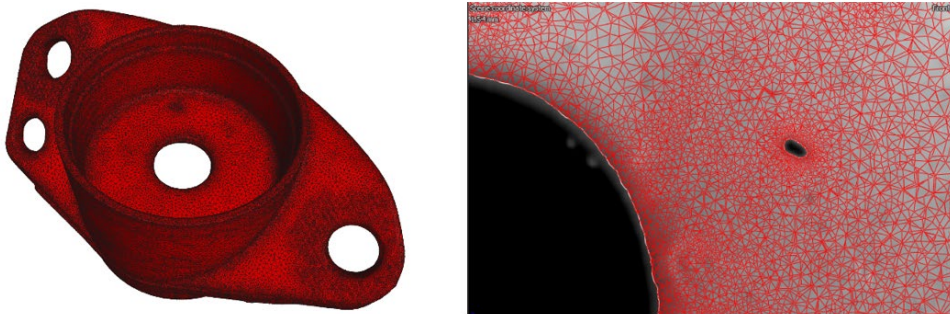


**Figure 4:** Tetrahedral mesh generated from CT data including critical pores

The generated mesh can further be enhanced by including the effect of the non-meshed pores in an averaged way by mapping a scalar porosity to a FE Mesh (Figure 5). By following this workflow, relevant information from CT can be used in a classical finite element simulation while maintaining computational and model build efficiency.

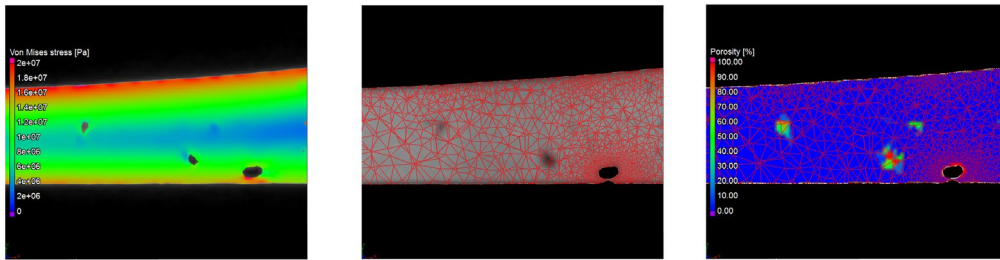


**Figure 5:** Von Mises stress from pre-simulation with SMS (left), mesh with reduced porosity (middle) and mapping of porosity values on FE mesh

## 5: Summary and Conclusion

The proposed workflow is shown in Figure 6. It enables the user to take advantage of the information on microstructural defects in a component detected by CT scanning and the full functionality, including advanced material modelling, that is provided by a classical finite element software. Thus, a significantly enhanced structural simulation can be performed, which simulates the manufactured component more realistically by considering microstructural defects.

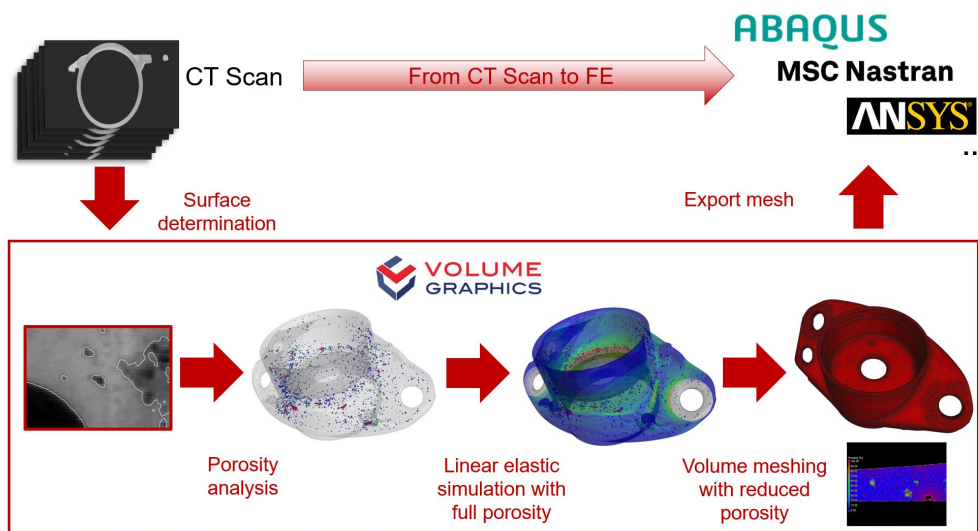


**Figure 6:** Workflow from CT scan to classical FE Simulation

## REFERENCES

- [1] Schillinger, D., Ruess, M. (2015): “The Finite Cell Method: A Review in the Context of Higher-Order Structural Analysis of CAD and Image-Based Geometric Models”, *Arch. Comp. Meth. Engin.*, 22(3), pp. 391–455
- [2] Fieres, J., Schumann, P., Reinhart, C.: “Predicting failure in additively manufactured parts using X-ray computed tomography and simulation”, *Procedia Engineering 2013 (2018)* 69-78
- [3] Fieres, J., Esposito, F. (2018): Accurate and efficient simulation of real pore geometries directly on CT images. White paper. <https://www.tec-eurolab.com/public/file/AnsysVsVG2TECEurolabsrl-7070-7668.pdf>

# **Novel multi-billion degrees-of-freedom FEA models for rapid simulation of the multi-physics behaviour of a complete aero engine**

*Neeraj Cherukunnath, Sandeep Shrivastava, Suvro Mukherjee, Nunzio Palumbo, Ed Green*

*Rolls-Royce Plc*

## **SUMMARY**

Simulation and modelling, enabled by high performance computing, have transformed the way aero-engines are designed and engineered. However, next generation engines will place demands on simulation that cannot be met by incremental changes to current techniques. There is a strong industry need to deliver efficient engines to the aerospace market in significantly reduced time-scale, but with a much higher level of maturity. High Performance Computing (HPC) offers a means of achieving this by providing fast, accurate, simulation of operational behaviour at all stages of a products lifecycle. This includes the accurate prediction of rotating and static engine part clearances using very large, high fidelity, coupled thermo-mechanical models at whole engine level. Under the EPSRC funded research programme ASiMoV, Rolls-Royce Plc is working with a number of academic and industrial partners, to develop an advanced, large scale multi-physics simulation system capable of running multi-billion degrees-of-freedom (DoF) models on HPC systems. This paper provides an overall summary of the work packages included in the research program.

This paper describes the complex process of model generation, meshing, application of complex boundary conditions and creation of complex flight profiles at whole engine level. The models are currently generated using in-house finite element system. The paper also covers the development and performance testing of a Message Passing Interface (MPI) based distributed parallel solver for finite element analysis (FEA), implemented on the public domain FEniCS code.

In the future, the focus will be to develop an advanced process to build large whole engine models representing better physics, faster generation of large meshes and implementation of advanced algorithms to improve parallel scalability in solution process in HPC systems. Further extension of the capability to multi-physics coupling with electromagnetics (EM) and computational fluid dynamics (CFD) will potentially lead to develop advanced large scale simulation of future hybrid/electric aero engines.



## 1: Introduction

The strategic vision of this Prosperity Partnership *Advanced Simulation and Modelling of Virtual Systems* (ASiMoV) is to enable the research and development of the next generation of engineering simulation and modelling techniques. The one of the aim of the project is to achieve a high fidelity coupled thermo-mechanical FEA simulation capability of a complete aero engine during operation. This will lead further expansion of the capability to more coupled multi-physics including EM and CFD for the simulation of future electric engines. This level of simulation will require breakthroughs at all levels, including physical models, numerical solvers, algorithms, software infrastructure, and Exascale HPC hardware. The driving ambition is to realise new simulation technology for the ultra-high resolution and extreme scale needed for meaningful virtual certification models. This virtual certification concept will potentially bring a major impact on overall cost reduction for the future product development programmes. This leads to the twin-track ambition shown in Figure 1.

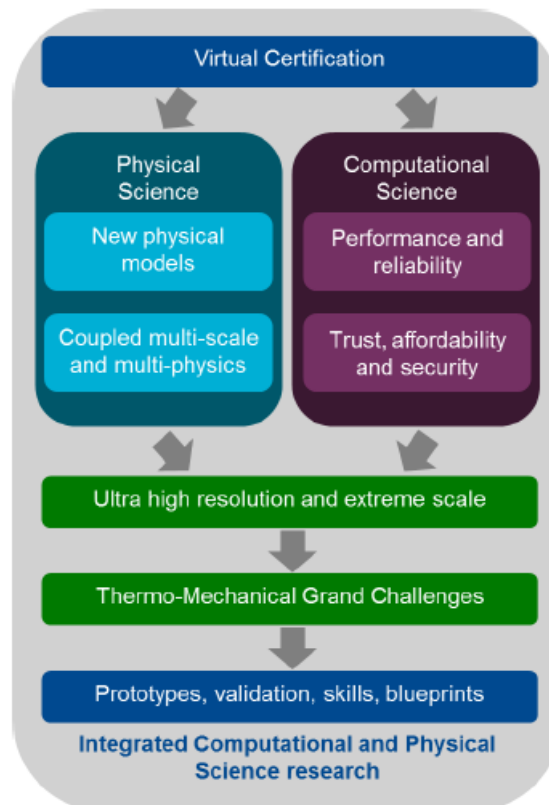


**Figure 1: Virtual certification capability concept**

The programme is broken down into seven work packages (WPs) led by industrial and academic partners:

- 1) **Grand challenge cases and integration** (Rolls-Royce): In order to integrate WPs 2-7, and to have benchmarks for progress, a set of scalable grand challenge use cases are under development through which we can prototype the simulation capability developed by the Partnership.
- 2) **Proto-type solvers** (Cambridge University): This WP addresses the development of extreme scale solvers with the requisite robustness and performance for engineering applications.
- 3) **Extreme computing** (Edinburgh Parallel Computing Centre): The research programme addresses challenges associated with extreme-scale computation and extreme volumes of data in particular. This includes extreme-scale parallelism, maximisation of processing performance, in-memory computing, multi-physics simulation workflow coordination, extreme data I/O and storage.
- 4) **Robustness of Physics** (Oxford University): This WP aim is to ensure scalability and robustness of relevant physically based models. Two particular problems of interest under consideration are scalability of contact mechanics algorithms, and an AI-based scaling of large computational mechanics simulations.
- 5) **Trusted computing** (Rolls-Royce): Protecting data on large shared HPC systems, including from system administrators, is an emerging area. Research is needed to minimise and maintain trust boundaries to the level needed for research on proprietary test cases, which cannot be desensitised without affecting the science that is being simulated. The two themes this research programme follows are trust boundaries for secure simulations and confidence in the simulations.
- 6) **Lean computing** (Warwick University): The requirements for new high-resolution physical models and full-system simulations will require calculations on trillions of cells and hundreds of millions of computing threads. Scaling to this level is not currently possible, as limits to computing hardware, software and infrastructure costs render this impracticable. The research programme follows five themes including HPC and Cloud Computing, Algorithmic Challenges for Lean Computing, Heterogeneous Computing for Low Power, Predictive Queuing and High-Level Abstractions for Energy Efficiency.
- 7) **Future computing platforms** (Bristol University): The aim of this WP is to develop new techniques that are able to exploit future Exascale

computer architectures, memory hierarchies and interconnects. This WP addresses fundamental computer architecture questions across five major themes including exploitation of future processor features, performance portability, leveraging emerging AI processors, future memory hierarchies and future interconnects.

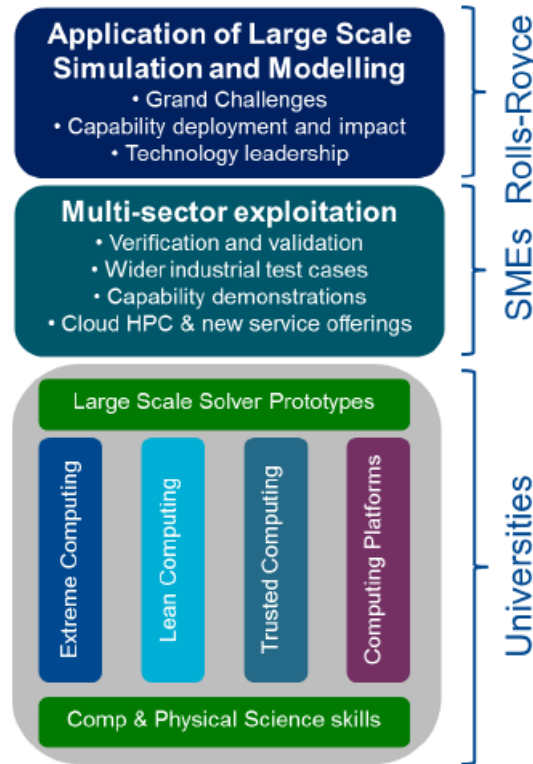


**Figure 2: Research Framework**

## 2: Grand Challenge Model Generation

In order to progressively develop efficient and robust advanced solvers in high performance computing environment, with the aim of improving the speed and accuracy of analysis of high fidelity models, a set of scalable grand challenge use cases are developed for prototyping the capability developed by the Partnership. As the simulation goals are well beyond today’s capabilities, these generic test cases allow us to scale model size, geometric and physical complexity. Full engine thermo-mechanical FEA cases will allow us to demonstrate the first ultra-high resolution thermo-mechanical simulation of a complete engine in operation, including the effects of contact and friction. Target model size is several billion elements using a representative geometry closer to manufacturing geometry.

The three benchmarks under current consideration are a large component model, a whole engine level static structure model and finally a large high fidelity model that is a close representation of a production aero engine (Figure 3). The largest model consists of six thousand components with complex thermal boundary conditions, structural constraints and loads. The loading conditions are representative of complex flight cycles. Multi-billion element meshes have been generated with advanced mesh generation processes. This results in the generation of large finite element binary input data for these models. To handle the large amounts of input data, mesh related data has been separated from data related to boundary conditions and loadings, which are linked to the external geometry. These geometry faces are tagged to finite element faces and this information is stored in an HDF5 formatted mesh file.

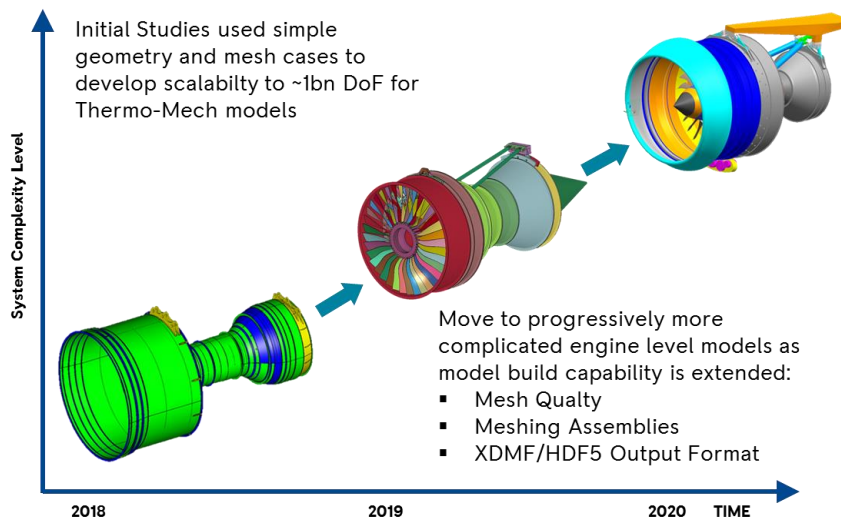


**Figure 3: Agile approach to model development**

### 3: Solver Development

The major challenge in developing scalable speed and accuracy is the development of solver technology, particularly iterative solvers for implicit coupled thermo-mechanical finite element analysis. After briefly presenting the algorithmic aspects of the solver developed by academic partners, this paper focuses on the performance aspects of the benchmark models under various solver parameters and pre-conditioners. In order to improve the scalability of the solver, codes are parallelised throughout the analysis, from reading input HDF5 files to writing results data after the parallel iterative solve. The input mesh data on multiple MPI processes have been partitioned using parallel partitioning algorithms and distributed to multiple processes. In the transient time stepping process, parts of large linear system are assembled from

evaluated element matrices in corresponding MPI processes and solved using a pre-conditioned iterative solver. The iterative solution process is based on the efficient usage of the public domain Portable, Extensible Toolkit for Scientific Computation (PETSc) and related codes. For representative verification test cases, the results, especially deflections, are compared between the in-house system and the FEniCS code.

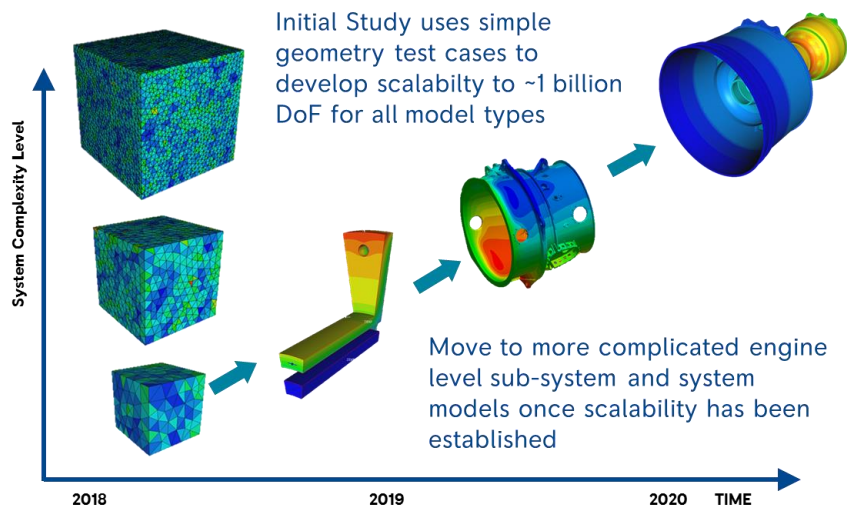


**Figure 4: Agile approach to solver development**

#### 4: Conclusion: Future Simulation Technologies

The major focus of the research is to address the computational challenges of simulation of large scale engineering systems in high performance computing environment. Prototyping of the above mentioned engineering grand challenge models leads to the demonstration of the first ultra-high resolution multi-billion thermo-mechanical simulation of a whole engine in operation, including the effects of contact and friction. The full engine coupled FEA and CFD case extends the previous case to include in-the loop coupled CFD analysis. This leads to perform the first engine-level simulations capable of exhibiting emergent system behaviour. The target model size is over one trillion cells. The coupled thermo-mechanical and electromagnetic FEA case extends the capability to predict transient behaviour of electrical machines (Figure 5). During the final stage of the project, the target is to develop fully coupled FEA (Thermo-Mechanical), CFD and EM prototype model to demonstrate multi-physics behaviour representing the future hybrid/electric engines (Figure 6).

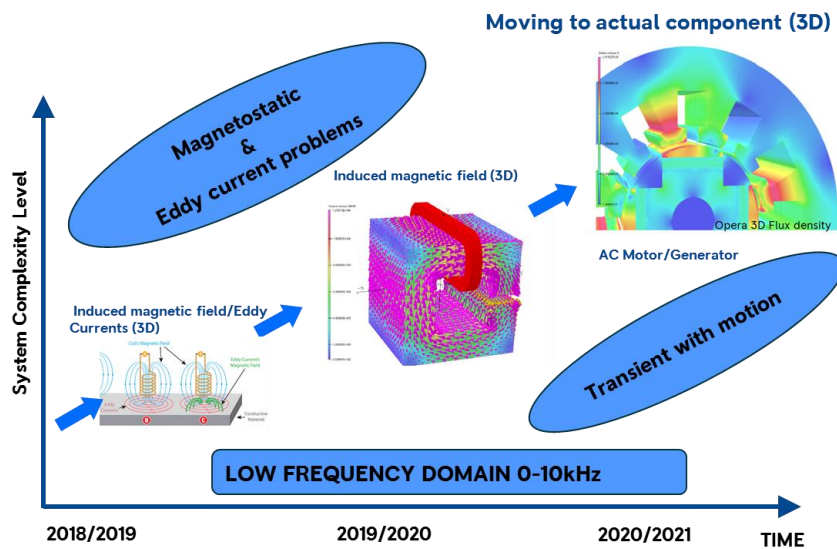


Figure 5: Agile approach to Electromagnetic Simulation

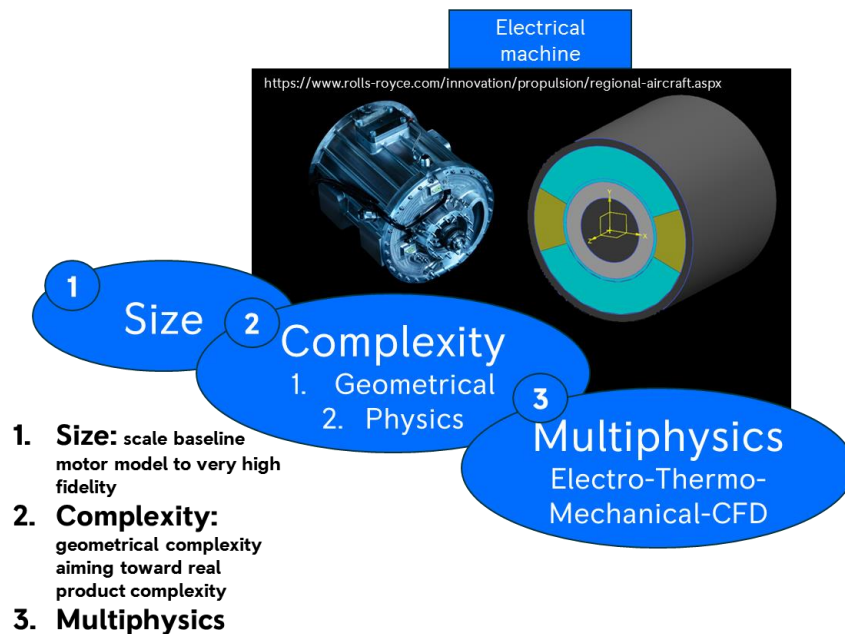


Figure 6: Multi-physics Simulation of Electric Machines

The permission of Rolls-Royce to publish this paper is gratefully acknowledged. This research forms part of the Rolls-Royce led EPSRC Prosperity Partnership (Grant Ref: EP/S005072/1) entitled “Strategic Partnership in Computational Science for Advanced Simulation and Modelling of Virtual Systems – ASiMoV”. Access to the UK national supercomputer service (ARCHER) is gratefully acknowledged.

We acknowledge Edinburgh Parallel Computing Centre (EPCC), University of Cambridge, University of Oxford, University of Warwick and University of Bristol for their contribution and support.

# **Understanding powder behaviour in an additive manufacturing process by using DEM**

*Marina Sousani  
Senior R&D Engineer*

## **SUMMARY**

The automotive, aerospace, food and healthcare sectors require the handling of powders when employing Additive Manufacturing (AM) as the latter enables the production of complex parts in a short amount of time. Thus, considered an established method to developing an agile manufacturing environment, that can drastically reduce the lead time from conception to the production stage.

Different powders are used in these AM processes and they are fed into various production equipment through delivery systems. These systems aim to deliver a precise quantity of fine powder for subsequent spreading, hence the reliability of their performance strongly affects the finished product quality. Powder is a unique material, sensitive to environmental and machine conditions, which makes its handling a challenging task. Therefore, establishing the optimal configuration by prototyping is both difficult and time-consuming.

This work presents a Discrete Element Method (DEM) simulation [1] of a commercial dosing system, used by the BARNES Groups Advisors for their AM processes. The latter uses a prescribed volume of mixed powders and controls their flow into the printers spreading systems, hence dictate the success or failure of the end product and influence the machine set-up. Specifically, the use of fine powders with different flowability poses a great challenge both to the design and operation phases as it affects the uniformity of the powder bed and speed of delivery.

## **1: Material characterisation**

Calibration is an important and necessary process that creates a link between the real application and the parameters used in the simulations. Furthermore, the success of the virtual model, predicting material behaviour and/or solving potential problems, is highly dependent on the choice of model input parameters and the physical measurements used as benchmarks. In this work, the input parameters of the model were optimised by using measurements from the FT4 powder rheometer as benchmarks.

The FT4 powder rheometer, which is a well-known powder tester measuring flowability shear strength and compressibility, was considered best as it operates in a dynamic flow regime and a low stress state [2] corresponding to the expected conditions in the dosing wheel. It used a 50 ml vessel including



blades that rotate with a helical velocity of 100mm/s. The test provides measurements of the force and torque on the shaft of an impeller blade, which passes through a bed of powder and calculates the total energy required to mix the powder material (Figure 1).

## 2: Calibration of DEM parameters

This paper introduces a robust workflow that correlates experimental data from the FT4 rheometer BFE tester with simulation results, to replicate real powders of different flowability (free-flowing and cohesive) in a computer environment. A meso-scopic modelling approach was employed, which made the physical particle size distribution less meaningful. The powder was modelled as a mono-dispersed system, in the interest of simplicity, and used the Edinburgh Elasto-Plastic Adhesion (EEPA) contact model [3,4] to capture the complex elasto-plastic-adhesive behaviour of the material. A parameter sensitivity analysis was conducted using a Plackett-Burman design of experiments configuration and a linear response fitting model to the data. The results (Figure 2) showed an excellent agreement between the experimental data and the simulation results, providing confidence on the virtual model and a good understanding of the material behaviour. Due to limited space only the results for the free-flowing material are presented below.

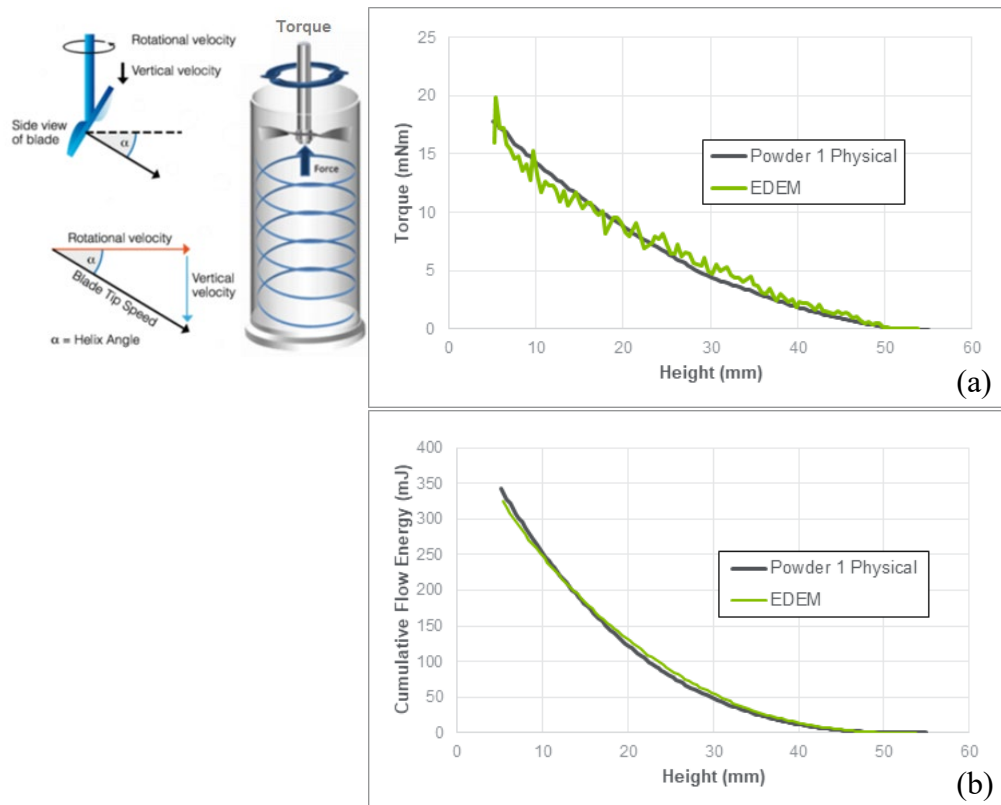


Figure 1: Comparison between experimental and simulated results for the free-flowing material.

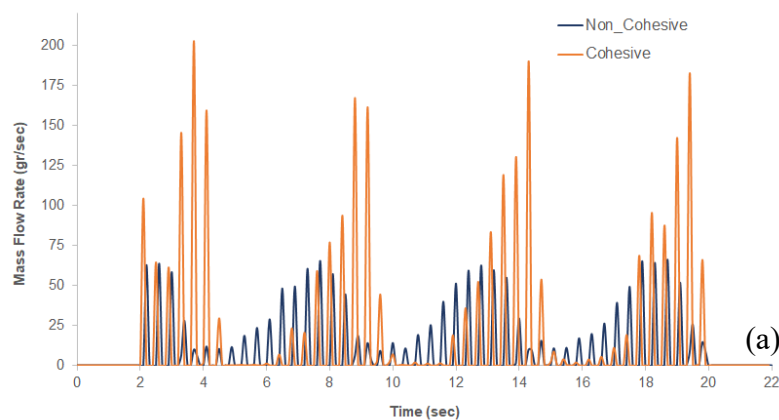
### 3: Dosing wheel application

The EDEM model replicated the real physical system in which a volume of powder filled the top of the apparatus and as the wheel rotated the powder was transported and discharged on top of a vibrating powder bed. The simulation was repeated twice using a free flowing and a cohesive powder material, respectively.  $1.2 \times 10^5$  bi-sphered particles were generated from the top, dropping under the effect of gravity and left to rest before the turning of the wheel. The simulation run for 22seconds of physical time and used a Graphic Processing Unit to accelerate the calculations.

Due to limited space only some of the results are presented herein. Exporting the mass flow rate at the discharge area (Figure 2(a)), it was observed that the free-flowing material was released abruptly followed by intervals of no flow, whereas the profile of the cohesive material appeared to be more uniform, continuous and with lower peaks. This behaviour can be attributed to the creation of agglomerates due to cohesion. This claim was verified by observing the contact vectors between the particles dropping on the powder bed. It can be observed that the cohesive material covers much larger area compared to the free-flowing one (Figure 2(b)).

Next the DEM data were visualised as continuum, based on the work of Goldhirsch, I. (2010). For this, a custom workflow was put together that extracts the discrete data from the simulations and applies them into the continuum equations. For that EDEMPy was used, a Python library for post-processing and analysis of EDEM simulation data that takes advantage of EDEM's hdf5 file structure.

The temporal average velocity (Figure 3) of the cohesive material created a bottleneck at the discharge area and was considerable slower demonstrating that the presence of cohesion hinders the flow, due to formation of agglomerates, resulting in a non-uniform distribution.



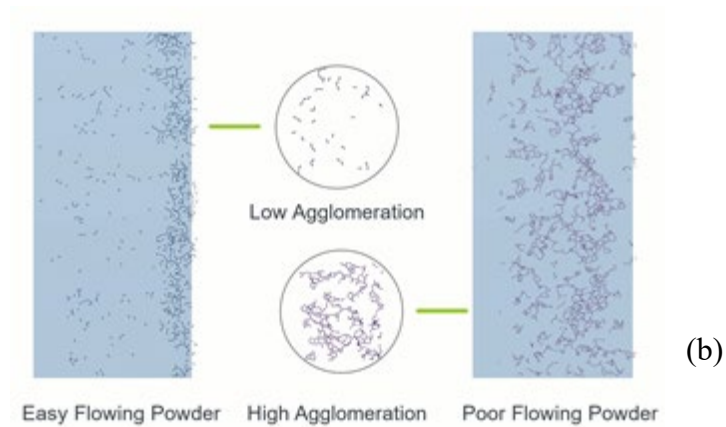


**Figure 2:** (a) Mass flow rate at the bottom for the free-flowing (blue) and the cohesive (orange) material and (b) top view and zoomed-in areas of the powder bed highlighting the creation of agglomerates based on contact vectors.

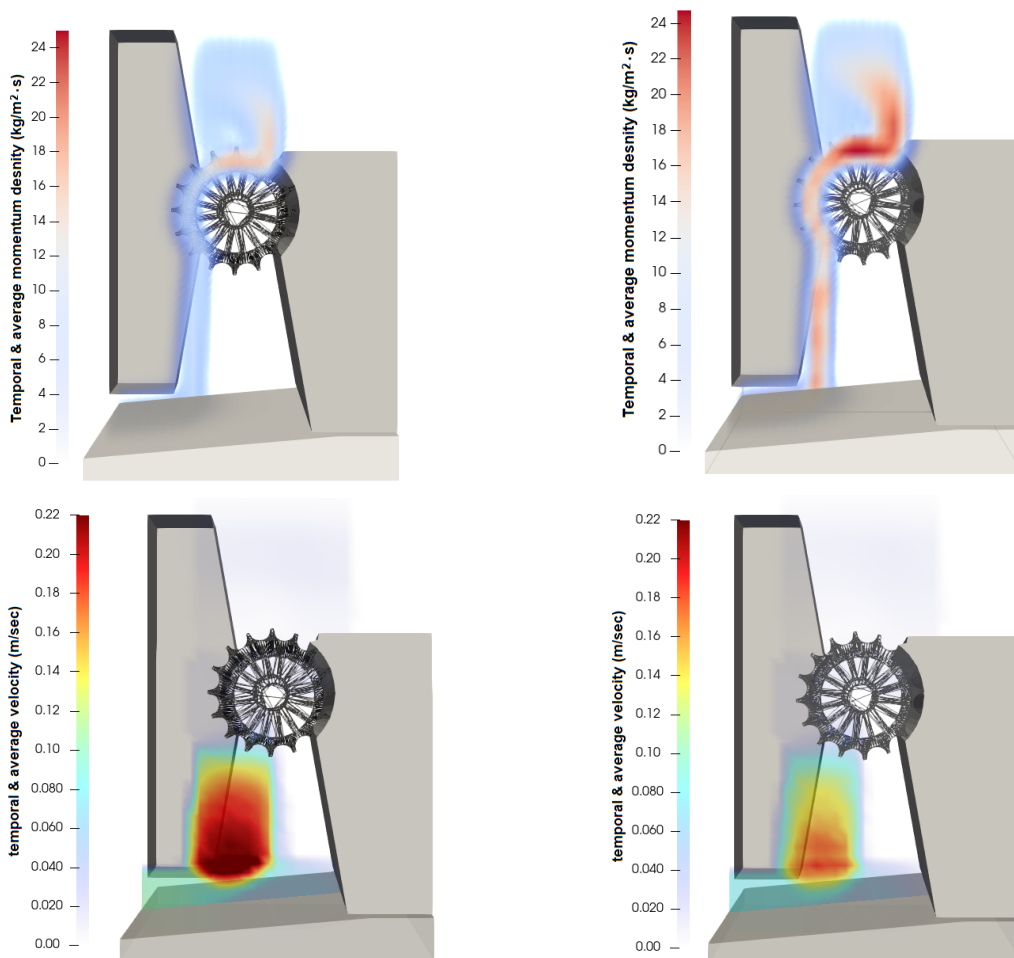


**Figure 3:** Comparison temporal average momentum density & temporal average velocity for the free-flowing (left) and the cohesive material (right).

#### **4: Conclusions**

This work presents EDEM material models that capture the complex micromechanical behaviour of powders and provide excellent quantitative predictions of the physical responses after calibration. The calibration methodology required only a small number of simulations, making the calibration of accurate models practical.

The coupled DEM-Coarse Graining methodology employed herein provided good understanding of the mechanics of the system and helped towards a reliable and precise powder delivery.

#### **REFERENCES**

- [1] Cundall, P.A. & Strack, O.D.L. A discrete numerical model for granular assemblies of the article. *Géotechnique* 1979, 29, 47-65
- [2] Freeman, R. Measuring the flow properties of consolidated, conditioned and aerated powders — A comparative study using a powder rheometer and a rotational shear cell of the article. *Powder Technology* 2007, 174, 25-33
- [3] Thakur, S.C., Morrissey, J.P., Sun, J., Chen, J.F. & Ooi, J. Micromechanical analysis of cohesive granular materials using the discrete element method with an adhesive elasto-plastic contact model of the article. *Granular Matter* 2014, 16, 383-400
- [4] Chung, Y.C. & Ooi, J.Y. Benchmark tests for verifying discrete element modelling codes at particle impact level of the article. *Granular Matter* 2011, 13, 643-56
- [5] Goldhirsch, I. Stress, stress asymmetry and couple stress: from discrete particles to continuous fields of the article. *Granular Matter* 2010, 12, 239-52

# **Understanding the Manufacturing Cost Drivers of Tolerances**

*Amanda Bligh, PhD  
aPriori Technologies*

## **SUMMARY**

Appropriate tolerancing is one of the critical components required in reaching the best manufacturing cost for a component, with tight tolerancing being a common reason for the selection of more expensive manufacturing processes. During a standard design and development process, it is generally difficult for an engineer to understand the impact of tightening or relaxing tolerances on manufacturing process selection and the resulting impact on manufacturing cost. This is especially true for newer engineers or those with limited experience in manufacturing. Ideally, an engineer with limited manufacturing experience would be able to investigate an extensive list of manufacturing and tolerances combinations and receive feedback on the cost from internal experts or suppliers to help build their intuition and knowledge. Completing this process, though, is time prohibitive and requires the involvement of many stakeholders. Automation of this process using available CAD, simulation, optimization, and simulation software tools would be a natural solution.

A geometry-based manufacturing and costing analysis solution which can read syntactic tolerances and includes common heuristics for manufacturing process selection can provide visibility to the impacts of tolerances on manufacturing process selection, cycle time, and cost more quickly and consistently than consulting an expert. By automating such a software with a multi-discipline design optimization tool, it now becomes feasible to understand the impacts of tolerance changes on manufacturing process requirements and find better solutions for both tolerancing and manufacturing options while keeping the cost impact of these changes in context.

In this study, tolerance and manufacturing options are investigated for a manufactured part through the automation of geometry-based manufacturing costing software using a multi-disciplinary design optimization tool. With this investigation it is possible to see opportunities for manufacturing improvement by using cost as the primary metric. Additionally, the output of such an analysis enables those with limited experience in manufacturing to make informed decisions regarding the manufacturing implications of tolerancing, thus providing an opportunity to further democratize aspects of the engineering process.

## 1: Introduction

A common workflow for engineers is to evaluate tolerances by ensuring they meet standards for fits and requirements to meet other design goals. As manufacturing engineers are intimately aware, though, parts are often designed with overly tight tolerances, leading to the use of expensive manufacturing processes and loops in the development process. While some feedback on expensive processes tolerances may drive is captured in tolerance optimization software, the full impact from a manufacturing cost or cycle time perspective is not commonly available. In this paper, the impact on product development of using a geometry-based manufacturing costing software to quantify the cost impact of tolerances is assessed for both a manual and automated use case.

## 2: Background

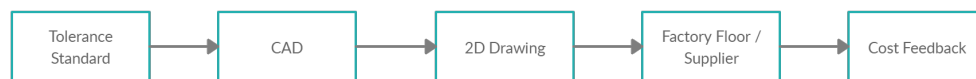


**Figure 1: Flow for cost feedback within a standard development process.**

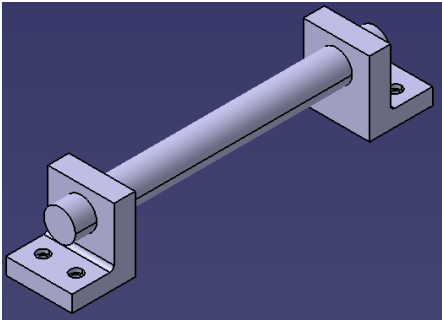
Previous work in manufacturing notes that 70% of the final cost of a product is driven by early design decisions [1]. These decisions include the selection of tolerances, often based on standards, from sources like the *Machinery's Handbook* [2], or gathered from specialized software considering complex GT&D. While there are methods for optimizing the cost of tolerances [3,4], they require a comprehensive knowledge of features' costs at multiple tolerance levels in advance to decide between process and tolerance options.

Figure 1 shows a workflow for cost feedback on tolerances within product development. A standard tolerance is added to either 3D CAD or the 2D drawing of a part. The drawing is sent to the internal factory floor or a supplier. Cost feedback is provided using the tolerances on the drawing. If standards are followed, the cost may be as expected. But, when product requirements drive tolerances to vary from the standard, the cost may be higher than the target, and requiring design changes. This work slows the development process, as several loops may be needed to reach acceptable tolerances and costs. For this reason, the design for manufacturing (DFM) literature recommends estimating the cost of a product based on the cycle time, setup time, and hourly rates for labour and machines early in development [1,5,6]. Such estimates are possible using a geometry-based manufacturing costing software during the design process.

## 3: Example with Manual Workflow

A simple case of a rod in a sliding fit with two mounts is used for this study, with a nominal diameter of 1.5 inches (38.1 mm) as shown in Figure 1.

Reviewing the standard tolerances definition for a rod of this size, the recommended ANSI tolerances for a sliding fit are: -0.00, +0.01 inches (-0.00, 0.254 mm) for the diameter of the mounting holes and -0.0021, -0.001 (-0.05334, -0.0254 mm) for the diameter of the rod. This information was included in the semantic PMI on the CAD parts.



**Figure 2: Case study assembly with two mounts and a rod interacting with a sliding fit with a 1.5” (38.1 mm) nominal dimension.**

The input assumptions for each part in the manufacturing cost estimation software (aPiori Professional) are shown in the table below, along with the resulting outputs of cost and cycle time. The software was set to read the PMI based tolerances.

Part	Routing	Annual Volume	Material	Region	Cost Each (USD)	Cycle Time (sec) Per Routing Step
<b>Rod</b>	2 Axis Lathe	5500	1010 Steel	USA	16.87	291
<b>Support</b>	Sand Casting / 3 Axis Mill	5500	Cast 1020 Steel	USA	5.92	154 / 15

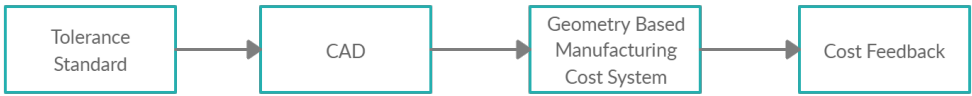


**Figure 3: Tolerance to cost flow with a geometry-based manufacturing cost system included.**

Using this approach provides the opportunity to receive cost feedback before contacting the factory or supplier for costing detail, allowing for real time manufacturing cost feedback based on the tolerances input by the engineer, as shown in Figure 3. If a tighter tolerance than the standard is required, this can be easily changed in the PMI and investigated. Such a capability eliminates

time during the development process and gives early confidence to the engineering team regarding tolerancing decisions.

#### 4: Example with Automated Workflow

While the workflow in Figure 3 provides some early insight into the impact of selected tolerances, it does not give a sense of the overall impact on cost as the tolerance is adjusted outside of the standard without manual intervention by the engineer. To investigate this, the workflow is automated. A constraint is included to maintain a clearance between the minimum and maximum value provided by the ANSI clearance standard for a RC4 sliding fit. Figure 4 shows this updated workflow.

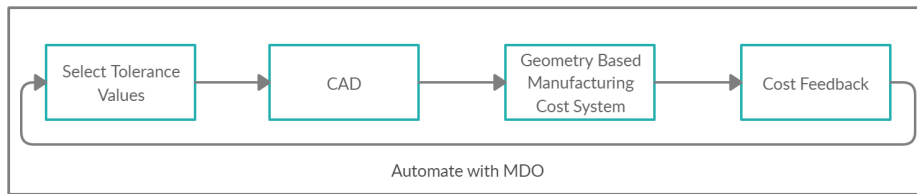


**Figure 4: Automating the flow with an MDO toolset.**

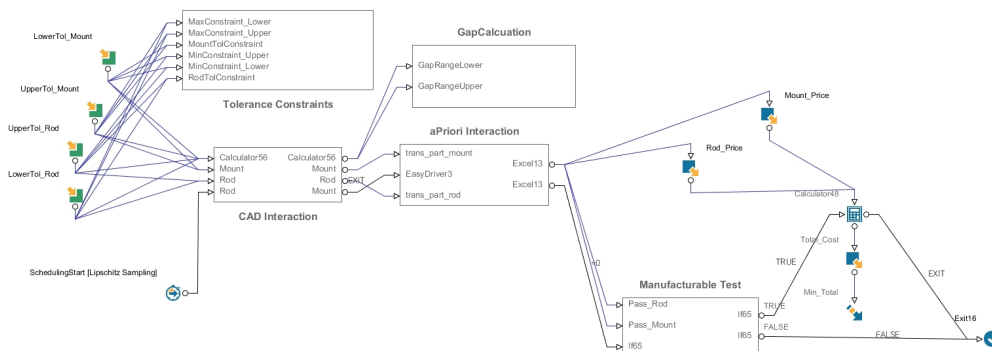


**Figure 5: MDO workflow for optimization tolerances for manufacturing cost.**

A total of 500 iterations were completed using a Lipschitz Sampling optimization algorithm, with the objective of minimizing the cost of the overall assembly. Of these 500 iterations, 339 met all required criteria and had manufacturable tolerances based on the USA baseline factory model used in the geometry-based manufacturing cost system. The workflow used, completed in modeFRONTIER, is shown in Figure 5.

In addition to the clearance constraints, a manufacturability test is also included. The test reviews feedback from the geometry-based manufacturing cost software regarding if a tolerance can be manufactured with the tolerances provided for the iteration.



Figure 6 shows the total cost graphed by the tolerance gap (absolute value of the difference between the high and low tolerance value), with the same data grouped by either the tolerance gap for the rod (x) or the tolerance gap for the mount (+). Two response regimes separated by \$2.50 are shown in the graph. The higher cost regime reflects the addition of outer diameter (OD) traverse grinding on the rod to reach the required tolerance, which is added when the tolerance is beyond that which finish turning alone can reach. When the rod tolerance is very tight, the mount tolerance varies, as shown in its series, creating a small impact (\$0.15) to cost.

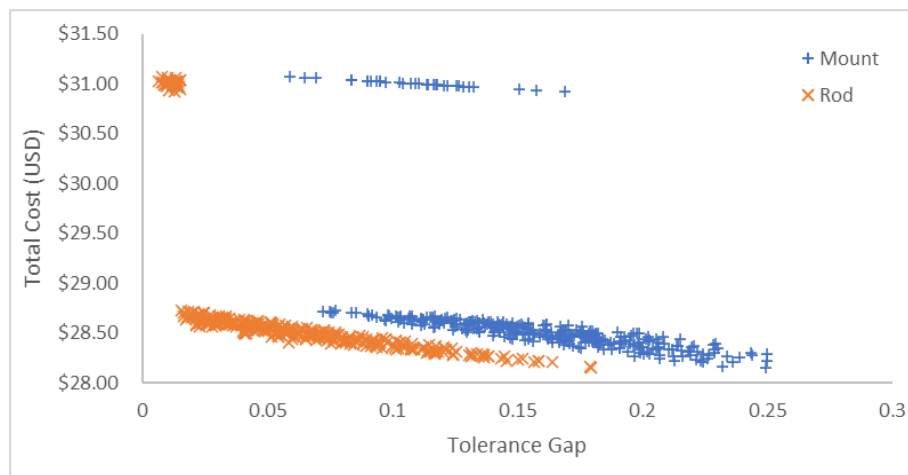


**Figure 6: Graph of Total Cost vs. Minimum Gap**

When OD traverse grinding is not required, there is more variation in the cost (\$0.57), as seen in the lower regime for both series in Figure 6. This reflects changes in the speeds and feeds as the tolerances on both the rod (completed with finish turning) and mount (completed with boring) tighten. The design engineer can gain from this analysis an understating of the acceptable tolerance gap and its cost impact.

## 5: Conclusion

Within the standard product development process, decisions based on the cost impact of tolerances and manufacturing breakpoints for designs often requires expert knowledge of manufacturing options and results in more development time to access that knowledge. A geometry-based manufacturing cost tool gives engineers the ability to see the impact of tolerances early in the manufacturing process and make decisions best suited for the lowest cost option. By further automating with an MDO tool, a best design option can be reached beyond only cost and tolerances to ensure both the performance and economic implications of a design.

## REFERENCES

- [1] Boothroyd, G., Dewhurst, P. and Knight, W. (2011). Product design for manufacture and assembly. Boca Raton: CRC Press - Taylor & Francis.
- [2] Oberg, E., Jones, F.D., Ryffel, H.H., and McCauley, C.J. (2016). Machinery's Handbook. 30th ed. New York: Industrial Press, Incorporated.
- [3] Chase, K.W., Greenwood, W.H., Loosli, B.G. and Hauglund, L.F., 1990. Least cost tolerance allocation for mechanical assemblies with automated process selection. Manufacturing review, 3(1), pp.49-59.
- [4] Chase, K.W., 1999. Minimum-Cost Tolerance Allocation. Dimensioning and Tolerancing Handbook.
- [5] Philpott, M., Dornik, N., Ellis, B., Hong, P., Warning, C., 2019. Design for Manufacture. Online.
- [6] Bralla, J., 1999. Design for Manufacturability Handbook. Boston: McGraw-Hill.

# Using fluid dynamics for simulating exterior ballistics phenomena

Véronique de Briey \*

Royal Military Academy, Brussels, Belgium

Benoît G. Marinus †

Royal Military Academy, Brussels, Belgium

Marc Pirlot ‡

Royal Military Academy, Brussels, Belgium

## Extended abstract

### I. Nomenclature

CFD		Computational Fluid Dynamics
RBD		Rigid Body Dynamics
RANS		Reynolds Average Navier-Stokes
$\vec{x}, \vec{y}, \vec{z}$		Body axes reference frame
$\vec{x}_g, \vec{y}_g, \vec{z}_g$		Ground-fixed reference frame
$\vec{x}_a, \vec{y}_a, \vec{z}_a$		Aero-ballistic axes reference frame (relative to the total velocity vector)
$\vec{V}$	m/s	Total velocity vector (tangent to the trajectory)
$u, v, w$	m/s	components of $\vec{V}$ in the body axes
$p, q, r$	rad/s	Angular velocities around the body axes
$\alpha, \beta$	rad	Pitch and sideslip angles
$\delta$ or AoA	rad	Total yaw angle or angle of attack ( $\delta \approx \sqrt{\alpha^2 + \beta^2}$ )
$I_x, I_y$	kg.m <sup>2</sup>	Longitudinal and Transverse moments of inertia
$\vec{F}_X, \vec{F}_Y, \vec{F}_Z$	N	Aerodynamical forces in body axes
$\vec{M}_X, \vec{M}_Y, \vec{M}_Z$	N.m	Aerodynamical moments in body axes
$C_D$		Drag force coefficient ( $C_D = C_{D_0} + C_{D_{\delta^2}} * \sin^2(\delta)$ )
$C_L$		Lift force coefficient ( $C_L = C_{L_\delta} * \sin(\delta) + C_{L_{\delta^3}} * \sin^3(\delta)$ )
$C_M$		Pitch moment coefficient ( $C_M = C_{M_\delta} * \sin(\delta) + C_{M_{\delta^3}} * \sin^3(\delta)$ )
$C_{i_p}$		Spin damping coefficient
$C_H$		Pitch damping coefficient
$A$	deg	Pitching Amplitude for the forced oscillation
$k$		Reduced pitch frequency
$N$		Number of global iterations per oscillation cycle
$i$		Number of inner iterations per global iteration

\*PhD candidate, Dept of Weapon Systems and Ballistics of the Royal Military Academy, veronique.debriey@dymasec.be.

†Associate Professor, Dept of Mechanical Engineering of the Royal Military Academy.

‡Professor, Dept of Weapon Systems and Ballistics of the Royal Military Academy.

## II. Background

IN external ballistics, trajectography is the combination of calculation methods and techniques for predicting the trajectory of projectiles launched from firearms. When the projectile is not guided, it is thus a question of being able to predict the point of impact as soon as it has left the weapon, or inversely, to know the orientation to be given to the weapon in order to hit a target. Depending on the application (artillery, small arms, anti-tank, etc...), more or less complex computational models must be considered, but generally speaking, by going beyond the scope of short-range firing, it is necessary to know the aerodynamic characteristics of the projectiles in order to calculate a trajectory. Nowadays, it is possible to characterise these projectiles aerodynamically by shooting in all velocity regimes, but the cost and the time needed to carry out the tests are still considerable, especially for large calibres [1, 2]. This is why it is interesting to be able to simulate the flows numerically in order to quickly and reliably generate their virtual fly out. Many CFD-based techniques have already been developed, but a major effort must still be carried out on the validation side of these techniques.

One of the applications generating a lot of interest is long-range shooting (sniping). Indeed, the trend for precision ammunition is to always hit a smaller target with a higher probability at an ever-increasing distance [3]. The last two decades revealed many new calibres, new weapon features and a large number of trajectory software's to reach this goal. However, there is no unanimous criterion yet to define properly and scientifically why a projectile is better than another one. Until recently, the calculation of trajectories for projectiles launched from rifles did not pose any real problems because as long as the projectile remained in the supersonic domain, its behaviour remained predictable and was characterized by mainly semi-empirical models. The existing software's are often drag based (Point-Mass Model [4]), with a fitting established to match real firing, but they do not account specifically for the sharp changes in aerodynamic forces when the projectiles reach the transonic zone. Nonetheless, the transonic domain has to be crossed by precision ammunition when reaching high operational ranges with the classical propulsion and its inherent velocities.

## III. Methodology

### A. Rigid Body Dynamics

The most complete model to characterize a trajectory is, as its name suggests, the six degrees of freedom model (Fig.1 on the left), which includes three translations in a  $x, y, z$  cartesian coordinate system, referred as body reference frame, as well as the three rotations around these same three axes [5, 6].

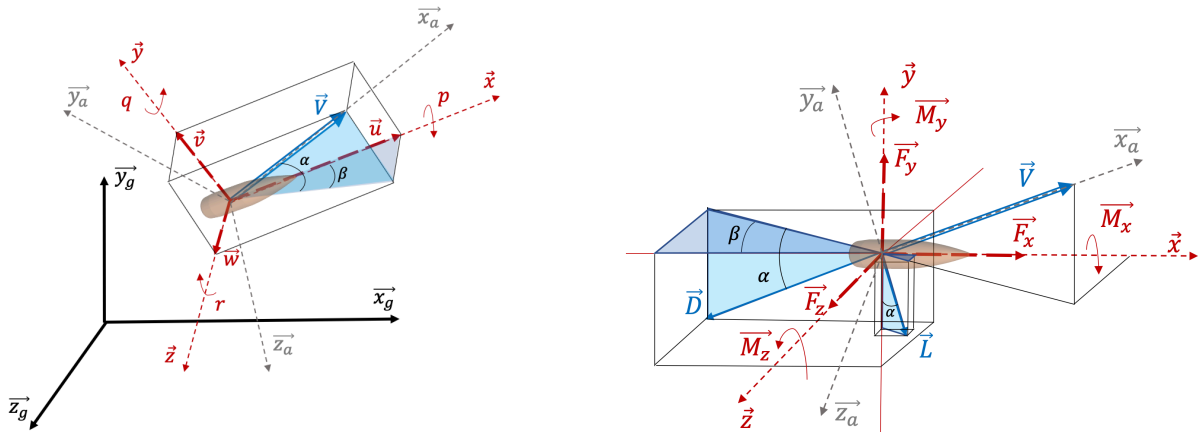


**Fig. 1 6 DOF Modeling and Representation of Aerodynamical forces.**

The resultant of the forces ( $F_x, F_y, F_z$ ) and moments ( $M_x, M_y, M_z$ ) related to the centre of gravity in relation to these three axes in all speed regimes must therefore be calculated with CFD to derive the aerodynamic coefficients. However, the aerodynamic coefficients are commonly given in what is called the aero-ballistic axis system (relative to

the velocity vector- Fig.1 on the right), and not in the body-axis system. The forces are therefore expressed mainly as a function of the lift and the drag, and secondarily as a function of Magnus' force, if the latter proves to be significant. The moments are expressed in function of the pitching moment coefficient, spin damping coefficient, pitching damping moment coefficient and if this is justified with the Magnus moment coefficient. The Magnus effect will not be included in the modeling below because its effect has not yet been extensively evaluated and the numerical sensitivity for capturing it has not yet been studied in depth.

In ballistics, it is common to consider rotational symmetry and therefore simplify the calculations with  $I_y = I_z$ . A predominantly used approach is that of Robert Mc Coy [4]: it allows to calculate forces and moments vectorially without having to work with transformation matrices to go from one reference frame to another. The results presented in this study are based on this simplified approach.

## B. Computational Approach

### 1. Mesh Characteristics and Turbulence Modeling

Any self-respecting approach that studies fluids numerically in different speed regimes should consider different meshes. While a supersonic definition requires very fine cells to capture all the shocks that develop near the projectile, but can admit a restricted domain in front of the object under study, a subsonic definition can afford coarser cells but the domain must be larger because of the propagation of disturbances upstream, against the flow direction [7, 8].

As this approach aims to define the aerodynamic coefficients in the different regimes but also in the transition between these regimes and with as little manipulation as possible, the idea was to use a trade-off approach. A large domain will therefore be used, with sufficiently fine meshes for the definition of shocks in the boundary layer. The mesh is consequently heavier, but it allows to reduce the number of manipulations to define a set of coefficients. Moreover, as the quality of the mesh is also essential, an hexagonal mesh is theoretically to be favoured. But again, to make the procedure as automatic as possible, a tetrahedral mesh is used in a parametric way according to the size of the projectile to be studied. A particular attention is nevertheless attached to the walls, which are defined in a prismatic way, in order to still insert structure and a mesh size that can satisfy the requirements of the boundary layer definition.

Finally, the mesh used for these steady and unsteady RANS simulations of the full projectile in free-air consists typically of 2 million elements with a prismatic boundary layer mesh comprising 30 layers resulting in an average value for  $y^+$  of one along the adiabatic no-slip walls. The domain extends to 20 projectile-lengths where pressure-far-field conditions are applied together with the desired angle of attack. The outlet boundaries in Fluent are defined as a pressure-outlet.

A  $\gamma$ -SST transition model [9, 10] was used for the calculations. In addition to blend the robust and accurate formulation of the  $k-\omega$  model [11] in the near-wall region and to use the freestream independence of the  $k-\epsilon$  model [12] in the far field, this model solves an additional transport equation for the turbulent intermittency. Like other engineering transition models, this model is best applicable to wall-bounded flows and not to transition in free shear flows.

### 2. Output: Aerodynamic coefficients

Between the different aerodynamic coefficients of interest, we can distinguish the so-called static coefficients, and the dynamic coefficients, linked to the different damping phenomena generated over time, which are more difficult to determine because of their connection to very unstable forces. While the first category is essential in all applications, the second category is above all necessary in the design phase of weapon-ammunition system, in order to ensure optimum projectile stability. If the damping in pitching is for instance too small or too high, there is a risk that the projectile will not finish its trajectory with the right impact angle on its target, missing the desired effect (shaped charge, armour-piercing projectile, non-lethal impact [13], etc...). However, when a system is well dimensioned, knowledge of the static coefficients alone is in most cases sufficient for a fairly accurate trajectory calculation.

Nevertheless, this study aims to determine a complete set of aerodynamic coefficients numerically, in order to have all the data required to calculate the trajectories of any new weapon-ammunition system and assess its performance. Leaving aside the Magnus effect, we still have 8 coefficients to determine for a spin-stabilised projectile, namely :

$$C_{D_0}, C_{D_{\delta^2}}, C_{L_{\delta}}, C_{L_{\delta^3}}, C_{M_{\delta}}, C_{M_{\delta^3}}, C_{l_p}, C_H$$

For all the static coefficients, a quasi-steady approach [14] was used in order to rapidly obtain entire curves of coefficients in function of the Mach number. As the coefficients are dependent on both the Mach number and the yaw angle, two complementary approaches have been used where each time one of the two parameters is fixed. In the case below, when the angle of attack is fixed, the velocity varies from Mach 3 to Mach 0.5, in steps of 0.005 Mach, which gives 500 global iterations with 40 inner iterations to reduce the residuals by a factor of about 100 between each step. When the velocity is set, the angle is varied between  $-10$  deg and  $+10$  deg in steps of 0.1 deg. The calculation is repeated for several velocities, which finally makes it possible to deduce both linear and quadratic or third-order coefficients (for lift and pitch).

Although it is a damping moment, and therefore transient, the  $C_{l_p}$  can be determined in the same way as the static coefficients. However, care must be taken to vary the rotation velocity in proportion to the translation velocity, i.e. to keep the adimensional angular velocity  $\frac{p d}{V}$  constant (even if we know that in flight this ratio tends to increase because the translation velocity decreases faster than the rotation velocity [8]).

The pitch damping coefficient is the one that requires the highest calculation effort. The transient planar pitching method was used [7, 8, 15, 16] and it consists in imposing a small-amplitude ( $A$ ) oscillation about a mean angle of attack, defined by a sinusoidal function. On the basis of the projectile's pitch response it is possible to deduce a damping over time. Like for the spin damping coefficient determination, an adimensional angular velocity is used, called  $k$ .

As this method is based on an hysteresis phenomenon in response to an induced disturbance to evaluate the damping, it seems obvious that a sensitivity study is necessary on a good number of input parameters ( $A, k, N, i^*$ ) in order to determine for which values of these parameters the solution has converged to the right solution [16].

#### IV. Results for a .308 inch Spin-Stabilized Projectile

Some results are presented below as raw numerical results obtained after calculation according to the methods set out above. **An uncertainty study must still be carried out in order to determine a margin of error with respect to these results.** In a first step, these results are compared with experimental test data from a key external ballistic reference [4].

##### A. Static aerodynamic coefficients

The following graphs presents both approaches explained in the previous section for drag, lift and pitch : Either the total force/moment is calculated by varying the angle of attack for different fixed velocities, and then on the basis of the quadratic or third order equations the different terms are extracted to represent the curves ( $Num\_AoA$ ). Or, the determination is done by a single calculation with a zero angle of attack for  $C_{D_0}$  and 3 degree angle of attack  $^\dagger$  for  $C_{L_\delta}$  and  $C_{M_\delta}$  and a Mach number ranging from 3 to 0.5, in steps of 0.005 ( $Num\_Mach$ ).

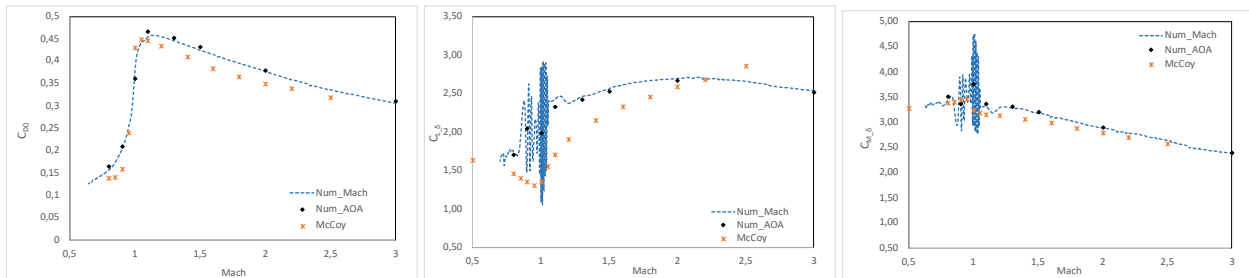


**Fig. 2 Comparison of numerical approaches for the determination of the principal static coefficients.**

For both quasi-steady methods, oscillations are observed for transonic velocities, but since the points obtained are quadratically interpolated in the AoA-approach, they are consistent with the other comparison data. However, there is a gap between the numerical results and the McCoy's experimental points, which is greater for the angle-of-attack-dependent term. In order to consider the validity of these numerical results the calculation of the total drag at 3 and

\*  $N$  and  $i$  being respectively the number of global iterations per oscillation and inner iterations per global iteration.

$^\dagger$  Because  $C_{L_\delta}$  and  $C_{M_\delta}$  varie linearly at low incidence [17].

10 degrees has been carried out (Fig. 3) and it is shown that the margin of error is very limited for small angles and increases as the angle increases. Calculations must therefore be further developed for larger angles to reduce the gaps.

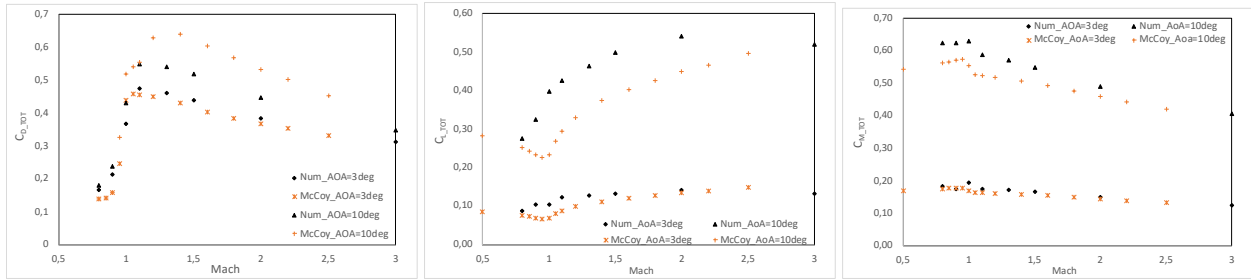


**Fig. 3 Total forces/moment for 3 degree and 10 degree Angle of Attack..**

For all static coefficients, one notices that the values converge for the two approaches, which can reduce the number of parameters to be put forward for the determination of the calculation uncertainty.

### B. Dynamic aerodynamic coefficients

While both methods again converge fairly well for the determination of  $C_{l_p}$  compared to the data from [4] (Fig.4 on the left), the results for  $C_H$  are quite different. However, the curve of  $C_H$  for this type of projectile is very similar to more recent experimental results given for equivalent projectiles [18], which led us to take the analysis further before calling the whole method into question. Other sources indeed reveal that McCoy's positive results do not seem realistic and possibly indicate an interaction with Magnus moment coefficient [8]. This assumption has therefore to be verified.

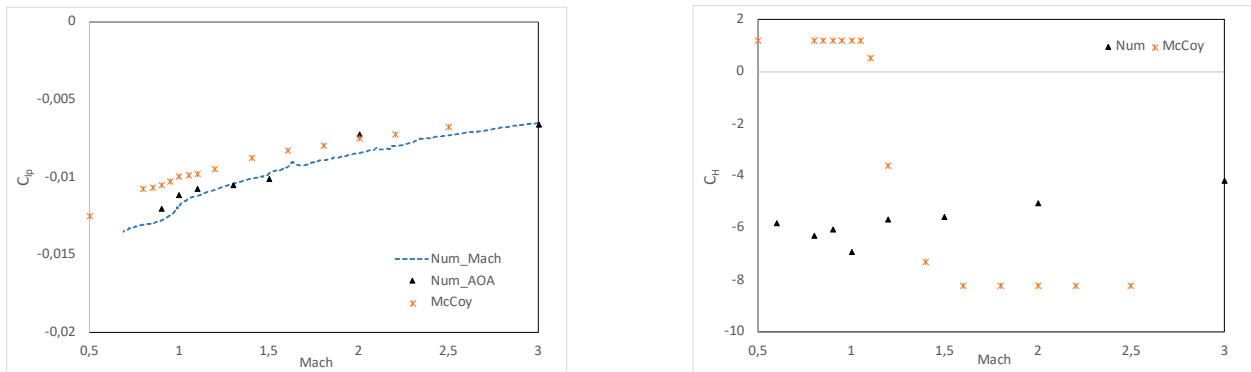


**Fig. 4 First Dynamic Coefficients.**

### C. 6DOF Trajectories

This last part aims to compare trajectories for the projectile studied in order to compare the relative importance of the different discrepancies found numerically. It will also shed light on the shortcomings linked to Magnus as well as the influence of damping on the stability of this spin-stabilised projectile.

## V. Conclusion

This multi-disciplinary study makes the link between ballistics, which for a long time was simply extrapolating experimental data to feed its trajectography models, with laborious fitting techniques, and computational fluid dynamics, which is already very advanced in many fields, including the characterisation of flying objects. The aim of this approach is to modernise the calculations with current CFD techniques and to set up "all-purpose" calculation methods to rapidly generate virtual fly-outs, regardless of the type, dimensions or velocity regime of the projectile under consideration. As there is a great amount of research in this field, there are many data available for validation, but this does not prevent the need to identify the error sources and to be able to quantify them in order to guarantee the expected accuracy.

## References

- [1] Fresconi, F., Guidos, B., Celmins, I., and Hathaway, W., "Flight Behavior of an Asymmetric Body through Spark Range Experiments Using Roll Yaw Resonance for Yaw Enhancement," 2015. URL <https://apps.dtic.mil/dtic/tr/fulltext/u2/a623629.pdf>.
- [2] Defence Research Establishment, V., "Ballistic Range Technology," 1970. URL <https://apps.dtic.mil/dtic/tr/fulltext/u2/713915.pdf>.
- [3] de Briey, V., Moumen, A., Marinus, G. B., and Pirlot, M., "Influence of the Transonic Crossing for Precision Ammunition," *31th International Symposium on Ballistics, Hyderabad*, 2019. doi:10.12783/ballistics2019/33109.
- [4] Mc Coy, R. L., "Modern Exterior Ballistics," 1999, Schiffer Publishing Ltd. : Atglen, PA.
- [5] Amoruso, M. J., "Euler Angles and Quaternions in Six Degrees of Freedom Simulations of Projectiles," *US Army Armament Research*, 1996.
- [6] Dimitrios, N. G., Elias, E. P., Dionissios, P. M., and Dimitrios, G. P., "A Six Degree of Freedom Trajectory Analysis of Spin-Stabilized Projectiles," *Journal of Spacecraft and Rockets*, 2007. doi:10.1063/1.2835958.
- [7] DeSpirito, J., Silton, S. S., and Weinacht, P., "Navier-Stokes Predictions of Dynamic Stability Derivatives: Evaluation of Steady-State Methods," *Army Research Laboratory Report*, , No. ARL-TR-4605, 2008.
- [8] Silton, S., "Navier-Stokes Predictions of Aerodynamic Coefficients and Dynamic Derivatives of a 0.50-cal Projectile," *29th AIAA Applied Aerodynamics Conference*, American Institute of Aeronautics and Astronautics, Honolulu, Hawaii, 2011. doi:10.2514/6.2011-3030.
- [9] Menter, F., Langtry, R., Likki, S., Suzen, Y., Huang, P., and Volker, S., "A correlation-Based Transition Model Using Local Variables: Part I Model Formulation," *Turbo Expo*, Vol. 4, 2004. doi:ASME-GT2004-53452.
- [10] Walters, D., and Cokljat, D., "A three-equation eddy-viscosity model for Reynolds-averaged Navier-Stokes simulations of transitional flows," *Journal of Fluids Engineering*, Vol. 130, No. 12, 2008, pp. 121–401.
- [11] Wilcox, D., "Turbulence Modeling for CFD," *DCW Industries, Inc. La Canada, California*, 1998.
- [12] Launder, B. E., and Spalding, D. B., "Lectures in Mathematical Models of Turbulence." *Academic Press*, 1972.
- [13] de Briey, V., Ndindabahizi, I., Marinus, G. B., and Pirlot, M., "Aerodynamical CFD Study of a non-lethal 12-Gauge fin-stabilized projectile," *Human Factors and Mechanical Engineering for Defense and Safety*, 2019. doi:10.1007/s41314-019-0020-x.
- [14] Silton, S. I., "Quasi-Steady Simulations for the Efficient Generation of Static Aerodynamic Coefficients at Subsonic Velocities," *35th AIAA Applied Aerodynamics Conference*, 2017, pp. 1–16. doi:10.2514/6.2017-3398.
- [15] Weinacht, P., "Navier–Stokes Predictions of the Individual Components of the Pitch-Damping Sum," *Journal of Spacecraft and Rockets*, Vol. 35, No. 5, 1998. doi:10.2514/2.3390.
- [16] Bhagwandin, V. A., and Sahu, J., "Numerical Prediction of Pitch Damping Stability Derivatives for Finned Projectiles," *Army Research Laboratory Report*, , No. ARL-TR-6725, 2013. doi:10.2514/1.A32734.
- [17] de Briey, V., and Marinus, B., "Aerodynamic Characterization of a Non-Lethal Finned Projectile at Low Subsonic Velocity," *AIAA Aviation 2019 Forum, Dallas*, 2019. doi:10.2514/6.2019-3696.
- [18] Silton, S., and Howell, B., "Aerodynamic and Flight Dynamic Characteristics of 5.56-mm Ammunition: M855," *ARL-TR-5182*, Army Research Laboratory Report, 2010. doi:10.21236/ada530895.



# Numerical and experimental evaluation of tile stoves mode of operation

Johannes Mantler (Austrian Tile Stove Association) , Florian Schüssler (ACAM Engineering) , Markus Trenker (flowdynamics)

## 1 Summary

The thermal behavior in a tile stove (Kachelofen) is complex and varies at all time. For this reason, a coupled thermal and numerical flow model was created within the funded FFG (Austrian Research Promotion Agency) project "KachelofenSimulation". The simulation models provide a good basis for considering thermal comfort in rooms and enables more specific experiment design for further research. The validation of the simulation models was carried out with measurements in the research institute of the Austrian Tile Stove Association. The literature research on thermal comfort shows the complexity and challenge of comprehensively describing this term. The essential parameters are temperatures, velocities, contents of the air as well as many individual influences.

With existing measurement results, a first tile stove simulation model was created. The solid was defined with the physical properties of chamotte and the negative volume ("air body") with the properties of air. The meshing was carried out after optimization by a convergence study. The results for the air volume are around 500 000 elements and about 75 000 elements for the chamotte body. Boundary conditions were defined for the combustion chamber heat output, the volume flow at the flue gas connector, the heat transfer to the environment and the ambient conditions.

The knowledge from meshing and the boundary conditions were applied to the other two simulation models. Additionally, the geometry of the heat-emitting volume in the combustion chamber was improved. Also, the boundary conditions of the heat transfer on the tile stove surface was enhanced by models and measurements. For the tile stove with an air gap between the inner and an outer chamotte layer an analytical calculation of the heat transfer was developed. These two simulation models were validated with built tile stoves in the research facilities of the Austrian Tile Stove Association. Temperatures on the surface, in the solid phase and in the exhaust gas were used for the validation.

The influence of the tile stove construction (structure of the chamotte layers, orientation of the flues, door arrangements and different combustion chambers), the influence of the room position (tile stove in the center or on the side of the room), the influence of wall material in the installation room (wood or concrete) as well as influence on fire protection were analyzed with the simulation models of the tile stoves.

The generated simulation models reproduce the reality of the tile stoves very good. They can be used in the future to investigate the interactions of tile stoves in rooms and buildings more closely.

## 2 Modeling, convergence studies and validation

The necessary parameters for the simulation for solids are the density, thermal conductivity, specific heat capacity and the emission coefficient [1]. These parameters have been extensively researched to provide a good basis for the calculations. In addition, the emission coefficient of chamotte was checked or more precisely determined in our own tests. In the material data of chamotte, the specific heat capacity and the thermal conductivity are dependent on the temperature. These sudden changes have a negative impact on the convergence of the simulation calculations. Therefore, the specific heat capacity and the thermal conductivity for the temperature range were replaced by a linear function. The thermal conductivity of chamotte is one of the main influencing factors in the simulation model. To achieve a good match between the simulation models and the measurement results, the thermal conductivity of the various models was varied somewhat in order to take into account the air inclusions and mortar joints.

The data for the gas phase or air were taken from the Siemens Simcenter simulation software [2]. It was assumed that the gas composition in the exhaust gas corresponds to the composition of air. The mass increase of the gas during combustion (approx. 5%) is neglected. Gases are assumed to be incompressible, but buoyancy due to the temperature difference is taken into account.

For the various tile stoves, CAD models were created with the Siemens Simcenter. An CFD model was created from the CAD model. Chamotte was assigned as a material to the solid in the model. The negative volume of the chamotte body was defined as the body of air. The tile stove and the air volume were calculated using different mesh sizes. The mesh should be fine enough to make the calculation as accurate as possible, but coarse enough to keep the software's computing time within a reasonable time

frame. The CFD- mesh was carried out after optimization by means of a convergence study and resulted in around 500,000 elements for the air volume and around 75,000 elements for the chamotte body. The process is shown in Figure 1.

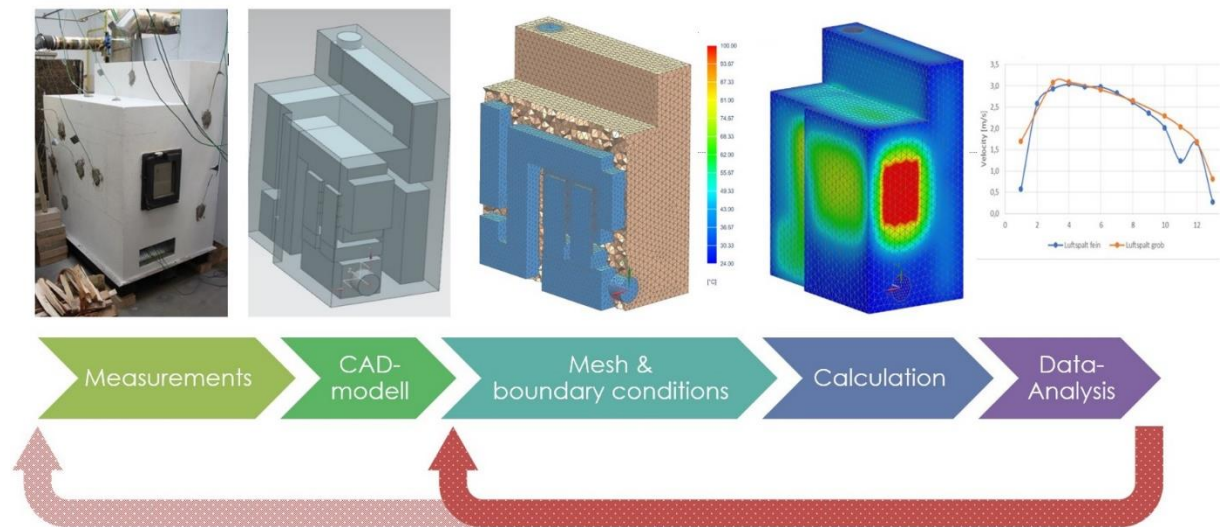
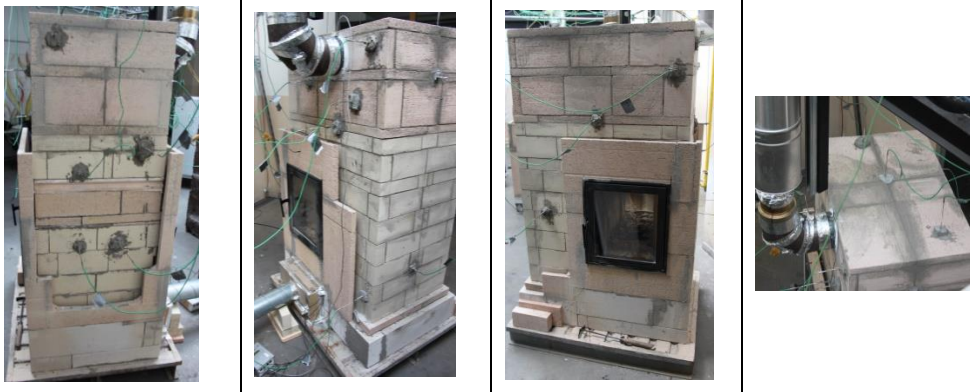
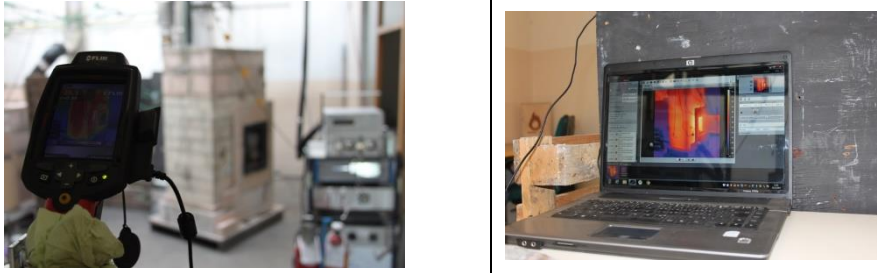
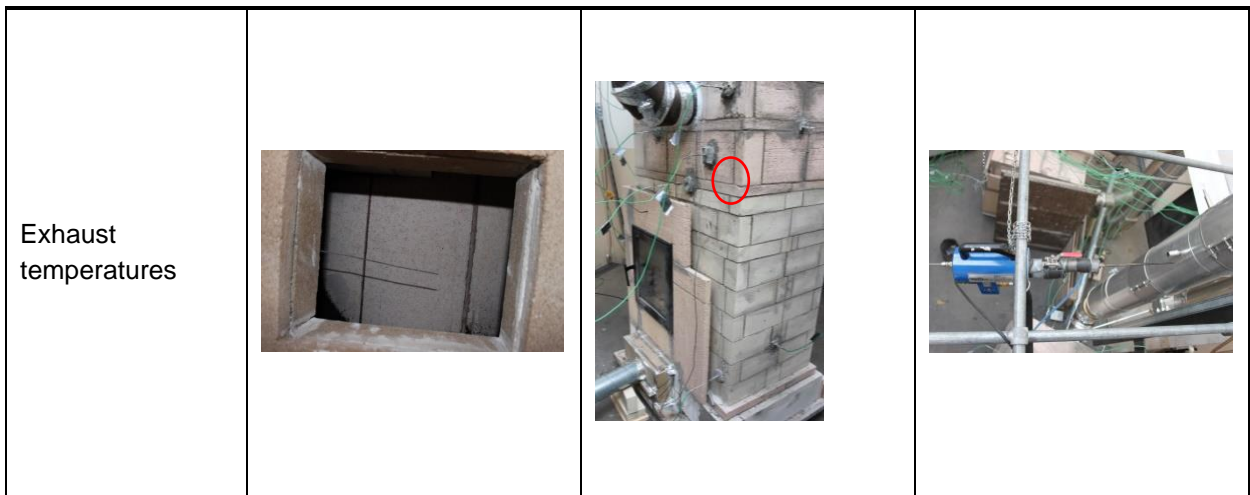


Fig. 1  
Methodology - overview

The simulation models were validated using measurements on real tile stoves in the research facility. In the measurements carried out for validation, the measured variables were recorded at the following positions, shown in Table 1.

Table 1 – Measurements for validation, excerpt

Measurand	Description of position
Room temperature	The room temperature was measured at a height of approx. 0.5 m outside the area of influence of the direct radiation from the tile stove.
Surface temperatures	Thermocouples (partly on the surface) [3]
	
Surface temperatures	Thermography camera [4]
	



The measurement data were compared with the simulation models. The following exemplary graphic in Figure 2 compares the surface temperatures during the measurements and the simulation model. The simulation model reproduces the temperatures very well.

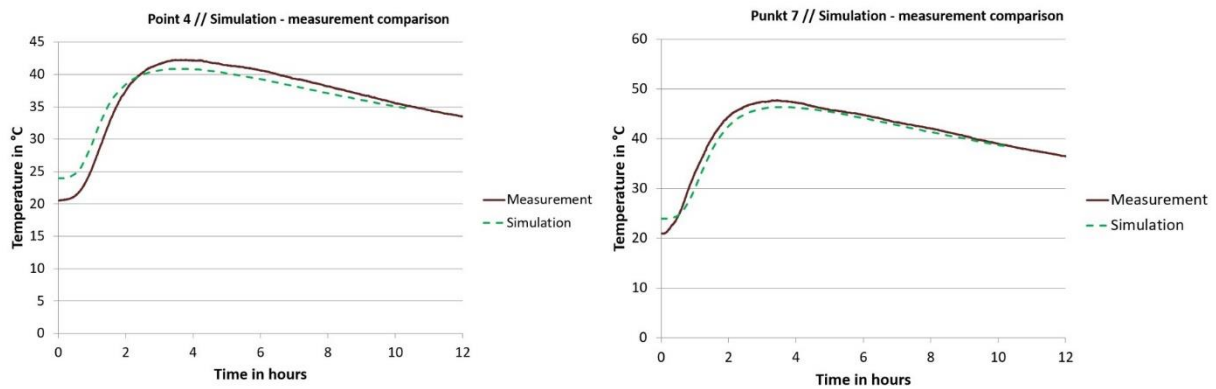
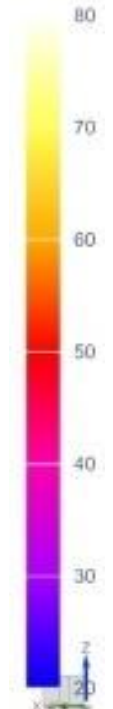
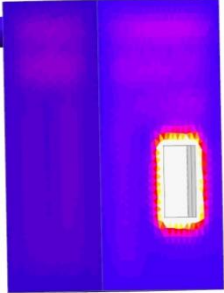
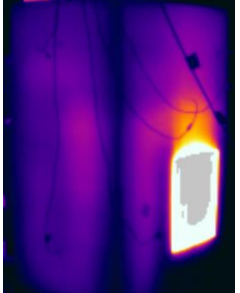
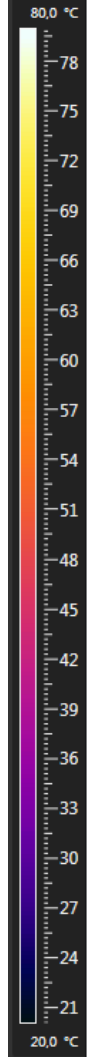
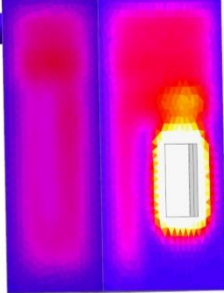
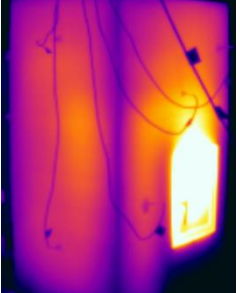
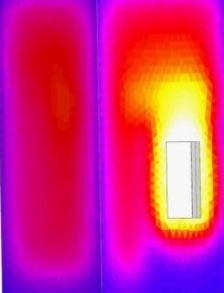
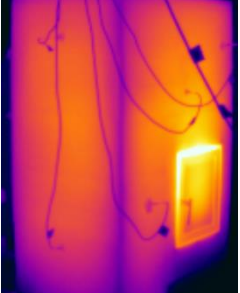
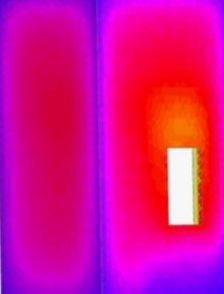



Fig. 2  
Comparison of simulation and measurement

In Table 2, the surface temperatures of the simulation model and the thermal imaging camera are compared. A similar profile of the temperatures can be seen in comparison.

Table 2 – result comparison

CFD Simulation		Measurement of thermal imaging camera	
 <p>in °C</p>	 <p>1 hour</p>	 <p>1 hour</p>	
	 <p>2 hours</p>	 <p>2 hours</p>	
	 <p>4 hours</p>	 <p>4 hours</p>	
	 <p>8 hours</p>	 <p>8 hours</p>	

The generated simulation models reproduce the reality of the tile stoves very good. They can be used for the investigation of the interactions of tile stoves in rooms and buildings, which is described below.

### 3 Transient consideration in buildings

The cyclical surface temperatures can be transferred to building models as 5-dimensional boundary conditions (position x, y, z; temperature, time). This makes it possible to examine various transient effects of building technology.

The influence of the spatial position of the tile stove was investigated with results of the surface temperatures. The room model is based on the living area of a specific house. To evaluate the influence of the room position, the tile stove was viewed in two different positions (central and sideward in the



room). In the simulation models, openings to the adjoining rooms were built through slots between the floor and the doors. The combustion air was also displayed through these adjoining rooms and the installation room itself. The adjoining rooms were assumed to be a temperature sink with a temperature of 20 ° C in the models. When the tile stove is positioned to the side, the air temperatures are higher than when the tile stove is in the central position. The difference can be explained by the fact that the tile stove is less able to emit radiation to its surroundings in the side position, as more surfaces are surrounded by walls and furnishings. As a result, the convective heat dissipation is higher and so is the air temperature. Using the example of the temperature curve at the sitting position on the couch, the difference between the two positions of the tile stove should be made clear again. A left seating area and a right seating area are defined on the couch in the living area. The temperature curve over time is determined for both seating positions for the "tile stove in central position" and "tile stove sideward" variant. The temperature curves are shown in Figure 3.

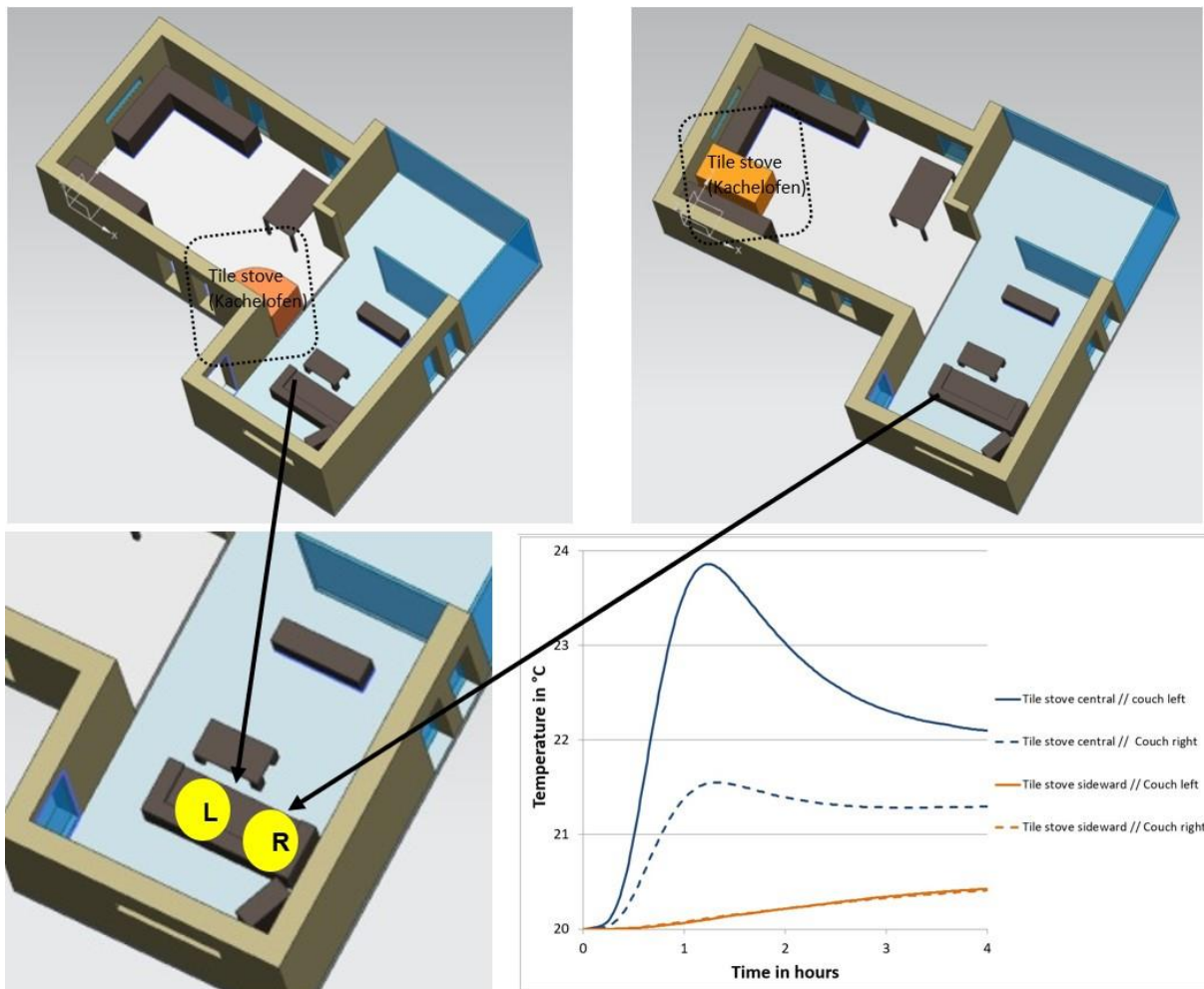
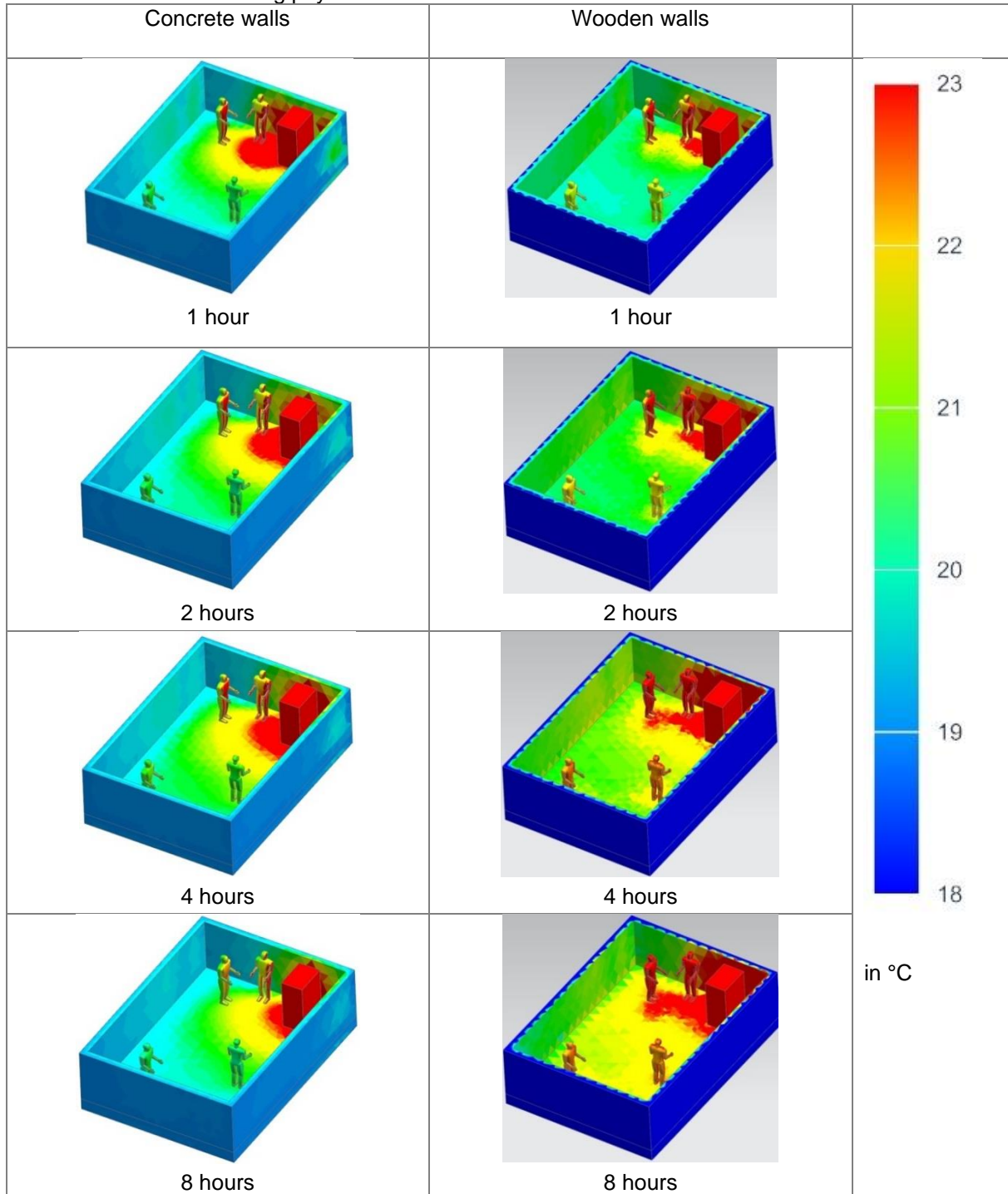


Fig. 3  
Effects on stove position

The influence of building physics was also examined. Concrete and wood were varied for the walls. The air volume and the geometry of the solid volume are identical in both wall structures. The temperature on the outside of the wall is selected so that the heat transfer for both materials is equivalent to the stored heat transfer coefficient. When comparing the wall structures made of wood and concrete, differences in surface temperatures and air temperatures can be determined. Due to the higher heat capacity and the higher thermal conductivity of concrete, more energy is stored in the wall surfaces than in the wall structures made of wood. As a result, the air temperatures in the wooden wall structures are 2 to 3 ° C higher than in the example with concrete walls, shown in Table 3.

Table 3 – Effects on building physics



#### 4 Outlook and future research question

The results of the research project provide a good and sound basis for the "Tile Stove System". This means that in the future the tile stove can be viewed as a "black box" for a detailed examination of the interactions of tile stoves in living rooms or entire building units and to promote traditional tile stoves as whole house heating. For this, however, it is necessary to consider longer periods of time (longer than the most commonly considered 12 hours). This requires long calculation periods and targeted simplifications in the models. In addition, consideration of the current weather conditions and weather forecasts can be relevant for the consideration of the comfort in the entire building. Another aspect is the interaction with ventilation systems in modern residential buildings and the distribution of heat via these systems.

In order to ensure a well-founded proof of fire safety issues, systematic practical tests in combination with simulation models would have to be carried out. A precise validation of these models is essential in such questions.

The work carried out in this paper forms the basis for future considerations. With the help of a 2D model, the heating output of a previously defined substitute gas for wood is validated. A CFD simulation is then carried out for a 3D model, taking the combustion into account. A 1D model for the flame is to be derived from this, which depicts the detailed combustion in a simplified manner. The model obtained will depend on some input parameters, such as the mass flow of the inlet air and have the character of a transfer function. Ultimately, this function will be used to be able to calculate 3D models of tile stoves with a reasonable amount of effort.

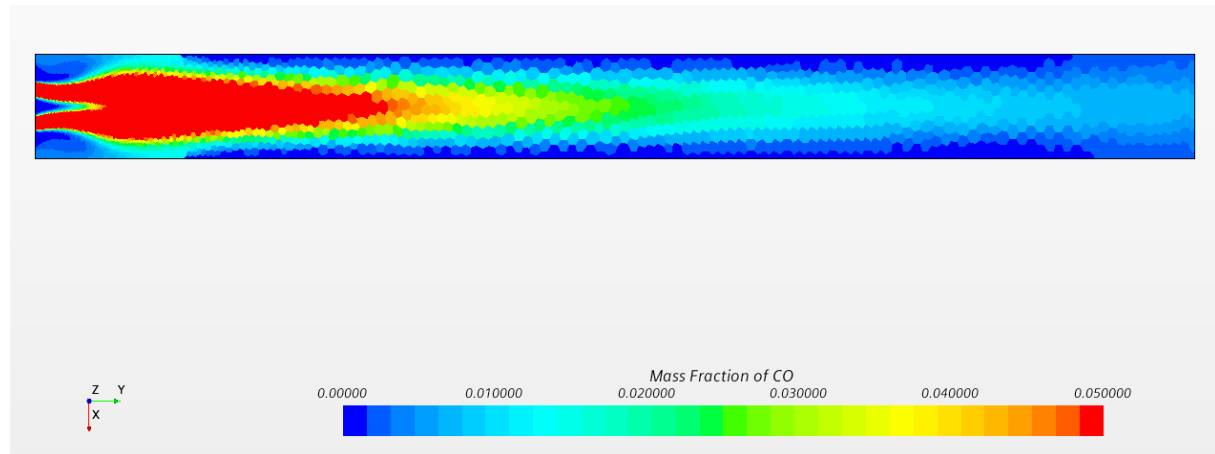


Fig. 4  
Extract of future results, mass fraction of 2D combustion analysis

Another aspect for possible future research questions is the linking of the relevant or selected comfort aspects in a simulation model in order to be able to make more targeted statements "at a glance" and to derive conclusions. These future considerations take place promptly and are funded by Austrian Research Promotion Agency (FFG) in a further project.

## 5 References

- [1] Simcenter 3D 2020.1, Thermal Solver Reference Manual, Maya HTT, 2019
- [2] Simcenter 3D 2020.1, Flow Solver Reference Manual, Maya HTT, 2019
- [3] Testo GmbH, Type: NiCr-Ni sheathed thermocouple - type K, Compensating cable: NiCr-Ni, Measurement accuracy: class 1
- [4] Manufacturer: FLIR, Model: i60, Serial number: 399021773

# **Increasing Product Reliability with Reduced Order Models**

*Dr John Parry, CEng. Dr Robin Bornoff, Byron Blackmore, John Wilson,  
Doug Kolak  
Mentor, a Siemens business*

## **SUMMARY**

This presentation describes the application of a novel Model Order Reduction approach for the construction of Dynamic Compact Thermal Models. With respect to previous approaches, this methodology allows reducing the complexity of the constructed models, from quadratically to linearly dependent on the number of independent heat sources. In such a way, the approach allows constructing Dynamic Compact Thermal Models practically without limitations on the number of heat sources.



## 1: Why Reduced Order Models?

Reduced Order Models (ROMs) offer considerable reductions in the size of the computational model while preserving the accuracy of the 3D model from which they are derived. They are Boundary Condition Independent (BCI), and so support the imposition of boundary conditions for downstream simulation. ROMs are orders of magnitude faster to solve. So much so, that they make previously impractical workflows feasible. An additional advantage is that internal details of the model can be hidden to protect sensitive IP, so BCI-ROMs have the potential to proliferate the supply chain.

## 2: BCI-ROM Workflows & Validation

BCI-ROMs are extracted as a matrix that represents a 3D conduction model with an unlimited number of heat sources. The technology is an extension of the FANTASTIC method pioneered by Prof. Lorenzo Codecasa [1, 2].

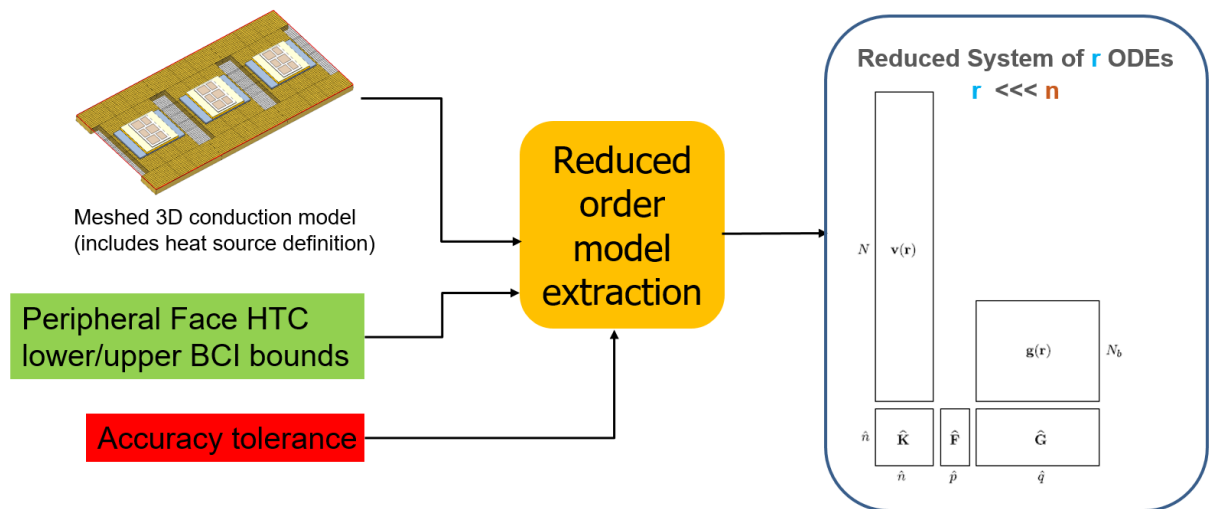


Figure 1: BCI-ROM Extraction Methodology.

The raw matrices are directly solvable in MATLAB or Octave, or can be converted into a Functional Mockup Unit (FMU) for use in 1D systems simulators such as Simcenter Flomaster. For a specific thermal environment they can also be converted into a SPICE thermal netlist sub-circuit or in VHDL-AMS for use in circuit simulators, making the electrical design flow “thermally aware”.

Not much needs to be said in terms of validation, as the mathematical method guarantees a user-specified level of accuracy relative to the original 3D conduction model that is high, with error bars in space and time below 1%. Examples are shown in the presentation.

### 3: Relevance of BCI-ROMs to Product Reliability

Most physical failure mechanisms in electronics increase with temperature, temperature gradients in space, and the rate of change of temperature with time. Temperature also affects circuit performance through electrothermal effects, with the situation getting more challenging as current densities in electronics have increased over time, leading to higher levels of Joule heating (DC IR drop). This is against a backdrop of electronics products finding increasing use in safety critical situations in aerospace & defense, and automotive and transportation. In the case of the latter, the environment for the electronics module is often hot and harsh. An industrial methodology is needed to ensure field reliability and prevent recalls and warranty costs.

### 4: Industrial Methodology for Power Electronics Reliability

Here we consider the inverter/converter module between the battery pack and motors in an electric vehicle, or hybrid electric vehicle.

#### a. Validation / Calibration of Detailed Model & ROM Extraction

The electrical test method is used to power and sense the semiconductor die and record the temperature change vs. time with high fidelity. This is repeated for the 3D conduction model, simulated in the test environment with the same powering condition. The temperature vs. time traces are converted into thermal structure functions that plot cumulative thermal capacitance vs. cumulative thermal resistance along the heat flow path to reveal the thermal structure of the part. These structure functions are compared, and a multi-curve fitting process is used to adjust nominated parameters in the model until the curves match to a high degree of accuracy (>99%).

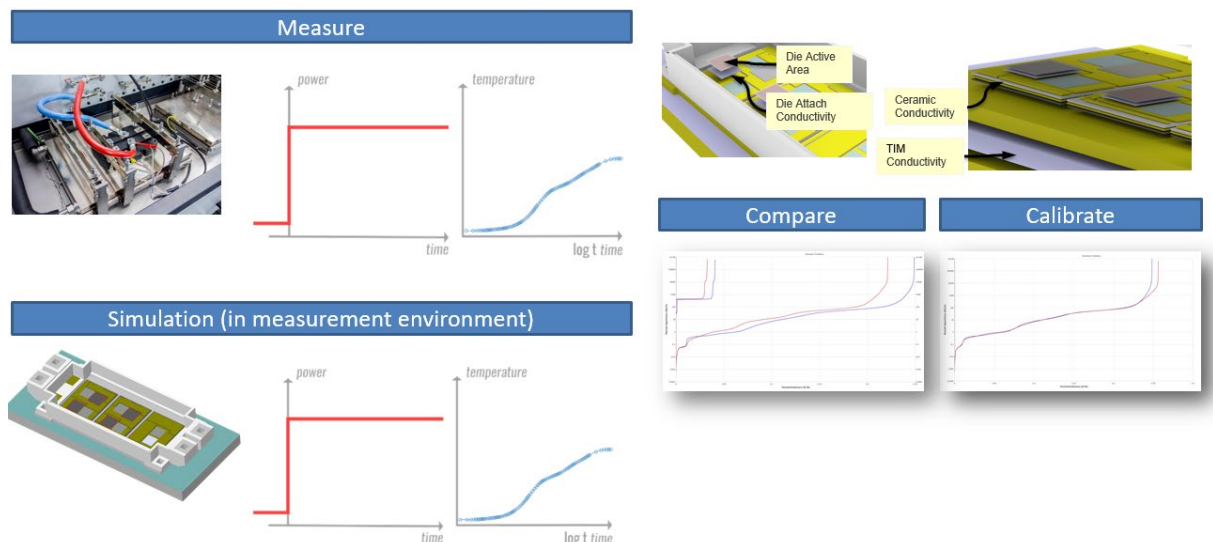


**Figure 2: Overview of Workflow to Create a Validated 3D Component Thermal Model.**

Once the 3D model is calibrated, the BCI-ROM is extracted as a FMU [3].

### **b. 1D System Simulation of the Vehicle Cooling System**

By simulating the electric vehicle's powertrain and cooling system, it is possible to determine the power required of the inverter over time based on a given vehicle configuration and driving cycle. This power can be applied as boundary condition to the FMU BCI-ROM, with that heat dissipating to the circulating coolant through the cold plate.

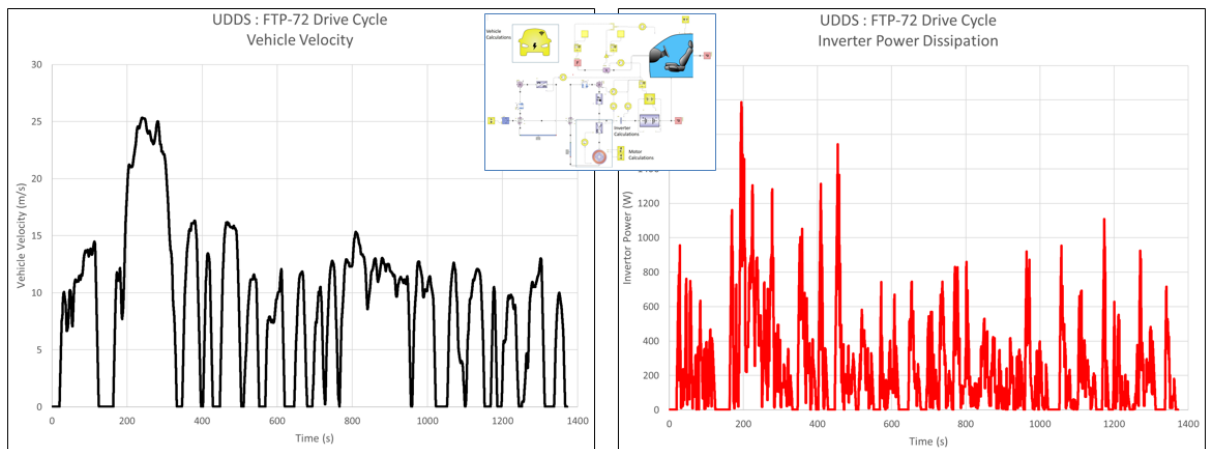


**Figure 3: Conversion of UDDS Drive Cycle into Power Dissipation for EV Converter/Inverter.**

The result is a temperature vs. time plot for each of the inverter chips in the module. Solving this with the 3D conduction model would take approx. 64 days, whereas with the ROM as part of the 1D system simulation it takes around 2.5 minutes, some 36,000 times faster and approximately 10X faster than real time.

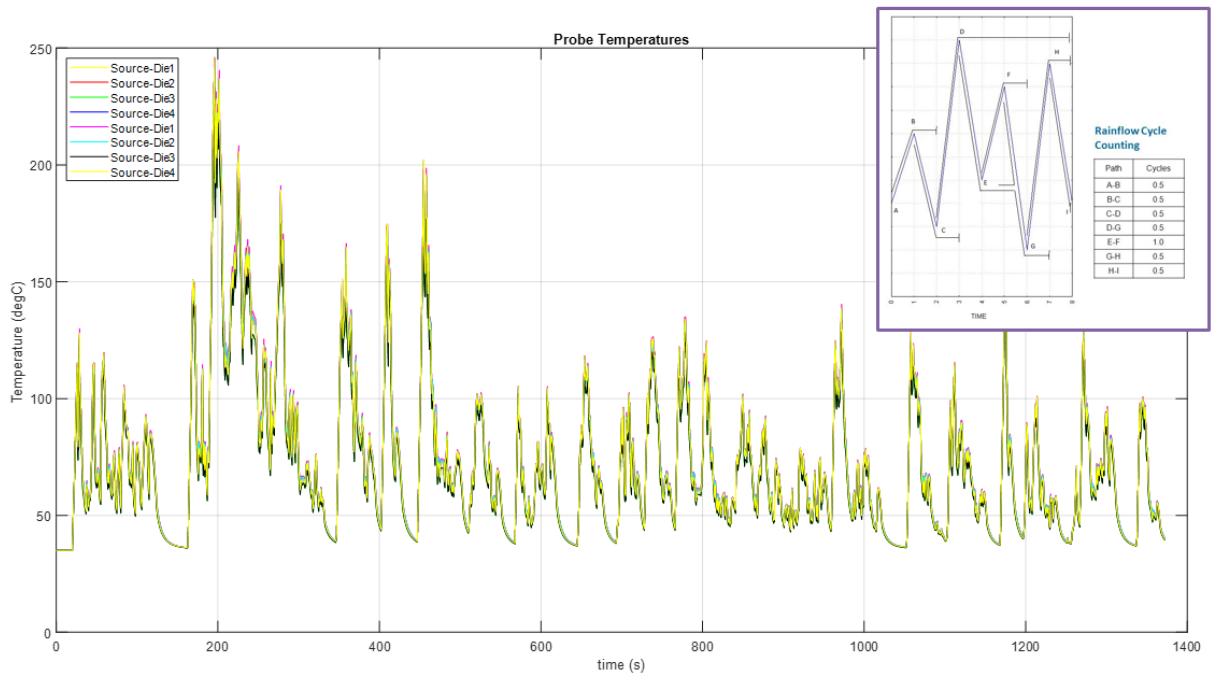


**Figure 4: IGBT Die Junction Temperatures Response across Drive Cycle with Rainflow Counting Inset.**

### c. 1D System Simulation of the Vehicle Cooling System

To predict field reliability requires a knowledge of failure rates under known (i.e. laboratory) conditions and field stress conditions. The temperature time history load conditions from the 1D system simulation are converted into stress-reversal fatigue cycles using rainflow counting. Lab data on lifetime as a function of temperature level and temperature swing per cycle, are used to calculate the life consumed by each stress-reversal.

## 5: Summary

BCI-ROM technology allows linear conduction problems with any number of heat sources to be solved with the almost same accuracy as the full 3D conduction model (>99%) and up to ~40000 times faster.

Accuracy of the ROM vs. the detailed 3D model is guaranteed by the mathematical method to match that specified by the user, with the 3D model itself calibrated against test data. ROMs hide the internal details of the original 3D model, allowing them to be transferred through the supply chain without concerns regarding intellectual property protection, and their boundary condition independent nature means that the BCI ROM can be used within any end user application environment. BCI-ROMs can be converted into a variety of formats for use within a range of downstream toolsets, such as computing environments like MathWorks MATLAB, electrical simulators like

SystemVision Cloud, and 1D system simulators like Simcenter Flomaster. Their accuracy and speed combine to facilitate hitherto impractical workflows, such as drive cycle field lifetime prediction

## REFERENCES

- [1] L Codecasa, V d'Alessandro, A Magnani, N Rinaldi, PJ Zampardi, “Fast novel thermal analysis simulation tool for integrated circuits (FANTASTIC)”, 20th International Workshop on Thermal Investigations of ICs and Systems (THERMINIC) article 6972507 United Kingdom, 2014.
- [2] “Partition-based approach to parametric dynamic compact thermal modeling” Lorenzo Codecasa, Vincenzo d’Alessandro, Alessandro Magnani, Niccolò Rinaldi, Andre G. Metzger, Robin Bornoff, John Parry. Microelectronics Reliability Journal, July 2017. DOI: 10.1016/j.microrel.2017.06.059
- [3] <https://fmi-standard.org/>.

# **The story behind building the world's fastest fully electric aircraft**

*Sabrina Hafid (ANSYS UK Ltd)*

## **SUMMARY**

Electrification is a subject which is on everybody's mind and Rolls-Royce is leading a small group of companies including Electroflight and YASA Motors who are wishing to emulate the VW Pike Peak success by building the world's fastest high-performance, full electric aircraft. The project, named ACCEL (Accelerating the Electrification of Flight) is also funded by the UK government (Aerospace Technology Institute).

In this context, the performance of the cooling system for the numerous battery packs on board must ensure maximum performance from the system in the space available. ANSYS was asked to optimise the design of the manifolds splitting the flow to the battery heat exchanger plates to ensure even flow split to each plate and minimise pressure drop. A two-staged workflow was chosen for this study:

- First, a visual rapid design of the fluid volume shape using an interactive GPU accelerated physics solver. This allowed to reach an optimal flow split.
- A second stage using traditional CFD to validate the flow split and perform an adjoint optimisation to minimize the pressure drop. This workflow enabled to obtain optimal manifold shapes that achieved an even flow split and an adjoint optimisation that reduced pressure drop up to 45%.

## 1: Background

The battery assembly, for the project ACCEL, is a large, energy dense assembly with one of the highest power densities in this industry. A crucial aspect of the project success is managing battery thermal performance, throughout the aircraft operation.

The batteries are assembled from individual, high performance cells, into multiple sub-assemblies and strings, each with active cooling systems. The cooling system comprises a series of heat-exchanger plates, feed by cooling water, through a series of inlet and outlet manifolds. The coolant flow direction can be reversed, for a limited period of time.

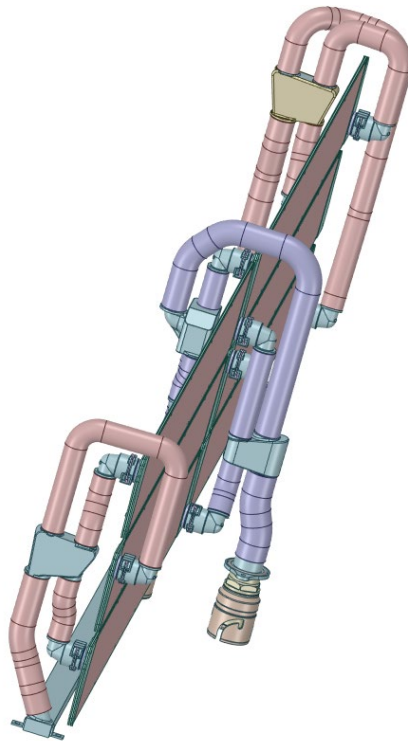


**Figure 1: Isometric view of the complete system with the 6 heat exchanger plates and the two-piping system. In the “normal direction” mode, the inlet system is composed of a main pipe feeding the fluid to two manifolds or plenums (purple) and two manifolds (red) collecting the fluid from the heat exchanger to the outlet**

The design of the inlet and outlet manifolds, in both forward and reverse flow, with a limited space envelope, an even flow split and with minimum pressure loss, is essential for the cooling system performance. In addition, the project, as a whole, is running to very tight timescales, so a fast turnaround at all stages is essential.

The aim of this study was to simulate the flow in the supply and return pipes and plenums which connect to the heat exchangers and to optimise the design of these components. The primary objective was to ensure that the coolant flow is divided equally amongst the six heat exchangers. A secondary objective was to minimise the pressure drop in the plenums and pipes which acts as a parasitic power demand on the feed pump and electrical system.

There was no restriction imposed on the complexity of the derived manifolds, as the intention was to make use of Additive Manufacturing for these parts.

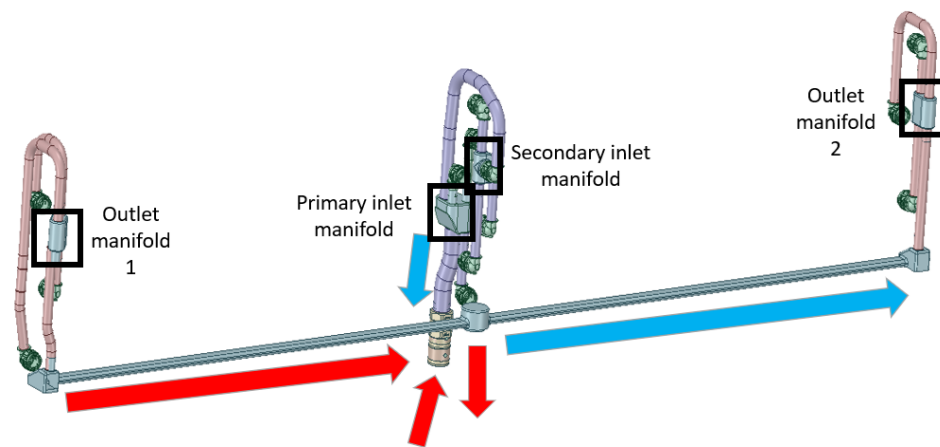


**Figure 2: Manifold and piping systems view – the red arrow describes the direction of the fluid in the normal direction while the blue arrow describes the reverse flow operation**

## 2: Method

The first stage involved a rapid design exploration of the manifold's fluid volume shape. These shapes needed to guarantee a balanced distribution of the fluid to the heat exchangers. For this step, a GPU solver was used to provide fast feedbacks on the state of the flow. The manifold's shapes were first optimized, considering no interaction with each other, then, the shapes were "refined" considering the rest of the system. A parameter study available inside the tool was also used to find a good position for the piping around the manifolds and a sensitivity to the mass flow rate was performed to investigate the robustness of the design.

A second stage involved a validation of the chosen design using traditional CFD tools and an Adjoint optimization to check if the pressure drop could be reduced by morphing the mesh of the chosen fluid volume.



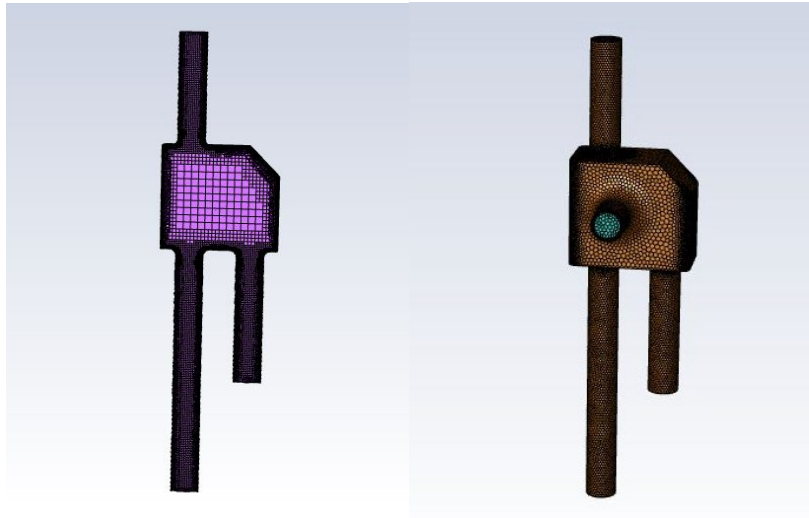


Figure 3: Secondary inlet manifold and piping poly-hexcore mesh

### 3: Results

An adjoint optimization on the pressure drop was performed during several iteration loops to obtain the optimal shape. An iteration loop is composed of a CFD analysis followed by an adjoint calculation and a mesh morphing step.

After nine iterations loops, the pressure drop was decreased up to 46% as seen on Figure 4.

Design Iterations	Pressure drop outlet 1 [Pa]	Pressure drop outlet 2 [Pa]	Pressure drop outlet 3 [Pa]
Design 1	420.4	418.5	409.7
Design 3	336.3	329.6	318.0
Design 5	285.4	277.2	272.5
Design 7	235.0	238.2	238.0
Design 9	223.9	224.8	226.5

Figure 4: Pressure drop results at the three branches of the secondary inlet manifold after a design iteration – Simplification by considering only one manifold

The final design considering the full system was simulated in a traditional CFD tool and the results for the flow in the normal direction are shown on Figure 5 below. The six outlets correspond to the entrance of the six heat exchangers.

<b>Monitors</b>	<b>Traditional CFD Results</b>
Crossflow (kg/s and L/min)	0.32025/18
Outlet 1 (kg/s and L/min)	0.053/2.98
Outlet 2 (kg/s and L/min)	0.054/3.04
Outlet 3 (kg/s and L/min)	0.054/3.04
Outlet 4 (kg/s and L/min)	0.053/2.98
Outlet 5 (kg/s and L/min)	0.052/2.92
Outlet 6 (kg/s and L/min)	0.054/3.04

**Figure 5: Mass flow rate results calculated at each heat exchanger**

The difference between the modules that are getting the least and the most flow is 3.5% which was below the tolerance of Electroflight for this system.

#### **4: Discussion**

This project has demonstrated that a combined approach of fast-interactive physics simulation and adjoint optimisation, can rapidly derive an optimal solution, replacing the need for otherwise lengthy parametric study.

Subsequent adjustments to the manifold arrangement, required due to changes in the feed pipes and adjustments to the space envelope, were easily addressed by revisiting the workflow process.

# **Artificially Intelligent segmentation of a shock absorber X-ray CT scan and beyond**

*E. Mezitis*  
*(BETA CAE Systems, China);*

*E. Karatsis*  
*(BETA CAE Systems, Greece);*

*P. Michailidis*  
*(BETA CAE Systems, Greece);*

*L.E. Baksiova*  
*(BETA CAE Systems, Greece);*

## **SUMMARY**

In this work, a CT-scanned shock absorber is virtually disassembled to inspect its anatomy. The complete process from CT data to CAE model is demonstrated through a realistic reverse engineering scenario ensuring high-quality meshed model for consequent finite element simulations. Artificially Intelligent algorithms used for image segmentation greatly reduce required user effort, while improving segmentation quality. Finally, a CAE model is created and the capabilities of the reverse engineered object are integrated through a fictitious durability analysis.

## **1: Background**

Advances in X-ray Computed Tomography (CT) have been remarkable during the last decade and have established the technique not only in biomedical applications, but also in other engineering fields. From Cone-beam X-ray CT (CBCT) scanners that achieve resolution of micrometers for nano-structure inspections, to full vehicle scanners, X-ray CT technology is present in most sectors of the automotive industry. It is rendered a suitable technique for product quality control, design evaluation and in general, a means of “digitizing” an existing, real object. In the Computer Aided Engineering (CAE) world, digitized real objects are ultimately converted into finite element models for realistic simulations and fast product development. X-ray CT provides a powerful, non-destructive method for achieving this even for complex multi-material assemblies. Limitations exist and are well known; however, emerging techniques in the field of tomography post-processing allow for minimization of uncertainty in material labelling and improvement of accuracy in segmentation.

## **2: Aim – Setting the target**

The target of the current study was to evaluate qualitatively and quantitatively the performance of a real object without destructing it, fully taking advantage of the information provided by a CT scan of it. This was achieved by disassembling it virtually and revealing its individual parts as well as by creating a CAE model that was further used in a fictitious durability analysis.

A key role during the progress of the works for this project was played by

- the leveraging provided by AI tools of RETOMO (BETA CAE Systems), the software for turning pixels to objects, enabling fast and accurate reconstruction of FE-data from CT-image,
- the complete and powerful range of mesh handling/processing tools available in ANSA (BETA CAE Systems), the pre-processor.

## **3: Segmentation process**

A 200 $\mu$ m resolution CT-scan of a shock absorber, provided by TECOSIM, was reverse-engineered in RETOMO [1]. Initially, the automatic material thresholding method was used to segment the object. Three different materials were assumed representing air, lower density material (assumed as oil) and higher density material, which included all the high density materials of the absorber (most of them were metallic parts). The standard seed-grow procedure was used to perform the initial material segmentation.

Despite the fact that this CT-scan was of high quality, there were still regions of inadequate quality. These artifacts were:

- artifacts due to window stitching probably from the reconstruction process
- beam hardening and scattering effects due to varying thickness and density.

In some regions, traditional tools (morphological filters and manual tools) were efficient in fixing these problematic areas. However, in other regions where these tools generated inadequate results, RETOMO's AI (Artificial Intelligence) engine was employed. This was a two-step process which required, first, a training phase for the AI engine and then the application phase. For the AI engine training, a mix of successfully and poorly segmented regions was marked on the image. These regions covered small portions of several slices, oriented in different coordinate axes. Within those regions manual tools were employed to fix any errors (see figure 1). Subsequently these regions were used as training data for the AI engine.

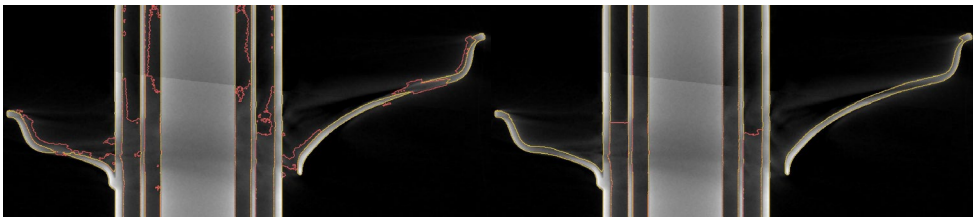


Figure 1: Slice before (left) and after (right) manual corrections

In the application phase, 3D regions of the segmented image were selected and the trained AI engine was simply applied. In figure 2 the improvement on the resulting mesh is shown achieved by the AI driven segmentation alone (i.e. no other filters or mesh processing has been used). This AI-driven segmentation approach led to approximately 95% time savings compared to manual material segmentation correction. Also, due to the semi-automated nature of the AI-process, a consistently high quality result was obtained. In contrast, a purely manual effort would show degradation in quality after some user fatigue.

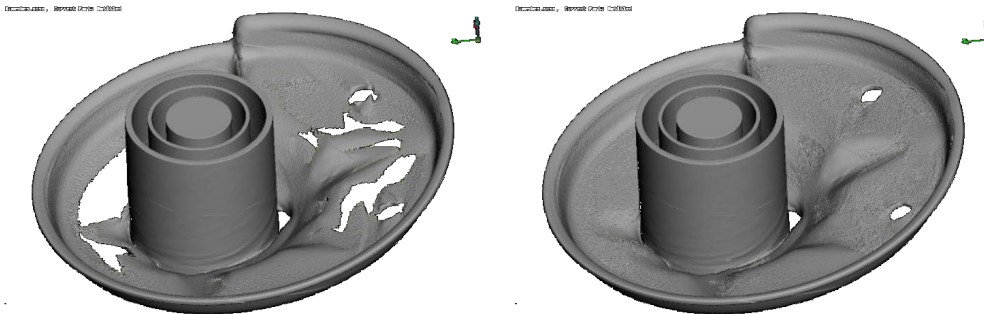
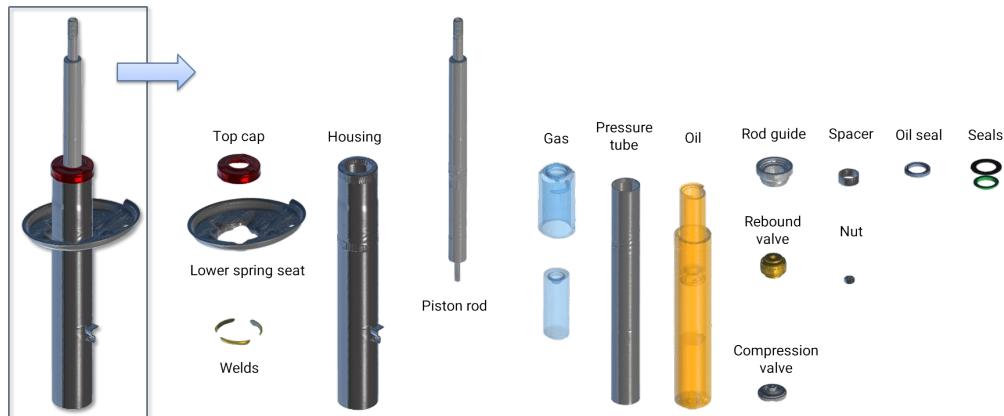


Figure 2: Spring seat mesh prior to (left) and after (right) applying AI segmentation

The result of the aforementioned procedure was a well segmented object into two different materials. However, parts of the shock absorber made of the same material were still stitched together. So, the next step was to isolate each part one by one with the aid of the manual tools. This was a time consuming process. Except for each part isolation, the welds that support the spring seat onto the tube, were also separated for the durability analysis. The final product of the segmentation was a watertight mesh surface for each part (see figure 3).



**Figure 3: Reconstructed individual components of the shock absorber item after segmentation in RETOMO, post processing in ANSA and photorealistic shading in META**

#### **4: Post-processing of segmented parts**

The surface meshes were then post-treated in ANSA [2]. There, it was possible to acquire some measurements of the shock absorber, such as the volume of the oil existing within the chambers and the diameter and length of the absorber. Feature-lines were introduced on the model, in order to ensure that during re-meshing the main features will remain intact. Then, the surface mesh was reconstructed to achieve a uniform element length. A zone with a finer mesh was created around the welding region for the durability analysis.

#### **5: Durability Analysis**

To highlight some of the possibilities of the reverse engineered object, a fictitious durability analysis of the spring seat welds was selected to be performed. The aim of this analysis was to compare the model's stress behavior when welds are replaced by the "ideal" welds as proposed by the ANSA tool. The welds were isolated during the segmentation and a separate surface mesh was created. This mesh was post-treated in ANSA along with the rest of components. The mesh size was finer in the region around the welds and coarser further away.

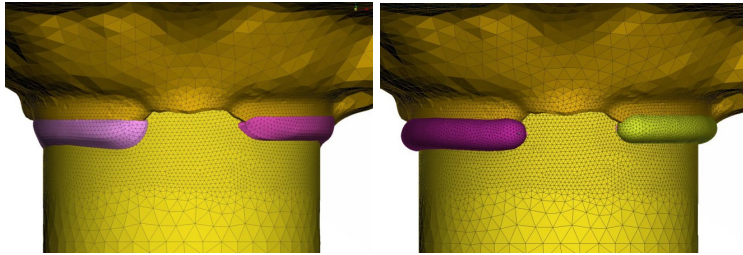


**Figure 4: Real (left) versus ideal (right) welds**

The parts that took place in the durability analysis were three: the outer tube of the shock absorber, the spring seat and the welds. The top and bottom regions of the tube were constrained; a fictitious load was distributed at the spring seat while gravity forces were neglected. Once the model was set up, it was subjected to a static analysis in Abaqus/Standard (Dassault Systèmes) [3] to obtain the stress distribution and concentration in the welds region.

Furthermore, a second model was created, whose welds were replaced by the “ideal” welds as proposed by the ANSA tool (see figure 4 for a depiction of the two different models). Following the simulations, the results were processed in META. The two models’ stress behaviour was compared (see figure 5). As expected, the stress distribution in the welds region is different in the real welds model versus ideal welds model. Similarly, one could easily modify any component’s design (e.g. using morphing functions available in ANSA) and re-evaluate the performance of the component or the assembly.

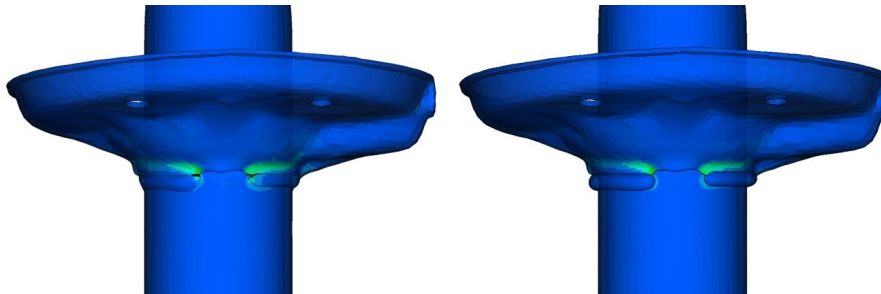


**Figure 5: Stress distribution on real (left) and ideal (right) welds**

## **6: Conclusions**

The current study demonstrates the complete process from pixels to running the generated CAE model in a fictitious durability scenario. Exploiting AI-assisted tools image segmentation is economical and consistently of high quality, regardless of the software user. Resulting meshes can easily be converted to versatile CAE-friendly models using recent advances in feature lines handling. Once obtaining such a model, several options are available. In this study, the effect of geometrical imperfections of a weld in a durability scenario is shown. The engineering value of modifying other design parameters would be equally straightforward to achieve.

## REFERENCES

- [1] BETA CAE Systems SA, (2019). *RETOMO version 20.1.0 User's Guide*.
- [2] BETA CAE Systems SA, (2020). *ANSA version 20.1.1 User's Guide*.
- [3] Dassault Systèmes, (2019). *Abaqus 2019 Abaqus/CAE User's Manual*.



# Process Optimisation in Robotic Arc Welding by Computational Fluid Dynamics

*Alessio Basso – TWI Ltd*

*Valerio Carollo – TWI Ltd*

*Tyler London – TWI Ltd*

## **SUMMARY**

Gas Metal Arc Welding (GMAW) is a joining process using the heat produced from an electric arc between a consumable metal wire electrode and the metallic work pieces to be joined. As a result, both wire and workpiece simultaneously melt, which will form the solidified joint. GMAW is well-established in industrial fabrication, particularly through the GMAW-Pulse variant – where electrical pulses are alternated between the high and low current to reduce undesired spattering.

Present requirements in industry tend to optimise costs, productivity and quality. Therefore, robotic arc welding has received increasing attention, owing to its capability of enabling more consistent, repeatable fabrications through the precise control of all the process parameters – e.g. wire feeding rate, voltage, travel speed and shielding gas inflow. As a result, the weld quality is dependent on the balance between the above parameters.

In manual welding, defects can be identified, controlled and mitigated by the welder, whereas in robotic arc welding, parameters are precisely specified a priori. Therefore, extensive experimental test programmes can be performed where different welding parameters are varied and functional correlations with the weld quality metrics are determined. Alternatively, engineering analysis tools, especially Computational Fluid Dynamics (CFD), can be used to perform virtual experiments.

In this work, a multi-physics CFD model was built to predict the weld melt pool shape in GMAW with given parameters, e.g. travel speed, power input, operating temperature, wire feeding rate. Results from numerical analysis will be fed into the robot algorithm which uses the prescribed process parameters to reproduce the same weld shape as from simulations.

## Background

The GMAW parameters have been widely investigated in the literature, these include the arc plasma on top of the weld pool (Azar, et al., 2012; Murphy, et al., 2009), or the interaction between the shielding gas and the metal vapour from the weld pool (Sharma, et al., 2014). One-pulse-one-drop GMAW simulations have attracted interest due to the reduced spattering of the weld pool (Cho, et al., 2019; Cho, et al., 2013). Parameters such as current, voltage and arc size are tuned and molten pool dynamics can be simulated and captured through high-speed flow visualisation.

Similar approaches were undertaken for narrow gap gas metal arc welding (NG-GMAW) (Duan, et al., 2018), where a dynamic model was implemented to simulate a rotating welding arc. Other methods to simulate the weld characteristics included artificial neural networks for automatic detection of the gap width (Vivek, et al., 2019; Fabry, et al., 2018; Cruz, et al., 2018). Similarly, Multiphase CFD simulations were implemented for prediction of similar processes, such as YAG Laser + GMAW (Kubiak, et al., 2016) and KPAW-GMAW (Wu, et al., 2020).

## Modelling approach

The current analyses characterise each mechanism separately: a) Droplet inlet mass; b) Localised Gaussian heat source; c) Pressure source due to the Joule heating effect. Once the model was verified, calibration of the full model including all the above contributions was performed to fine-tune model parameters. Finally, a Design-of-Experiment analysis was undertaken to establish the most statistically significant working parameters and to build up response surface functions relating inputs and outputs.

## Experimental Validation

Validation of the numerical models is being undertaken through the comparison of liquid fraction contours from CFD and the solidified weld shape from the workpiece sections. Weld metrics, such as penetration, toe angle, bead width and bead height, are also being assessed.

## Results and conclusions

Preliminary results show encouraging match from simulations and data from experiments, suggesting that the model setup is correct to represent the flow physics involved in the GMAW process. Owing to delays incurred through the COVID-19 situation, the validation has been delayed.

## References

- Azar, A., Sigmund, K. & Akselsen, O., 2012. Determination of welding heat source parameters from actual bed shape. *Computational Material Science*, Volume 54, pp. 176-182.
- Cho, D.-W., Park, J.-H. & Moon, H.-S., 2019. A study on molten pool behaviour in the one pulse drop GMAW process using computational fluid dynamics. *International Journal of Heat and Mass Transfer*, Volume 139, pp. 848-859.
- Cho, D.-W., Song, W.-H., Cho, M.-H. & Na, S.-J., 2013. Analysis of submerged arc welding process by three-dimensional computational fluid dynamics simulations. *Journal of Materials Processing Technology*, Volume 213, pp. 2278-2291.
- Cruz, J., Torres, E. & AbsiAlfaro, S., 2018. Modelling and control of weld height reinforcement in the GMAW process.. *Mechanical Science Engineering*, Volume 40, p. 164.
- Duan, B. et al., 2018. Parameter analysis and optimization of the rotating arc NG-GMAW welding process. *International Journal Simulation Model*, 17(1), pp. 170-179.
- Fabry, C., Pittner, A. & Rethmeier, M., 2018. Design of neural network arc sensor for gap width detection in automated narrow gap GMAW. *Weld world*, Volume 62, pp. 819-830.
- Kubiak, M., Piekarska, W., Saternus, Z. & Domanski, T., 2016. Numerical prediction of fusion zone and heat affected zone in hybrid Yb:YAG laser + GMAW welding process with experimental verification. *Procedia Engineering*, Volume 136, pp. 88-94.
- Murphy, et al., 2009. CFD Modelling of arc welding - The importance of arc plasma. *Seventh International Conference on CFD in the Minerals and Process Industries, CSIRO*.
- Sharma, Y., Kini, C., Deepak & Shamrao, J. P., 2014. A computational fluid dynamic study on transient thermal characteristics of two-phase gas metal arc welding process. *International Journal od recent advances in mechanical Engineering*, 3(2).
- Vivek, S., Chandrasekaran, M., Samanta, S. & Thirugnanasambandam, M., 2019. *Artificial neural network modelling of the weld bead characteristics during GMAW of nitrogen strenghtened austenitic stainless steel*. s.l., s.n.

Wu, D. et al., 2020. Analysis of heat transfer and material flow in hybrid KPAW-GMAW process based on the novel three dimensional CFD simulation.. *International Journal of Heat and Mass Transfer*, Volume 147.

# **A value-focussed approach to the deployment of Simulation Data Management in Aerospace**

*Mark Norris, Consultant, theSDMconsultancy*

*Lionel Fine, Predictive Stream Leader, Airbus Helicopters*

*Gwenael Neveu, Consultant, Digital Product Simulation*

**Keywords : Simulation Data Management, System of Record, SDM, Simulation Process and Data Management, SPDM, Simulation Management, Simulation Lifecycle Management, SLM**

## **SUMMARY**

Simulation Data Management (SDM) is a class of application pioneered by Automotive and Aerospace OEMs and Tier 1 suppliers that rely upon simulation within their product development processes to achieve industry-leading performance. Typically SDM has been deployed for critical processes such as automotive crash simulation or for new simulation processes such as Virtual Testing of critical systems. This ensures that critical simulation processes are secured and has been found to yield productivity and engineering throughput improvements.

While SDM solutions have proved highly effective at leading companies, the overall adoption of information systems to manage simulation data by simulation engineers is still extremely low at 1%-2%. Two reasons for low uptake are the cost and time to implement SDM and negative experiences of software offerings that lack basic SDM capabilities.

Best practice to deploy SDM has been to implement one end-to-end process at a time, providing end-to-end process traceability. There are two principal disadvantages with this sequential approach: Firstly, simulation engineers working in less critical domains have to wait potentially years to gain benefit from SDM. Secondly, digital traceability of important simulation data-sets is incomplete until all domains have been implemented in SDM. This is unsatisfactory to support regulatory compliance in safety critical industries.

We proposed a different value-focussed approach: to deploy a System of Record (SoR) for simulation data on an SDM platform for all simulation domains. This delivers digital traceability of important simulation data-sets and provides value to all simulation engineers and to the enterprise immediately. The innovation here is to adopt the MOSSEC approach as an internal data standard first as the basis for a System of Record as well as preparing its use for external exchange.

Further benefits of this approach are that a repository of simulation information is valuable input to the deployment team and will accelerate the SDM roll-out.

## 1: Introduction

Simulation Data Management (SDM) is a class of application pioneered by Automotive and Aerospace OEMs and Tier 1 suppliers that rely upon simulation within their product development processes to achieve industry-leading performance. It allows them to build and maintain the Digital Thread of both the data used and the decisions taken to predict the performance and lifetime of engineered products.

While SDM solutions have proved highly effective at a small number of leading companies, the overall adoption of information systems to manage simulation data by simulation engineers is still extremely low at 1%-2%. The SimBest study[1] conducted interviews of 170 simulation engineers in UK companies and found no one using an SDM or other solution to manage their simulation data-sets. The study concluded that "there is little formal use of SPDM even though it is seen as important and necessary" and that "SPDM and SPLM systems are perceived as very costly".

Best practice to deploy SDM has been to implement one end-to-end process at a time, providing end-to-end process traceability and enabling a simulation team to migrate from notebooks and shared drive file systems to a robust information system. Typically SDM has been deployed for critical processes such as automotive crash simulation or for new simulation processes such as Virtual Testing of critical systems. This ensures that critical simulation processes are secured and has been found to yield productivity and engineering throughput improvements. But because large simulation organisations typically have 100 simulation applications, complete SDM deployment takes several years.

There are two disadvantages with this sequential approach:

- Other simulation engineers have to wait potentially years until the project phase in which their process chain will be implemented in SDM to gain any benefit from SDM
- Digital traceability of simulation results is incomplete until all domains have been implemented in SDM which is unsatisfactory in safety critical industries.

## 2: Project Approach

The first step was to carry out a survey, requesting input from the hundreds of simulation engineers and their managers. The main request from the survey was a system in which engineers could archive their simulation work and find it again at a later date. In the aerospace industry, similar simulations are run several times at the different stages of a program: concept evaluation, preliminary design, detail design, design validation/virtual test, design validation based on loads from flight testing, aircraft performance upgrades and in-service. There is therefore a significant benefit both to simulation engineers and the organisation if all the formal information related to a simulation is catalogued in a system of record and the key files are immediately accessible for re-use. Aircraft program staff also request a formal record of all simulations used to support certification. So there was a common requirement for a catalogued simulation archive.

A simulation archive has apparently nothing in common with a classic SDM approach of end to end deployment by domain. Best practice to deploy SDM has been to implement one end-to-end process chain at a time with integration of every application used in the process chain. This enables the transition from notebooks and file systems for the team responsible for this process chain, provides

full traceability and assures data quality. This approach enables the most critical processes to be implemented first. The main disadvantage is that some simulation engineers have to wait potentially years until the project phase in which their process chain will be implemented in SDM to gain any benefit from SDM

Based on the common requests from the engineers, their managers and the programs for a single source of simulation data, we re-evaluated how SDM technology could be deployed for an aerospace OEM. Major research programs such as CRESCENDO propose the MoSSEC standard based around the Simulation Study for collaboration across the virtual aerospace enterprise.

We examined the idea to use the MoSSEC study construct as the basis for a simulation System of Record (SoR) which we intend to deploy for all domains as the first step in an SDM deployment. That is to say to use MoSSEC as the basis for an internal data standard rather than just as an exchange standard.

Analysis of a System of Record-based deployment approach reveals that it has many advantages compared to the classic SDM deployment approach one domain at a time:

- a system of record (SOR) based on an SDM solution can be deployed rapidly, in less than a year
- a SOR provides value to all simulation engineers who have a single source of simulation data and a single place to archive their simulations
- an SOR provides digital traceability of all simulations supporting business decisions or certification
- application integration is not required in the first instance, reducing the cost of the first deployment phase.
- such a deployment leads to standard simulation data being stored and accessible in the SDM solution, saving analysts' time, supporting multi-discipline collaboration and preparing for the deployment of SDM one process chain at a time
- this approach enables the SDM implementation team to ramp up their skills by implementing the less technically demanding SOR functionality first.
- This implementation approach is particularly appropriate in an aerospace context in which the same simulation is repeated at each project phase and then potentially while the aerospace system is in-service.

Once the SoR has been deployed, the classic SDM deployment approach can be applied based on the urgency of the need for detailed SDM support in particular domains, see figure 1. Then frequently used processes can be automated based on need and potential benefits.

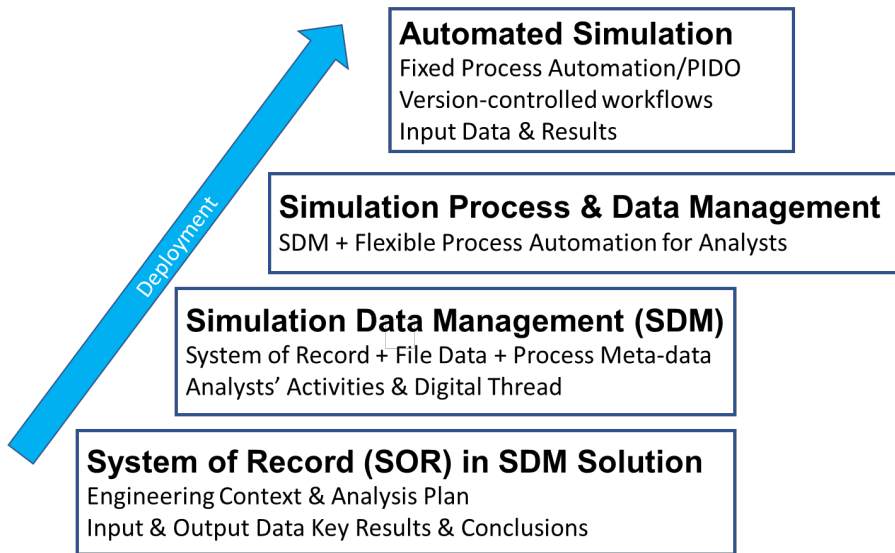


**Figure 1: System of Record based deployment approach**

The immediate value of System of Record-based deployment approach is shown in figure 2. In an aerospace context, this benefits the simulation engineers, the SDM deployment team and the enterprise.

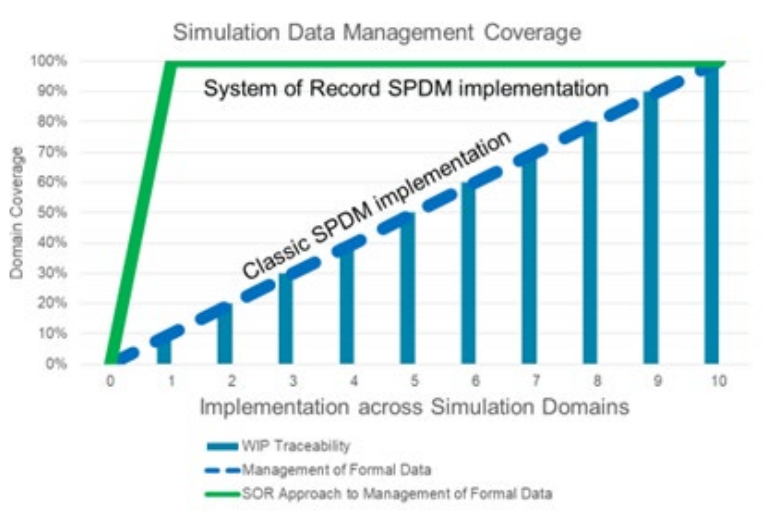


**Figure 2: Data management coverage from a System of Record based approach**

### 3: Conclusion

A System of Record based deployment of Simulation Data Management offers many benefits and has no obvious disadvantages, at least in the context of an Aerospace OEM. The only requirement is that the SDM solution must provide the core SDM capability of study management. Thus a fit for purpose SDM solution is as important for this approach as for the classic SDM deployment approach by domain.



# **Hardware And Software System For Managing The Life Cycle Of Gas Turbines**

*S.A. Akinin, A.I. Boltaev, D.S. Gluzdov, E.A. Dobretsov, D.O. Pimanov  
Satratek, Novosibirsk, Russia*

## **SUMMARY**

The paper presents the current progress of company Satratek, Novosibirsk city, Russia on setting up a digital twin for the one-stage one-shaft ground-based gas turbine engine with an annular combustion chamber. This product will allow to equip gas turbines that are transferred from planned to condition-based maintenance and are not serviced by the manufacturer with a modular system. The developed system is based on mathematical models that describe the gas flow and the behaviour of equipment materials in the combustion chamber under the cyclic and constant thermal loads and oxidation. Our modelling approach is to use network models at the system level together with the finite element procedures to estimate the residual life of individual system components. Thus, a software product that receives data from SCADA system and interacts between the modules had been developed.

## **1: Introduction**

At present, gas turbine plants are widely used in the Russian Federation and the rest of the world to generate electricity and heat, as well as in gas transportation. Most of these plants have a long operating time and are not serviced by the manufacturer. Also, maintenance and repair procedures are in transition from planned to condition-based.

This project will allow equipping gas turbines that are not serviced / warranted with a modular system to solve a wide range of industry tasks: early detection of emergencies, optimisation of the operational mode, predictive maintenance and repair, reduction of condition-based maintenance risks. To solve these tasks a hardware and software system is being developed.

The hardware and software system consists of the following elements: a modular system for collecting and storing information; an integrated model of a gas turbine that combines the models of critical elements; data analysis and predictive analytics module; software module for solving optimisation problems; graphical user interface for data visualisation and issuing recommendations.

The data gathering module collects data from sensors installed on a gas turbine. It is responsible for the conversion of signals from analogue to digital, buffering, pre-processing and data transfer. Data is collected from the SCADA and control system as well as additionally installed sensors. The data is stored for subsequent analysis.

An integrated physical and mathematical model of the turbine is deployed on several different levels of detail. It combines the simple network approach and nonlinear finite element (FE) analysis. The network model allows to estimate the working substance state, meanwhile, the FE method results are used to predict individual component life.

Hardware, software architecture and system-level models are designed for a gas turbine engine of a given class. At the same time, finite element models require geometry and material data that are specific to each device. Computational method to evaluate the residual life is being developed and can be used individually for a specific turbine.

## **2: Gas turbine maintenance optimization problem**

The design of the gas turbine engine in question includes an annular combustion chamber with a set of 24 burners. The engine is one-stage and one-shaft. The critical temperature-induced loads in the chamber are perceived by

removable metallic shields covered by thermal barrier coating. Cooling air mass flow rate goes through several holes in the flame tube and impinges on the shields inner unprotected surfaces to be cooled.

According to the design, the expected life of the heat shields is significantly less than the life of the turbine at large. Thus, the engine maintenance consists of periodically repeated inspections of the combustion chamber or blading section that are executed to preventively find components at risk and replace it before the failure. Alternating the large and small inspections allows minimising the system downtime by inspecting the turbine blades and barrier shields with different frequencies. During each small and large inspection, defective tiles must be found and replaced as the components that are most susceptible to wear. Finding the optimal intervals between the inspections with due regard for cost minimisation and breakdown risk control is the problem, which is being solved numerically. Some approaches to solving this problem can be found in the literature. [1]

A purely statistical approach to this problem can be implemented, but it requires a large amount of statistical data collected over the years of operation. In contrast, the physical and mathematical simulation of damage accumulation processes under random loading must be based on a representative number of laboratory tests to have predictive power. Moreover, not all the processes occurring in the combustion chamber could be treated with reliable and at the same time accessible calculation techniques.

### **3: Modelling approach**

To develop the numerical procedure that could predict the damage level of one shield with known running time the number of mathematical problems was established. The material models are being created for the nickel-chromium-based superalloy, the bond coat alloy and the ceramic. The models of alloys can also describe low-cycle fatigue and creep behaviour and could be implemented to the finite element analysis. The combination of ductile and creep damage can additionally be a point to predict crack initiation.

To convert real-time data received from sensors and the automation system into a spectrum of temperature loads for each of the components a network model of the turbine-is being developed.

Finite element modelling is performed for consumable components (heat shields) for typical loading cycles and their combinations. When assessing damage level to materials, transient thermal and structural analyses are performed.

Mechanisms that can cause spalling of the ceramic coating are complicated and as such are subject to various environmental factors. [2] The thickness of the temperature-grown oxide layer can be considered as one of the main parameters to defy the strength of a barrier coating. [3]

#### 4: Results

The Armstrong-Frederick model and Norton model were chosen, implemented and calibrated separately as main models for low-cycle fatigue and creep behaviour of Inconel 738LC superalloy. The system-level network model of the gas turbine Ansaldo Energia V64.3A in the Flownex Simulation Environment is developed and calibrated on the technical data sheets. To test the implemented software interaction between sensors, Flownex environment and reduced-order models obtained from the kerosene burner CFD simulation, a digital model of the fire resistance test stand was created and put to trial.

#### 5: REFERENCES

- [1] Martínez, A., Lara, G., Pascual, R., and López Droguett, E. (2015). 'Optimal Failure-Finding Intervals for Heat Shields in a Gas Turbine Combustion Chamber Using a Multicriteria Approach.' *ASME. J. Eng. Gas Turbines Power*. July 2015; 137(7): 072501. <https://doi.org/10.1115/1.4029202>
- [2] Evans, A.G., Clarke, D.R., and Levi, C.G. (2008). 'The influence of oxides on the performance of advanced gas turbines.' *J. Euro. Ceramic Society*. January 2008; 28(7); pp. 1405-1419. <https://doi.org/10.1016/j.jeurceramsoc.2007.12.023>
- [3] Meier, S.M., Sheffler, K.D., Nissley, D.M. (1991) Thermal barrier coating life prediction model development, phase 2. Contractor Report. NAS 1.26:189111.

# **A conceptual study of an externally cooled, high voltage underground cable crossing**

*Stephen M King*

*Industry Process Consultant Senior Specialist – Dassault Systemes UK Ltd*

## **SUMMARY**

The objective of the numerical simulation described in this paper was to assess the viability of using induced natural convection to cool underground, high voltage power cables that are in close proximity with each other.

Inevitably, with the continually developing UK power network infrastructure, new cable circuits may, in some cases, have to traverse existing underground circuits that have been operating successfully for many years. This can cause significant problems as underground power cables are carefully designed to be able to transmit the required amount of power without exceeding the limiting conductor temperature of 90 degrees centigrade. In cases where cable circuits are in close proximity, then some degree of mutual heating will exist and this must be assessed in order to ensure the integrity of the cables. In complex cable crossings, this is not a trivial calculation and generally requires numerical simulation by finite element or finite difference methods. If external, fluid-driven cooling mechanisms are also included, then this further complicates the calculation.

In order to mitigate this mutual heating effect on the cable circuits, one possible solution is to provide additional cooling via air-ducts that are placed between the cable circuits. These ducts are open to the atmosphere at either end and provide a mechanism for delivering air at ambient temperature to the cable circuits; the air flow being created by either induced natural convection or by forced convection using fans.

A numerical simulation of the heat transfer within the cables, ground and air-ducts was completed using Dassault Systemes's **3DEXPERIENCE** platform incorporating the 3DSFlow Navier-Stokes fluid dynamics solver. This provided the means to construct a three-dimensional model of the complete cable system including geometry and mesh generation, and to perform heat transfer simulations utilising conjugate heat transfer effects for both naturally induced and forced convection conditions. The post-processing of simulation results produced essential data indicating whether induced natural convection could be relied upon to provide adequate cooling for all likely seasonal operating conditions.

## 1: Model set-up and scenario

The general arrangement for the simulation model comprised two, established 132kV power circuits (total of 6 cables) that were being crossed by a single, new 400kV power circuit (total of 3 cables) at a shallow angle. The 400kV circuit passes underneath the existing circuits with a number of air ducts placed in-between them to provide a cooling mechanism via the flow of air; either by naturally induced convection or by forced convection.

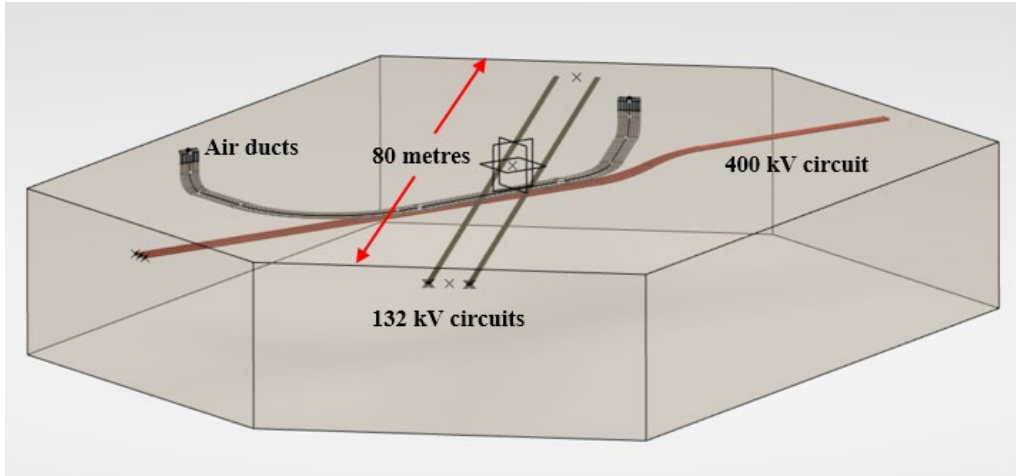


Figure 1: General arrangement of simulation model

Heat generated at the cable conductors, together with power losses generated in the insulation and sheath, were transmitted through the buried cable backfill and ground, generally towards the ground surface which is treated as an isotherm at ambient temperature. This heat raises the temperature of the air in the ducts in the vicinity of the crossing. As the ducts are at a slight angle to the horizontal, and if ambient conditions allow, a naturally induced air flow is generated, commonly known as the ‘chimney’ effect, which takes heat away from the cables.

Ideally, for naturally induced convection to be most effective, the location of the duct inlet and outlets should be as close to the crossing point as possible. However, in this instance, geographical constraints meant that the inlets and outlets had to be where they are, at some distance from the crossing.

## 2: Meshing

The physical size of the model was determined by the location of the duct inlet and outlets and by the need to have boundary temperatures that would not influence the cable temperatures at the crossing. This resulted in a physically large model, approximately 80m x 80m x 15m deep.

Despite this large size, the cables themselves are only about 80 mm (132kV) and 140 mm (400kV) in diameter, and so in order to capture the higher temperature gradients, the mesh in the vicinity of the cables required greater fidelity than the mesh at the extremities of the model. This was achieved using the Hex Dominant Mesher (HDM), which can quickly provide a mesh that satisfies this requirement. Originally designed for discretising fluid domains, it also works very well for solid regions; in this case the representation of the ground between the cable circuits and ducts.

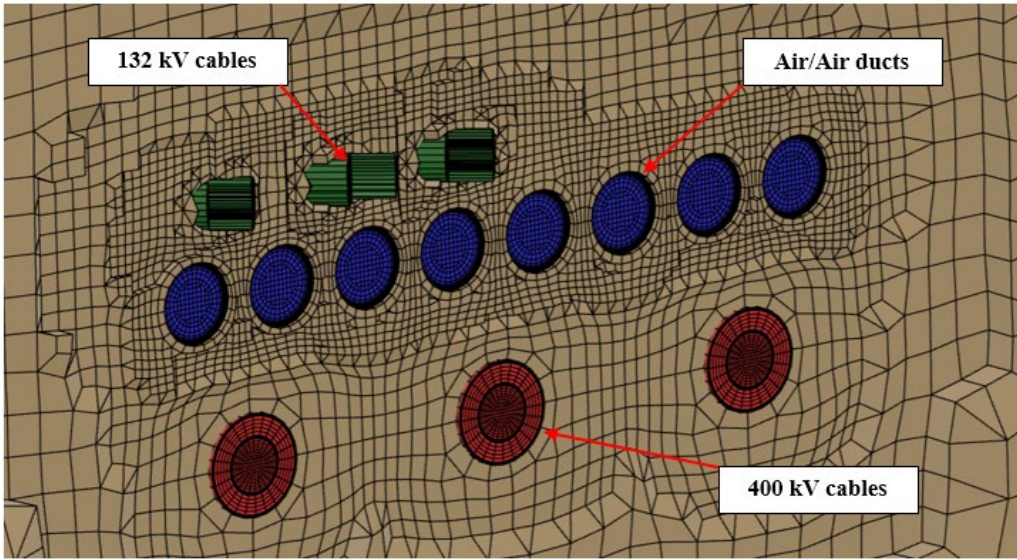


**Figure 2: Discretisation of ground surrounding cables and ducts**

The mesh used for the cables and ducts was generated by extruding a two-dimensional mesh along a path which allowed control over the size and location of the elements representing the constituent parts.

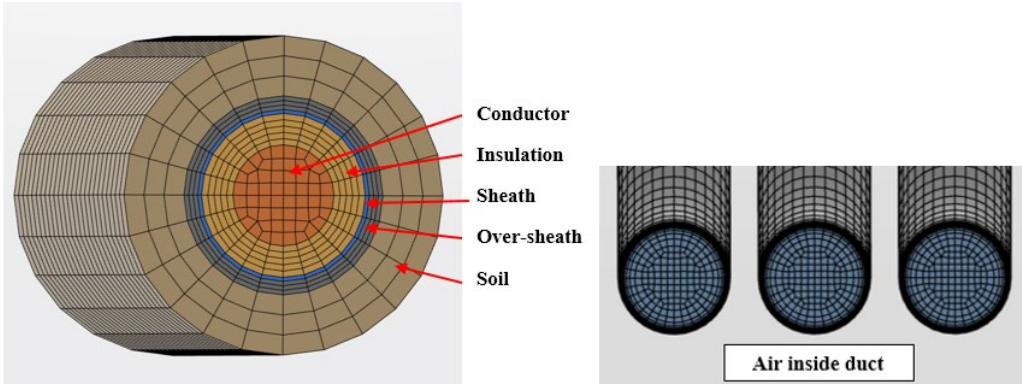


**Figure 3: Mesh discretisation used for cables and ducts**

The combination of mesh extrusion and mesh generation using the HDM resulted in model of approximately 19.5 million elements, 14.8 million of which were generated by the HDM to represent the ground.

### 3: Simulation and results

A number of simulations were completed using loading and boundary values that reflected operating conditions likely to be experienced at different times of the year.

Power losses in the conductors, dielectrics and sheaths of the cables were defined as volumetric heat sources and boundary conditions including ground surface temperature and ambient air temperature were set for each seasonal scenario. The remote ground temperature remained constant at 15 degrees centigrade. Stagnation pressure boundaries were defined at the outlet end of the air ducts and either a stagnation pressure boundary (induced flow) or a volumetric flow condition (forced flow) defined at the inlet end.

Each simulation was run as a steady-state analysis using the 3DSFlow Navier-Stokes solver incorporating conjugate heat transfer. A K-Epsilon turbulence model was used for the duct air flow and the software automatically created non-conformal thermal interfaces at the solid/solid and solid/fluid boundaries.

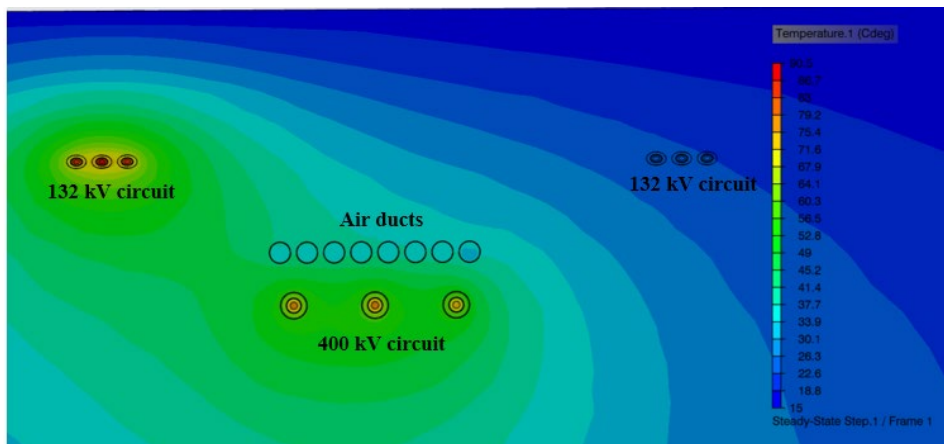


Figure 4: Temperature contours surrounding cables and ducts

In accordance with the objectives of the project, a steady-state solution was obtained for a range of seasonal scenarios. In some cases, typically when the ambient temperature was low, induced flow was instigated in the ducts and the cables were adequately cooled. However, in other cases when the ambient temperature was high, the buoyancy forces of the heated air were insufficient to overcome the frictional resistance of the duct air flow and hence longitudinal duct air flow was not developed. This resulted in conductor temperatures that were not within acceptable operational limits.



# VMAP enabling interoperability in integrated CAE simulation workflows

Klaus Wolf, Priyanka Gulati

*Fraunhofer Institute for Algorithms and Scientific Computing – SCAI, Sankt Augustin GERMANY*  
[Klaus.Wolf@scai.fraunhofer.de](mailto:Klaus.Wolf@scai.fraunhofer.de) [PriyankaGulati@scai.fraunhofer.de](mailto:PriyankaGulati@scai.fraunhofer.de)

Gino Duffett

*NAFEMS GmbH, Munich, GERMANY*  
[Gino.Duffett@nafems.org](mailto:Gino.Duffett@nafems.org)

**Keywords:** interoperability, standards, manufacturing simulation, software interfaces, data mapping, material models, ontologies, simulation workflows

## Introduction



With the progress in CAE simulation leading to more complicated and integrated workflows, data control and transfer becomes essential. This is extremely important in the manufacturing industry where complicated simulation workflows are necessary in tracking material changes throughout the manufacturing process. Traditionally this has led to many one-off solutions created by engineers in their desire to solve their design-process problems within the defined timescales. Naturally, the result was that many methodologies for transferring information became available but were stand-alone and/or unavailable to different departments or entities.

The VMAP data standard is the first to address this issue and solve the problem by standardising the data being transferred to enable complete software interoperability. Additionally, VMAP provides a library of IO routines to help engineers speed-up the creation of their workflows thereby removing the emphasis for considering data formats. This enables easier and more flexible data transfer, use of different software for different simulations and the creation of re-useable processes that can be easily adapted to include more or different data. Moreover, this enables software interoperability for post-processing and data manipulation and processing.

VMAP is cost-free and is supported by the international VMAP Standards Community comprising independent software vendors (ISVs), developers, academia and other entities and provides the CAE industry with a focus group to provide guidance, collaborate, evolve and maintain VMAP.

This paper describes the VMAP standard and IO libraries, example of its successful implementation via various use cases. The important roles of the VMAP Standards Community are also described.

## The VMAP Standard

VMAP is defined as a vendor neutral standard for CAE data-storage to enhance interoperability in virtual engineering workflows.

The data standard is based on HDF5, a widely accepted implementation platform for many IO related applications. The data formats currently included in the release version 0.4 relate to geometry and discretization, coordinate and unit systems, result and state variables, parameters for (material) models as well as meta- and user-defined data. The list is under continual enhancement.

Many ISVs, both large and small players, will implement the VMAP Standard directly within their software to extract the maximum speed and efficiency, shown schematically in Figure 1.

However, all data defined within the standard can be written or read using the IO software library provided as part of the VMAP Standard, also shown schematically in Figure 1. This enables engineers

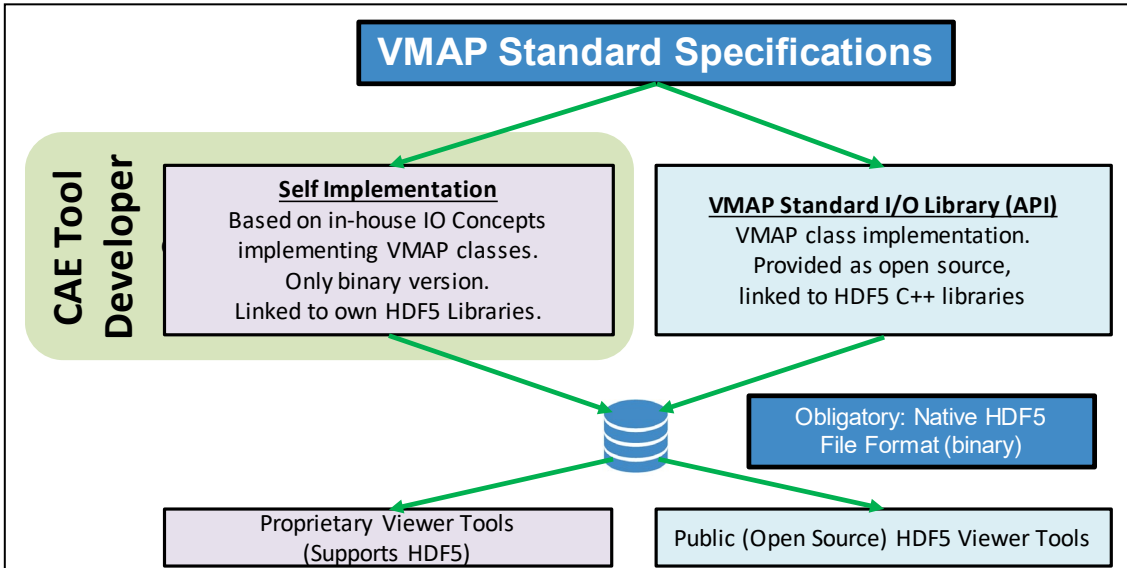


Figure 1: VMAP Standard implementation either within ISV software or utilising the supplied IO software library.

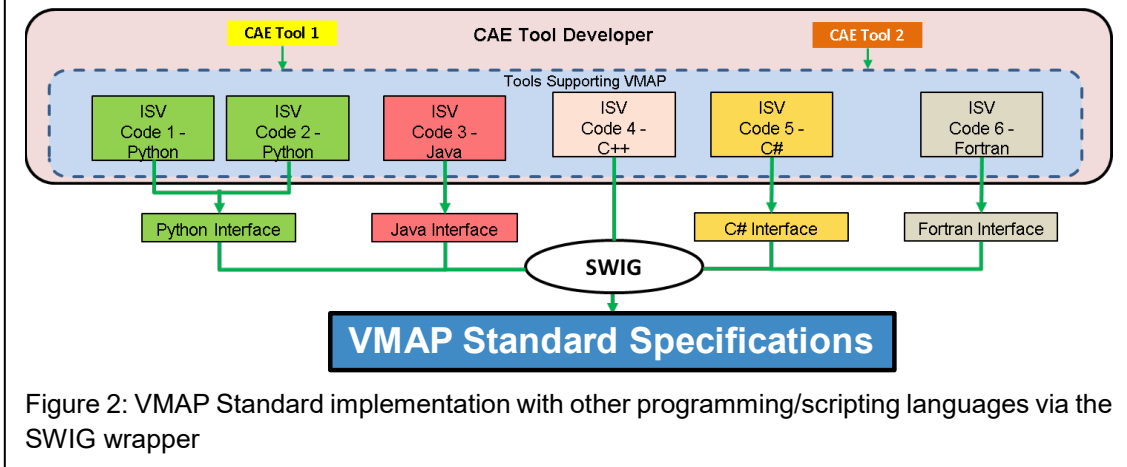


Figure 2: VMAP Standard implementation with other programming/scripting languages via the SWIG wrapper

to utilise VMAP without having any knowledge of the standardised data formats. The freely available SWIG wrapper tool can be utilised to bind the VMAP IO software library into software written in any other programming or script language, see Figure 2. As such the VMAP IO library is universally available.

To aid users and implementers a series of simple test cases are supplied within the release pack so that implementations can be quickly verified.

In summary, the complete VMAP Standard release includes:

- defined VMAP Standard (document),
- use case descriptions and background information (document),
- IO software library (software),
- a set of test cases to verify any implementation (files),
- contact information for the VMAP Standards Community (document).

Figure 3 shows a few ontology levels in VMAP. The green text represents a group, blue text represents datasets and red text represents attributes, all containing further details about a model. The HDF5 format stores the data in a similar format with groups, datasets and attributes.

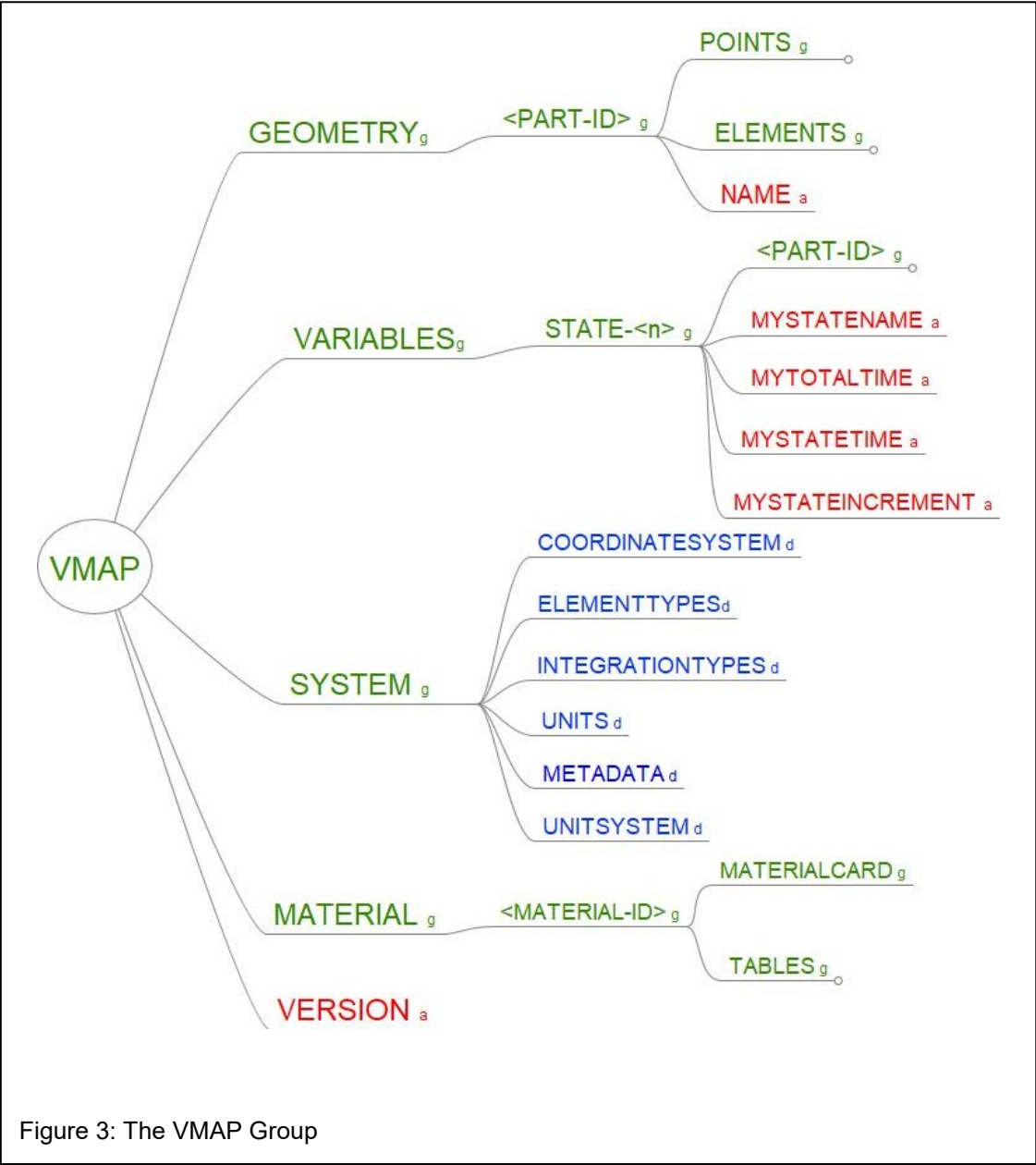


Figure 3: The VMAP Group

As can be seen in the ontology, VMAP is capable of storing dynamic time based analyses. The VMAP library can also offer the possibility to store multiple process simulation steps in the same VMAP file, useful for SMEs who do not wish to invest further in DBMS systems.

## COTS Software Implementations

To date the VMAP Standard has been implemented in many Commercial-Off-The-Shelf (COTS) software. This list, shown in Figure 4, is growing with discussions continuing with other groups regarding the VMAP implementation and creation of use cases defined by themselves (not listed).

## Use Cases

The VMAP Standard has been verified by many industrial use cases; some examples are shown in Figure 5. All these use cases include complex simulation processes requiring the tracking of material information throughout the process to ensure the correct component design with its desirable characteristics and to accurately design the manufacturing process details. Use cases that are being created in collaboration with entities external to the project are not defined here.

- **Blow Forming:** The blow moulding use case (4 simulation stages, 4 softwares) shows the detailed prediction of shrinkage and warpage of plastic bottles and containers. The product range of extrusion blow-moulded plastic parts ranges from thin-walled packaging products like bottles or cans, to highly stressed technical parts like fuel tanks or intermediate bulk containers (IBC).

The process simulations provide information, for example, about the wall thickness distribution and the shrinkage and warpage, which significantly influences the product properties of the final part. Therefore, all the information regarding the process history (e.g. temperatures, residual stresses, or wall thickness) needs to be stored and transferred between the different simulation steps. In combination with advanced material models, this integrated simulation approach makes it possible to predict the product properties of blow moulded parts with a very high accuracy.

More accurate simulation methods enable higher product performance of blow moulded plastic parts with less material consumption and shorter design/manufacture cycle times. Due to standardization and automation of the CAE workflow, time consuming data transfer between the different simulation stages can be avoided.

This case is representative for many blow moulded components as the material interfaces can easily be expanded.

Software	Platform(s)	Integration Type	VMAP import	VMAP export
4a FIBREMAP/MICROMECC		Integrated	v 0.4.0	v 0.4.0
ANSYS Mechanical		External Wrapper	(under development)	(under development)
Autodesk FUSION 360 Platform		Integrated	(technical evaluation)	(technical evaluation)
Autodesk Moldflow		External Wrapper	(under development)	v 0.4.0
Beta CAE Ansa		Integrated	v 0.4.0	v 0.4.0
Beta CAE Eplysis		Integrated	(under development)	(under development)
DYNAmore Envyo		Integrated	v 0.4.0	v 0.4.0
ESI Visual Environment		External Wrapper	v 0.4.0	v 0.4.0
e-Xstream Digimat		Integrated	v 0.4.0	v 0.4.0
Forge (Transvalor)		Integrated	(technical evaluation)	(technical evaluation)
inuTech Diffpack		External Wrapper	v 0.4.0	v 0.4.0
inuTech OOT		External Wrapper	(under development)	(under development)
MSC Marc		External Wrapper	v 0.4.0	v 0.4.0
OpenFOAM		External Wrapper	v 0.4.0	v 0.4.0
SCAI MpCCI Mapper		Integrated	v 0.4.0	v 0.4.0
Simcon CADMould		Integrated	v 0.4.0	v 0.4.0
Simulia Abaqus		External Wrapper	v 0.4.0	v 0.4.0

**Legend:**

- v 0.4.0 Existing tool available
- v 0.4.0 Tool development in progress
- v 0.4.0 Tool in planning stage

Figure 4: VMAP Standard ISV implementations. All release versions prior to the latest release 0.4.0 are compatible.

- **Composites for Lightweight Vehicles:** The lightweight vehicle composites use case (4 simulation stages, 5 softwares) shows an application of the continuous virtual process chain to a practical-oriented automotive structural part. An automated and accelerated workflow for product verification including both manufacture process and product design is available.

Mapping of results from solid to shell mesh is the most crucial point here and this has been achieved with a VMAP standardized data storage format. Most common variables include fibre orientation, volume & density.

Standardization of the data format will facilitate a complete CAE workflow for high-performance composites in relevant structural automotive applications.

- **Injection-Moulding:** This includes four sub cases: Impact, Foaming, Fatigue and Creep. These 4 plastic moulding use cases (2 to 4 simulation stages, 3 to 6 softwares) show the engineering potential of low-cost materials available for lightweight and safety applications.

Short- & Long-Fibre Reinforced Thermoplastics are used and fibre orientation including weld lines are transferred from an injection moulding simulation to a structural simulation, the main issue being the mapping of fibre orientation and other parameters.

With a completely integrated simulation process higher product performance with reduced product development times can be achieved.

- **Additive Manufacturing (AM):** The additive manufacturing use for plastic components and parts case (4 simulation stages, 4 softwares) demonstrates the needs and capabilities for AM in plastics. The product performance of additively manufactured parts is highly influenced by the process conditions. Therefore, the whole process history needs to be transferred between several simulation stages also involving different solvers and meshes. The main challenge is the transfer of time dependent boundary conditions from printer to simulation. This can be carried out effectively with the standardized VMAP data storage format.

A standardized format will help reduce efforts & cost during product development times.

- **Hybrid Modelling of Consumer Products:** The consumer lifestyle use case explores the complex improvement of the production processes and the performance of shaver products. The goal is to have a complete virtual process chain which, prior to VMAP, not been possible. Now, with using VMAP the teams are working on developing a virtual process chain which will enable seamless virtual product development.



Figure 5: Some components simulated in the defined use cases.

- **Composites in Aerospace:** The aerospace composites use case (5 simulation stages, 6 softwares) shows how standardized information can be passed between all the relevant simulation modules for the different phases of commercial aeronautics product development program utilizing the autoclave manufacturing process. The computational fluid dynamics simulation requires a different mesh and boundary conditions than for the thermo-chemical simulation, saturated flow, and stress/deformation simulations. So far, VMAP has been developed with a focus on structural simulation, however, it is possible to store and transfer data from and to other analyses types. Developing the standardized material models to enable process simulation will significantly accelerate and optimize the many simulation steps of an aerospace composite component development program.

## VMAP Standards Community

The VMAP Standard Community (VMAP-SC) supports and promotes the complete VMAP Standard. Current members comprise ISVs, developers, academia and other entities committed to evolve VMAP into a truly international Standard used by the CAE sector. Membership is open to any entity involved and working with VMAP but the VMAP-SC meetings are open to all interested parties. These are held about once every 3 or 4 months, with at least one face-to-face meeting a year.

During 2020 there has been a full plan of events including the VMAP International Conference on CAE Interoperability and the VMAP Project final project presentation.

All VMAP Standards Community information can be found on the website [vmap.eu.com/community](http://vmap.eu.com/community)

## Acknowledgements

ITEA is the EUREKA Cluster programme supporting innovative, industry-driven, pre-competitive R&D projects in the area of Software-intensive Systems & Services (SiSS). ITEA stimulates projects in an open community of large industry, SMEs, universities, research institutes and user organisations.

The Austrian part of the joint project is funded by the Austrian Research Promotion Agency (FFG). (number: Projekt 864080 – EUREKA ITEA 3 2017 VMAP Moulding).

The Belgian part of the joint project is funded by the companies partaking.

The Canadian part of the joint project is funded by the Scientific Research and Development Tax Credit Program (SR&ED)

The German part of the joint project is funded by the German Federal Ministry of Education and Research (BMBF) with 3.5 million euros via the ITEA 3 cluster of the European research initiative EUREKA. (number: DLR-Projektträger, Softwaresysteme und Wissenstechnologien – Funding Sign 01|S17025 A – K).

The Netherlands part of the joint project is funded by the Netherlands Enterprise Agency

The Swiss part of the joint project is funded by the companies partaking.